

Conformations and interactions of charged dendrimers in implicit and explicit solvents

Inaugural-Dissertation
zur Erlangung des Doktorgrades
der Mathematisch-Naturwissenschaftlichen Fakultät
der Heinrich-Heine-Universität Düsseldorf

vorgelegt von
Sebastian Huißmann
aus Kevelaer

Düsseldorf, Mai 2011

Aus dem Institut für Theoretische Physik
der Heinrich-Heine-Universität Düsseldorf

Gedruckt mit Genehmigung der
Mathematisch-Naturwissenschaftlichen Fakultät
der Heinrich-Heine-Universität Düsseldorf

Referent: Prof. Dr. Christos N. Likos
Koreferent: Prof. Dr. Jürgen Horbach
Tag der mündlichen Prüfung: 04. Juli 2011

The work described in this Thesis has been published in a number of papers, which constitute the following self-contained chapters:

Chapter 2

S. Huißmann, A. Wynveen, C. N. Likos, and R. Blaak,
The effects of pH, salt and bond stiffness on charged dendrimers,
J. Phys.: Condens. Matter. **22**, 232101 (2010).

Chapter 3

S. Huißmann, C. N. Likos, and R. Blaak,
Conformations of high-generation dendritic polyelectrolytes,
J. Mat. Chem. **20**, 10486 (2010).

Chapter 4

S. Huißmann, R. Blaak, and C. N. Likos
Explicit vs. implicit water simulations of charged dendrimers,
(in preparation) (2011).

Chapter 5

S. Huißmann, C. N. Likos, and R. Blaak
Effective interactions between charged dendrimers,
Soft Matter, DOI: 10.1039/c1sm05516j (2011).

Chapter 6

A. Wilk, S. Huißmann, E. Stiakakis, J. Kohlbrecher, D. Vlassopoulos, C. N. Likos, G. Meier, J. K. G. Dhont, G. Petekidis, and R. Vavrin
Osmotic shrinkage in star-linear polymer mixtures,
Eur. Phys. J. E **32**, 127 (2010).

Summary

Dendrimers are highly ordered polymeric macromolecules with a tree-like architecture. Advanced synthesis techniques provide control over their microscopic properties, such as a regulation of the overall charge by the pH of the solvent or the location of the ionizable groups within the molecule. We investigate the conformations and interactions of dendrimers with different spacer lengths between the subsequent generations under a changing environment. To this end, monomer-resolved molecular dynamics (MD) simulations in combination with the Ewald summation technique are employed.

For the analysis of the conformations of dendrimers in implicit aqueous solution, a variation of the spacer length is modeled both in an effective fashion, by tuning the bond stiffness, and explicitly, by inserting chains of monomers between the subsequent generations. A change of the pH value of the solution is modeled by charging the dendrimers in different ways. The effect of salinity on the conformation is examined by adding monovalent salt molecules to the solution. The dendrimers with rigid bonds reveal a shell-like structure, whereas the soft bonds result in a larger size of the dendrimer and more homogeneously distributed monomers within the molecule. By comparing the density profiles measured in the simulation with the results from Poisson-Boltzmann theory, we find very good agreement for the soft-bond model. A considerable stretching of the dendrimers can be observed for large generation number and spacer length. Upon charging dendrimers with high generation and long spacer chains, an opening-up of large voids within the dendrimer is found. Furthermore, uniform charge distributions of monomers result. The effect of explicitly modeled solvent molecules on the conformation of dendrimers under varying pH conditions is studied by employing the SPC/E model for water. Electrostatic interactions dominate over other solvent mediated effects. For end-group charged dendrimers a reduced swelling due to the hydrophobic interior of the dendrimer can be observed with respect to implicitly simulated water. In contrast, fully charged dendrimers show very good agreement. The water-intake increases with the charge of the dendrimer.

Furthermore, we investigate the influence of the dendrimer charge as well as the

salinity on the interaction between dendrimers of varying spacer length. A stronger repulsion is obtained the higher the charge of the dendrimers, while the interaction becomes softer for larger spacer lengths. By adding divalent salt molecules to the solution, the effective force can be reduced down to values of neutral dendrimers. The addition of monovalent salt has only a minor effect on the conformation and effective interaction of the dendrimers.

Finally, we analyze theoretically experimental results (obtained in FZ Jülich and FORTH) on the deformation of star polymers upon addition of homopolymer chains in good solvent conditions. The experimental observation of the osmotic shrinkage of multiarm star polymers in star/linear polymer mixtures is accurately predicted by describing the force balance on a star polymer by taking into account the classic Flory contributions as well as the osmotic force due to the linear chains, provided the latter lie above their own overlap concentration. No measurable shrinkage is induced on the stars when the linear polymer is dilute.

Zusammenfassung

Dendrimere sind hochgeordnete Polymere mit einem baumartigen Aufbau. Moderne Syntheseverfahren ermöglichen die Kontrolle ihrer mikroskopischen Eigenschaften, wie etwa eine Steuerung der Gesamtladung durch den pH-Wert des Lösungsmittels oder die Position der ionisierbaren Gruppen innerhalb des Moleküls. Es werden die Konformationen und Wechselwirkungen von Dendrimeren verschiedener Längen von Spacern zwischen den aufeinanderfolgenden Generationen in einer sich ändernden Umgebung untersucht. Zu diesem Zweck werden monomer-aufgelöste Molekulardynamik-Simulationen (MD) in Kombination mit der Ewald Summationstechnik eingesetzt.

Zur Analyse der Konformationen von Dendrimeren in impliziten wässrigen Lösungen wird eine Änderung der Spacerlänge sowohl effektiv durch Verstellen der Bindungssteifigkeit, als auch explizit durch Einsetzung von Monomerketten zwischen die aufeinanderfolgenden Generationen modelliert. Eine Änderung des pH Wertes des Lösungsmittels wird modelliert, indem die Dendrimere auf verschiedene Weise geladen werden. Die Wirkung des Salzgehaltes auf die Konformation wird durch Hinzufügen von monovalenten Salzmolekülen zur Lösung untersucht. Die Dendrimere mit steifen Bindungen zeigen eine Schalenstruktur auf, wohingegen die weichen Bindungen zu einer größeren Ausdehnung des Dendrimers und einer homogeneren Verteilung der Monomere innerhalb des Moleküls führen. Durch Vergleiche der in der Simulation gemessenen Dichteprofile mit den Ergebnissen aus der Poisson-Boltzmann-Theorie finden wir sehr gute Übereinstimmung für das Modell mit weichen Bindungen. Eine beachtliche Ausdehnung des Dendrimers kann für hohe Generationszahlen und Spacerlängen beobachtet werden. Für aufgeladene Dendrimere mit hohen Generationen und langen Spacerketten wurden sich öffnende große Hohlräume im Innern gefunden. Desweiteren ergibt sich eine gleichmäßige Verteilung von Monomeren. Der Effekt von explizit modellierten Lösungsmittelmolekülen auf die Konformation von Dendrimeren bei unterschiedlichen pH-Werten wurde studiert, indem das SPC/E-Modell für Wasser eingesetzt wurde. Elektrostatische Wechselwirkungen dominieren über andere Lösungsmittelleffekte. Für Dendrimere mit geladenen Endgruppen kann eine geringere Zunahme aufgrund des

hydrophoben Inneren des Dendrimers im Vergleich zum implizit simulierten Wasser beobachtet werden. Demgegenüber stimmen vollständig geladene Dendrimere in dieser Hinsicht sehr gut überein. Die Wasseraufnahme nimmt mit der Ladung der Dendrimere zu.

Wir untersuchen außerdem sowohl den Einfluss der Dendrimer Ladung als auch des Salzgehaltes auf die Wechselwirkung zwischen Dendrimern verschiedener Spacernlängen. Eine stärkere Abstoßung erhält man, je höher die Ladung des Dendrimers ist. Hingegen wird die Wechselwirkung bei längeren Spacern weicher. Durch Zufügen von divalenten Salzmolekülen zur Lösung kann die effektive Kraft auf Werte von neutralen Dendrimern reduziert werden. Monovalente Salzmoleküle haben nur einen geringfügigen Einfluss auf die Konformation und effektive Wechselwirkung der Dendrimere.

Abschließend analysieren wir theoretisch die experimentellen Ergebnisse (erhalten im FZ Jülich und FORTH) zur Verformung von Sternpolymeren durch Zufügung homopolymerer Ketten im guten Lösungsmittel. Die experimentellen Beobachtungen des osmotischen Schrumpfens von Sternpolymeren hoher Funktionalität in Stern-/Linearen-Polymer-Mischungen wird treffsicher vorhergesagt, indem das Gleichgewicht der auf ein Sternpolymer wirkenden Kräfte beschrieben wird. Hierzu werden die klassischen Flory-Beiträge ebenso berücksichtigt wie auch die osmotische Kraft, die von den linearen Ketten ausgeht, wobei vorausgesetzt wird, dass die Letzteren oberhalb ihrer eigenen Überlappkonzentration liegen. Es kann kein messbares Schrumpfen der Sterne für Mischungen mit verdünnten linearen Ketten beobachtet werden.

Contents

1	Introduction	1
2	Effects of pH, salt and bond stiffness on charged dendrimers	7
2.1	Introduction	8
2.2	Simulation Model	9
2.3	Theory	13
2.4	Effect of pH on dendrimers	14
2.5	Summary and conclusions	22
3	Conformations of high-generation dendritic polyelectrolytes	27
3.1	Introduction	28
3.2	Simulation model	30
3.3	Results	33
3.3.1	The radius of gyration	35
3.3.2	The bond lengths	37
3.3.3	The Radial Density Distribution	39
3.4	Conclusions	45
4	Explicit vs. implicit water simulations of charged dendrimers	47
4.1	Introduction	48
4.2	Simulation Model	50
4.3	Results	53
4.4	Conclusions	61

5	Effective interactions between charged dendrimers	63
5.1	Introduction	64
5.2	Simulation Model	66
5.3	Effect of Spacer	68
5.4	Effect of pH	71
5.5	Effect of Salt	79
5.6	Conclusions	83
6	Osmotic shrinkage in star/linear polymer mixtures	85
6.1	Introduction	86
6.2	Experimental	87
6.2.1	Materials	87
6.2.2	SANS	88
6.3	Results and discussion	89
6.3.1	SANS data	89
6.4	Theoretical analysis	93
6.5	Concluding remarks	101
7	Conclusions and outlook	103
	Bibliography	107

Chapter 1

Introduction

Soft matter is an integral part of our daily life. Aerosols, emulsions, foams like e.g. smoke, hairspray, fog, printing ink, blood, milk, mayonnaise are only a glimpse on what is encountered as soft matter.¹ All these systems are composed of colloidal particles whose defining characteristic is the mesoscopic length scale, lying roughly between 1 nm and $1\mu\text{m}$. When colloids, which can be of solid, liquid or gaseous nature, are dispersed in a continuous phase of a different composition these systems are also called colloidal dispersions, complex fluids or colloidal suspensions.¹⁻⁴ It is essentially their mesoscopic structural length scale that makes such systems soft, i.e. their rigidity against mechanical deformation is several orders of magnitude smaller than that of atomic materials.³ Based on the microscopic components, the goal of soft matter physics is the quantitative prediction of structural and dynamical properties of the system on a macroscopic scale. The high importance of soft matter systems is further supplemented by the possibility to tune and control material properties in a particular way by adjusting the microscopic parameters of the system. An in-depth understanding of the liquid state is therefore of vital interest for a large number of biological and technological applications and for fundamental research. To examine the structure and properties of soft matter, experimental techniques like X-ray, small angle neutron scattering (SANS) or electron scattering have been employed. However, the high densities of liquid phases and concomitant non-trivial short- and long-range correlations between the particles are challenges to a theoretical treatment of soft matter systems.³ To overcome this problem, a

concept called coarse-graining, or equivalently tracing out the degrees of freedom of the smaller particles in the solution has been established. A simplified effective one-component system can be obtained by deriving an effective Hamiltonian to describe the interactions between large colloids in a sea of small solvent molecules. With the resulting effective interaction and standard tools of liquid state theory^{5,6} it is possible to determine the structure of the complex fluids, which in turn allow for direct contact with experiments.³ The development of powerful computers not only lead to more sophisticated theories but also opened the way to test the validity and accuracy of the models and theories by means of computer simulations.^{7,8} Theory and simulations rely to a large extent on the separation of universal mechanisms from specific molecular details and have emerged as an important cornerstone besides experiments for the investigation of soft matter systems.

Polymers are macromolecules composed of repeating building blocks, the monomers, a number of atoms or group of atoms. The monomers interact via a short-ranged steric repulsion resulting in a self-avoiding polymer. Advanced synthesis techniques allow for the modification of their architecture. By polymerization, a mixture of monomers can be converted into a polymer of well-defined structure with, e.g., chain, star, brush or dendritic geometries. The properties of polymers are contingent on the architecture of the macromolecule and the possibility of modifying it has led to a large variety of polymeric architectures.

Polymer chains consist of a sequence of N monomers, where N is called the the degree of polymerization that can reach values of e.g. $N > 10^5$ for polystyrene. A sufficiently large degree of polymerization guarantees that the addition or removal of one or a few monomers, the properties of the chains are essentially unchanged. By connecting f chains to a common core, a star shaped molecule can be obtained, called star polymer.^{9,10} Here, f is the functionality of the star. Star polymers are a very interesting model systems that can bridge the gap between flexible polymer chains and hard colloidal particles by varying the functionality.³ For good solvents an analytical expression for the effective star-star interaction could be derived. And its validity is now established by many experiments and simulation studies.^{3,11}

Another class of synthetically prepared polymeric macromolecules but with a tree-like architecture are dendrimers. They have a highly branched and regular in-

ternal structure and were firstly synthesized in the late 1970's.^{12,13} The branching nodes of the dendrimer can be assigned to different shells, the so-called generations. Of special interest are their well-defined number of surface group together with the possibility to modify their chemical functionality. A large number of different dendritic architectures made it necessary to introduce a systematic nomenclature.¹⁴ Currently, Poly(amidoamine) (PAMAM) and poly(propyleneimine) (PPI) dendrimers are the most widely used dendrimers in experimental research. Many experimental and simulation studies have been performed on neutral dendrimers in order to examine their conformations,^{15,16} interactions¹⁷⁻¹⁹ and phase behavior.^{20,21} Dendrimers are an ideal model system for theoretical research due to their unique characteristics. Besides their well defined structure, neutral dendrimers possess a Gaussian interaction potential^{17,18} and combine many properties of colloidal and polymeric systems.¹⁵

Dendrimers can be found in a vast number of technological applications like solubility enhancement or in biomedical imaging as contrast agents. Furthermore, much effort is put into the question of how dendrimers can be used effectively in drug- and gene delivery. Some effective medicaments cause harmful side effects or can not be used at all due to their water insolubility. The possibility to synthesize biocompatible dendrimers that are capable of absorbing water-insoluble drug molecules has led to a very promising perspective. For example, hydrophobic drugs can be complexed into the hydrophobic interior of a dendrimer with water soluble surface groups making the whole complex water-soluble.²²

Polyelectrolyte dendrimers have properties that go beyond that of neutral dendrimers. Dendrimers can be synthesized in such a way that a variation of the pH value of the solution leads to dissociation of ions from the monomers thereby charging of the whole molecule. For polyelectrolyte chains and stars^{23,24} it is known that an increase of the charge results in electrostatic swelling of the macromolecule. The observation of conformational and size changes of dendrimers upon variation of the pH value of the aqueous solution has boosted the idea of using dendrimers as encapsulation agents in pharmaceutical applications. By changing the pH of the solution the dendrimer would either trap or release the drug molecule depending on its conformational state and degree of charging. Newkome *et. al.* were the first

who synthesized a dendrimer where a variation of the solution's pH value led to electrostatic swelling of the dendrimer according to which type of functional groups were used for the terminal generation.¹⁴ By means of diffusion ordered spectroscopy they observed a swelling of the size of about 35% when acidic or basic terminated 3rd-generational dendrimers were used.²⁵ However, other experimental and simulation studies resulted in a different view on the pH responsiveness of polyelectrolyte dendrimers. Nisato *et. al.* have found in SANS experiments that the size of a 8-th generational PAMAM dendrimer is essentially independent of charge density or ionic strength.²⁶ A pioneering simulation study of dendrimers under varying ionic strength predicted conformational changes from a dense-core to a dense-shell conformation.²⁷ Such contradictory observations have initiated a long debate about whether such conformational changes are completely absent or can be attributed to the steric crowding between the dendrimers of higher generations. Experimental and theoretical studies are therefore necessary to gain a better understanding of the conformational properties and the interaction between charged dendrimers.

We performed MD-simulations of charged dendrimers in implicitly and explicitly simulated water. Charged entities were simulated with the explicit Coulomb interaction, employing the Ewald summation technique. This Thesis is organized as follows. In chapter 2 the effect is studied that a variation of the pH value of the solution has on the conformational properties of dendrimers. Two types of dendrimers are considered, firstly dendrimers with rigid bonds between the nodes, and secondly, dendrimers with soft bonds. Additionally, monovalent salt is added to the solution. In Chapter 3 we show that flexibility is of crucial importance for the conformational properties of the dendrimers. We present a systematic study of the conformations of dendrimers with low and high generations and with different lengths of the spacer and under varying conditions of the pH value of the solution. By employing the SPC/E model for water²⁸ we explicitly take into account the granular nature of the aqueous solution in Chapter 4. Terminally and fully charged dendrimers with and without a spacer monomer between the nodes are considered and are compared to the simulations with implicit water. We proceed with the measurement of the effective force between neutral and charged dendrimers of different lengths of the spacer in Chapter 5. Furthermore, monovalent and divalent salt are added to the

solution, leading to different behavior of the dendrimer. Upon increasing the spacer length, dendrimers obtain properties that become more and more similar to that of star polymers and chains. In Chapter 6 the osmotic shrinkage of star polymers in a solution of linear homopolymer chains is theoretically analyzed and compared to experimental results (obtained in FZ Jülich and FORTH). The star radius is calculated by taking into account the classic Flory contributions to the free energy as well as the osmotic force exerted by the linear chains on the star. In Chapter 7 we conclude with an outlook on future research.

Chapter 2

Effects of pH, salt and bond stiffness on charged dendrimers

We have performed Molecular Dynamics simulations of charged dendrimers with various charge distributions, and including both rigid and soft bonds between the monomers. Whereas the rigid bonds result in a shell-like structure, the soft bonds lead to a larger dendrimer size and a more homogeneous monomer distribution. The measured density profiles of counter- and co-ions are compared with those stemming from Poisson-Boltzmann theory. The latter is in very good agreement with simulations for the soft-bond model, whereas for rigid bonds, significant discrepancies arise caused by the fact that Poisson-Boltzmann theory neglects finite-size ion effects. The addition of monovalent salt has no significant influence on the behavior of the dendrimers.

2.1 Introduction

Dendrimers are macromolecules with a highly and regular branched internal structure. They have been synthetically prepared since the late 1970's¹² and steady progress has led to efficient synthesis techniques²⁹. The abundant freedom in modifying their architecture makes them attractive for numerous technological applications. Previous research activities on neutral dendrimers showed that, due to back-folding of end-groups, they are found in a compact, dense-core conformation even for high generation numbers^{30,31}. The finding of a dense-core conformation has been confirmed by a large number of simulation studies^{15,32}, self-consistent field calculations³³, and scattering experiments^{34,35}. Dendrimers are also an interesting model system for colloidal/nanoparticles with a tunable stiffness^{18,19} that can bridge the gap between flexible polymers and rigid spheres.

However, neutral dendrimers only form a restricted subset of all possible architectures. An interesting question is that of how the introduction of charge, e.g., through variation of the pH value of the solution, influences the shape of the dendrimer²⁶. Whereas in the case of polyelectrolyte chains and stars in which changing the charge of the constituent atoms induces a transition from coiled to rod-like conformations^{23,24}, the charging of dendrimers might also lead to a stretched, open conformation which would allow for the absorption of smaller guest molecules in the "hollow" host. The addition of salt further influences the screening of the Coulomb interaction between the charged segments, leading to a collapse of the dendrimer for higher valences of salt ions^{36,37}. By means of quantitative SANS data analysis and experiments^{26,38-42} it has been found that the size of the dendrimer is only weakly dependent on changes of the pH, the latter being a direct way to influence the degree of charging of the molecule.

Previous simulation studies^{36,37,43,44} focused mainly on changes of pH and salinity for fixed model interactions. Here we will study the effect of bond stiffness under varying pH conditions and salt concentrations on the behavior of dendrimers. We employ MD simulations to show that softening of the bonds has a huge impact on both size of the dendrimer and its conformational properties. In Sec. 2.2 we give a short overview of the model and the simulation technique used. In Sec. 2.3 we de-

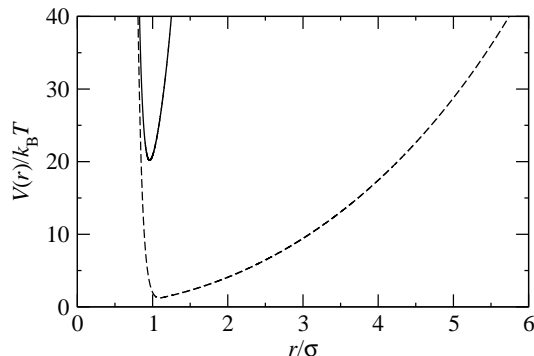


Figure 2.1: The total interaction potential $V(r)$ for two connected beads within a dendrimer, resulting from the sum of the steric [Eq. (2.1)] and bonded [Eq. (2.2)] potentials. The potentials for rigid and soft bonds are denoted by the solid and dashed lines, respectively.

scribe a theoretical approach used to ascertain the charge distribution of the counterions and co-ions around the dendrimer by an application of Poisson-Boltzmann theory. The results are presented in Sec. 2.4, where we focus on the influence of the pH of the solvent as well as considering effects of added salt, up to physiological concentrations, on the structure of the dendrimers. We conclude in Sec. 2.5 with a brief summary and outlook.

2.2 Simulation Model

In order to model the dendrimers, we employ a bead-spring model. A single pair of monomers, generation 0, forms the center of the internal structure of the dendrimer. Successive generations are added by connecting two additional monomers to each site of the highest generation only. A dendrimer thus formed will contain 2^{g+1} monomers in every generation g , whereas G denotes the total number of generations. Here we will focus on a dendrimer of generation $G = 4$, which has a total of 62 monomers.

In order to prevent monomers from coming arbitrary close, each pair of monomers at a relative distance r interacts via the purely repulsive, truncated and shifted

Lennard–Jones potential⁴⁵:

$$V_{\text{LJ}}(r) = \begin{cases} 4\epsilon \left[\left(\frac{\sigma}{r}\right)^{12} - \left(\frac{\sigma}{r}\right)^6 + \frac{1}{4} \right] & r \leq 2^{1/6}\sigma \\ 0 & r > 2^{1/6}\sigma, \end{cases} \quad (2.1)$$

where the interaction strength ϵ fixes our unit of energy and the monomer diameter σ will be our unit of length. The latter can be identified as the persistence length^{3,46}.

The connectivity between monomers is described by the so-called finite extensible nonlinear elastic (FENE) potential:

$$V_{\text{FENE}}(r) = \begin{cases} -U_0 \left(\frac{R_0}{\sigma}\right)^2 \ln \left[1 - \left(\frac{r}{R_0}\right)^2 \right] & r \leq R_0 \\ \infty & r > R_0. \end{cases} \quad (2.2)$$

Here R_0 is the maximal bond length between two monomers and U_0 is a measure for the spring constant.

In our simulations, we examine two types of bond stiffness: rigid bonds ($U_0 = 15\epsilon$, $R_0 = 1.5\sigma$) and soft bonds ($U_0 = 1\epsilon$, $R_0 = 10\sigma$). The values used for the stiff bonds are a realistic and yield excellent agreement between theory and experiment⁴⁷. Softer bonds could be obtained by the introduction of spacers. The resulting bond interactions $V(r) = V_{\text{LJ}}(r) + V_{\text{FENE}}(r)$, including short-range repulsion, for both kinds of bonds are shown in Fig. 2.1.

The short-range repulsive interaction between monomers ensures that for dendrimers with rigid bonds the unphysical crossing of bonds does not occur⁴⁸. Such crossings, however, are possible for the soft bonds. Since we will here focus mainly on static quantities, such unphysical movements should not affect the results presented here. Although these bonds are too soft for the microscopic/atomistic scale, and have not yet been employed on the mesoscopic/colloidal scale, they can nevertheless serve as a simple approximation for a short sequence of monomers that acts as spacers between the nodes of the dendrimer.

The electrostatic interaction between charged monomers is described by the Coulomb potential

$$V_{\text{Coulomb}}(r) = k_{\text{B}}T\lambda_{\text{B}} \frac{Z_i Z_j}{r} \quad (2.3)$$

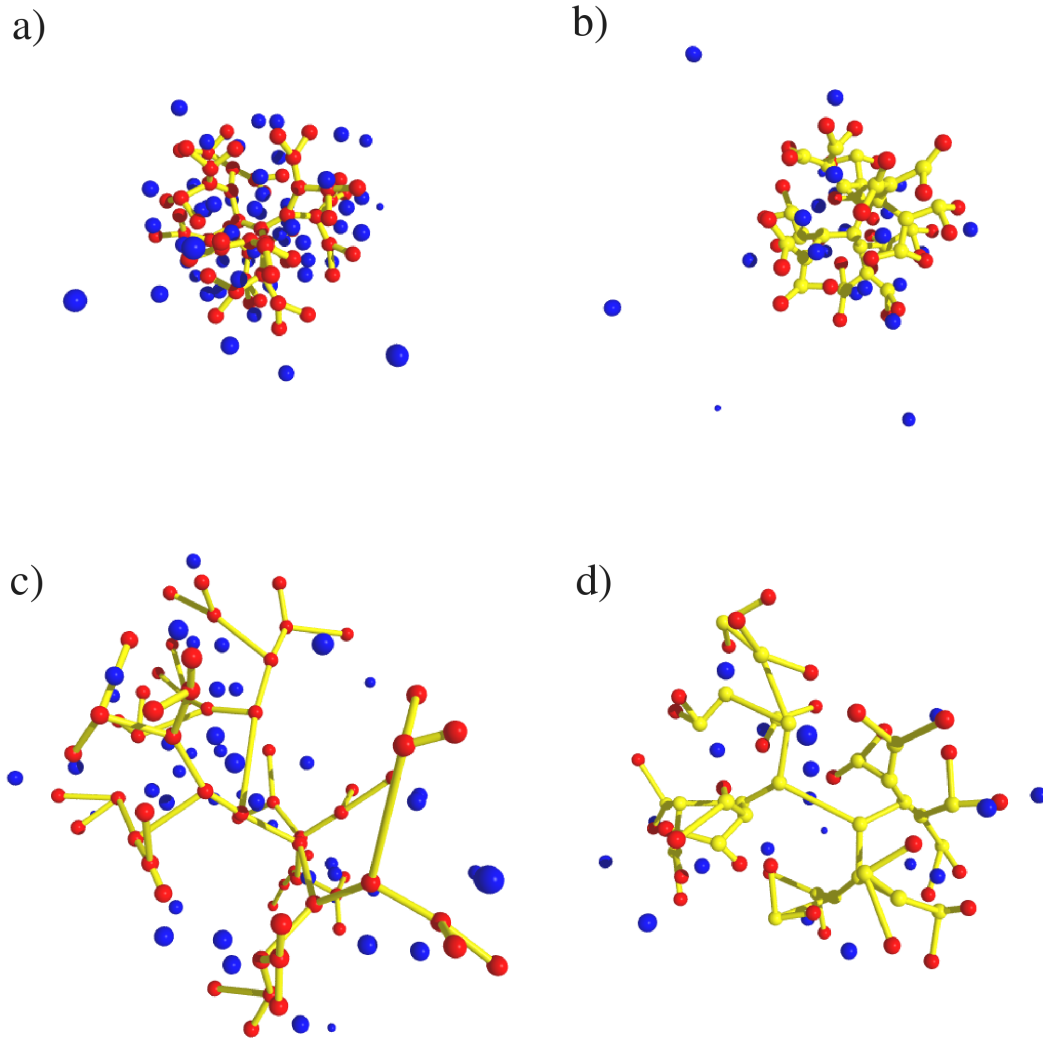


Figure 2.2: Snapshots from simulation for dendrimers with rigid bonds [(a),(b)] and soft bonds [(c),(d)]. The dendrimer types are fully charged, $Z = 62$, in (a) and (c) and only end-group charged, $Z = 32$, in (b) and (d). Neutral monomers are denoted by light gray (yellow), charged monomers by dark (red), and counter-ions by dark (blue), unbounded spheres. All monomers are rendered as spheres with half their Lennard-Jones diameter, for clarity.

with Z_i and Z_j the charge numbers, k_B the Boltzmann constant, T the temperature and λ_B the Bjerrum length given by

$$\lambda_B = \frac{e^2}{\epsilon_r k_B T}, \quad (2.4)$$

where ϵ_r is the relative permittivity.

For the solvent of our simulations we use implicit water at room temperature, which is modeled by choosing $\epsilon_r = 80$, $\lambda_B = 3\sigma$, and a temperature $k_B T = 1.2\epsilon$, which is maintained via an Andersen thermostat. This results in a particle diameter $\sigma = 0.238$ nm for our unit length. The monomers are chosen to be either neutral or monovalently charged. For charged dendrimers, the counter-ions released by the ionizable groups are included to guarantee overall charge neutrality. All counter-ions and co-ions interact, in addition to their Coulomb interaction, via the same short-range repulsion Eq. (2.1) as the monomers of the dendrimer.

The simulation box was chosen to be cubic in shape with length $L = 60\sigma$. The long-range Coulomb interactions are handled by the Ewald summation method, with the appropriate parameters for the box size and concentrations at hand. Time is measured in units of $\tau = (m\sigma^2\epsilon)^{1/2}$ and up to 5×10^6 and 10^7 time steps of $\delta t = 0.002\tau$ have been used for systems with rigid- and soft-bonded dendrimers, respectively, to gather good statistics. Initial configurations have been allowed to relax for a sufficiently long time to enable the counter-ions to diffuse into the core of the dendrimer and to reach a steady state for the inward and outward flux.

In our simulation we consider five kinds of dendrimers, which differ only in the way in which they are charged and can be characterized by their total charge number, denoted by Z . In addition to the fully neutral dendrimer with $Z = 0$ as a reference system, we obtain successive types by charging the highest neutral generation available. Therefore the next type $Z = 32$ has only its 32 monomers of the terminal generation charged. If we additionally charge the 16 monomers of generation 3, we obtain the type characterised by $Z = 48$. The next type with $Z = 56$ has all monomers of generation 2, 3, and 4 charged. The last type we consider is the fully charged dendrimer with $Z = 62$. This process of charging can be realized through a variation of the pH value of the aqueous solution. For instance, the dendrimer can be synthesized in such a way that the monomer units

are protonated, and thus charged, at low pH values but remain neutral at high pH values¹⁵. By the use of appropriate functional groups as monomer units, such as secondary and tertiary amines, only the monomers of the outer generations acquire charges at intermediate pH values. To examine the effect of salt on the behavior of the dendrimers, we have restricted ourselves to monovalent salt at concentrations of 10, 50, and 100 mM, where the corresponding ions were modelled in the same fashion as the counter-ions.

Representative snapshots from the simulations are shown in Fig. 2.2, where the difference between the rigid and soft dendrimers is apparent. The effect of the charges in the former case is to reorganize the monomers to minimize electrostatic interactions by maximizing the distances between charged monomers, whereas the size is almost insensitive to pH changes. In the latter case, the soft bonds allow the dendrimer to stretch, which reduces the electrostatic energy in a fashion not available to a dendrimer with rigid bonds, and leads to a more open structure and much more flexibility with respect to internal rearrangements.

2.3 Theory

Poisson-Boltzmann theory is a tool widely used for analysing charged, aqueous systems; we will demonstrate here how it may be applied to the dendrimer systems being probed. Results stemming from this method will be compared with simulation results as a check on the simulations and to determine the applicability of such an approach. We calculate the distribution of the counter-ions and co-ions in the solvent around the charged dendrimer by solving the Poisson-Boltzmann equation within a spherical cell of radius $R = (3/(4\pi))^{1/3}L$, i.e., the radius of a sphere whose volume is the system size, L^3 , which is given by:

$$\nabla^2\psi(r) = -4\pi\lambda_B [Z_m\rho_m(r) + Z_c\rho_c^\infty e^{-Z_c\psi(r)} + Z_{co}\rho_{co}^\infty e^{-Z_{co}\psi(r)}]. \quad (2.5)$$

Here $\psi(r)$ denotes the dimensionless electrostatic potential as a function of distance r from the center of mass of the dendrimer, ρ_c^∞ and ρ_{co}^∞ are the bulk number densities of counter-ions and co-ions, respectively, and $\rho_m(r)$ is the charge-number density of the

dendrimer. The latter is the radial charge density profile obtained by the simulation that is then used as an input in the equation in order to self-consistently determine the remaining, counter-ions and co-ion, charge density profiles. The charge numbers are $Z_m = Z_{co} = -Z_c = 1$, and the boundary conditions $\nabla\psi(0) = 0$ and $\nabla\psi(R) = 0$ have been applied. The former condition is a result of spherical symmetry, whereas the latter stems from overall charge neutrality of the full cell volume.

The solution to this nonlinear differential equation was obtained by means of the finite-difference method for the salt free cases. For higher salt concentrations we employed the Gauss-Seidel iteration method⁴⁹ using the solutions at lower concentrations as initial guesses.

From the solutions of Eq. (2.5) for the electrostatic potentials $\psi(r)$, we obtained the density profiles $\rho_c(r)$ and $\rho_{co}(r)$ for the counter-ions and co-ions, respectively:

$$\rho_c(r) = \rho_c^\infty \exp[-Z_c\psi(r)]; \quad (2.6)$$

$$\rho_{co}(r) = \rho_{co}^\infty \exp[-Z_{co}\psi(r)]. \quad (2.7)$$

By integrating the density profiles, we obtain the number of absorbed counter-ions N_{in} as:

$$N_{in} = 4\pi \int_0^{R_{max}} dr r^2 \rho_c(r), \quad (2.8)$$

where R_{max} is the maximum distance from the center of mass where the monomers of the dendrimer have been found in simulations.

2.4 Effect of pH on dendrimers

In this section we will focus on the effect that the pH of the solvent has on the conformational properties of dendrimers. It should be noted, however, that the pH is modeled in an implicit fashion, because we assumed that the change in pH will lead to a change in the overall charge configuration of the dendrimers, as described for the five different cases discussed in Sec. 2.2. Typically, the isoelectric points of annealed polyelectrolytes are found for a pH in the range 4 – 5.

A good measure for the typical size of a dendrimer is the radius of gyration R_g ,

Z	Rigid	Soft
62	2.87	5.6
56	2.81	5.3
48	2.76	5.1
32	2.70	4.8
0	2.51	3.8

Table 2.1: Radius of gyration R_g measured in units of the monomer diameter σ for rigid and soft bonds in a salt-free solution.

given by:

$$R_g^2 = \left\langle \frac{1}{N} \sum_{i=1}^N (\mathbf{r}_i - \mathbf{r}_c)^2 \right\rangle \quad (2.9)$$

where N is the number of monomers and \mathbf{r}_c the center of mass of the dendrimer. The simulation results for varying pH are shown in Table 2.1 for both the soft and rigid-bonded dendrimers. The short-range Lennard–Jones repulsion models the excluded volume effects present in the neutral dendrimers. Upon charging, the dendrimers swell monotonically, which is mainly due to the electrostatic repulsion between the charged monomers. The increase in size, however, also makes it easier for counterions to diffuse within the dendrimer, thus screening the repulsive forces to some extent. The swelling is restricted to about 15% for the fully charged dendrimer compared to the neutral one in the case of rigid bonds. The possibility to stretching the bonds in the soft-bonded dendrimers allows for a significantly larger swelling of almost 50%, which is not surprising considering the shapes of both bond interactions shown in Fig. 2.1.

It is clear that the swelling of the overall size of the dendrimers, which can only partially be explained by rearrangement of the monomers within the existing dendrimer structure, needs to be caused by increasing the distances between connected particles. Although all the bond interactions within a dendrimer are the same, the stretching of individual bonds depends on their location within the dendrimer. This can be seen in Table 2.2, where we list the average bond length for the different

Z	$b(0)$	$b(1)$	$b(2)$	$b(3)$	$b(4)$
62	2.5	2.3	2.1	2.0	1.7
56	2.4	2.2	2.0	1.9	1.7
48	2.4	2.2	1.9	1.8	1.7
32	2.2	2.1	1.8	1.7	1.6
0	1.8	1.7	1.7	1.6	1.5

Table 2.2: Average bond length $b(g)$ in units of σ for a monomer in generation g linked with its parent of generation $g - 1$ (except for $g = 0$) for the soft-bonded dendrimers.

dendrimer types with soft bonds separated with respect to their generation, i.e., the average bond length $b(g)$ is formed by the connection between a monomer of generation g and its parent of the lower generation $g - 1$. The bond $b(0)$ is the single central bond between the two generation 0 monomers. The same observations apply to the bond lengths of the dendrimer types with rigid bonds. However, the changes in bond lengths are very small and are therefore not shown.

It should be noted that the bond stretching observed is not only a direct consequence of the electrostatic repulsion of the particles participating in the bond, but a collective effect of all repulsive forces in the dendrimer. This is clear from the $Z = 32$ dendrimers for which the central bond $b(0)$ is stretched significantly with respect to the neutral dendrimer, even though only the end-group monomers carry charges. Not only do the bond lengths increase with increasing dendrimer charge, but also the stretching increases with decreasing generation. This is not unexpected, if one realizes that by stretching a single central bond, on average most monomer distances between monomers of different branches are increased, thus diminishing the electrostatic potential. In fact this argument is not restricted to the electrostatic interaction, because even for the neutral dendrimer the stretching of a central bond will be beneficial for the short-range repulsive forces and, at the cost of a somewhat higher energy, will increase the entropic freedom.

A better understanding of the internal structure is offered by the radial density

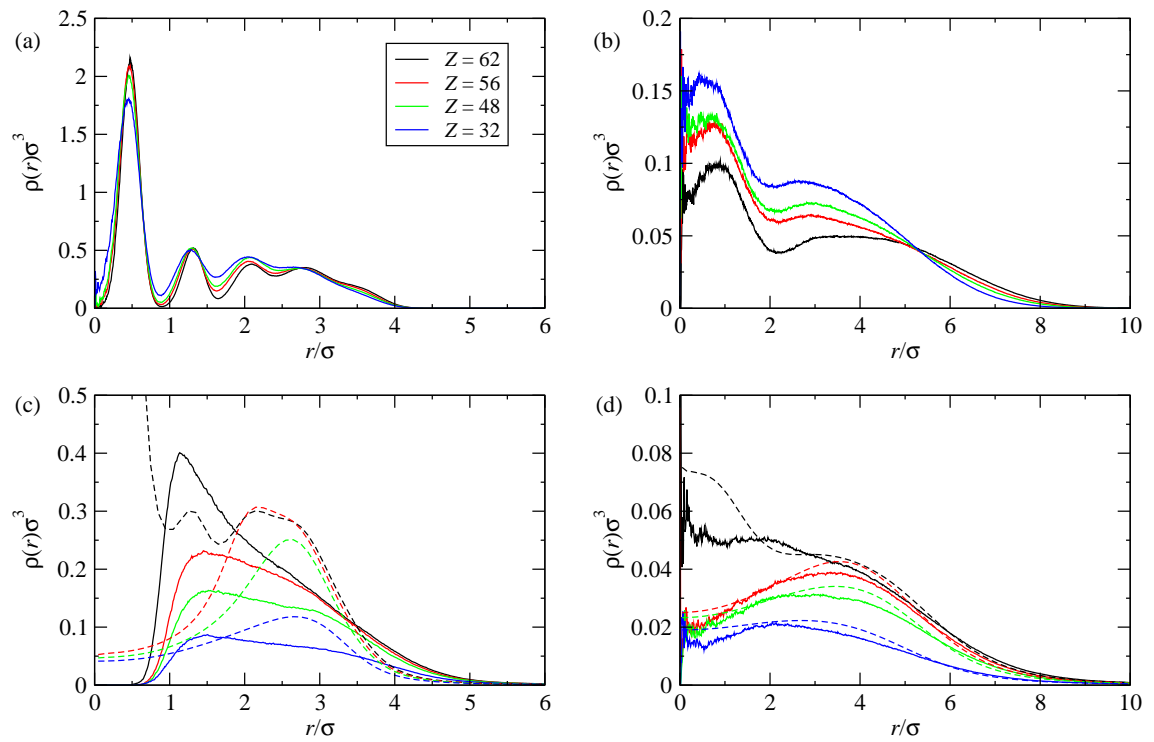


Figure 2.3: Simulation results for the radial density profiles [(a),(b)] and counter-ion distributions [(c),(d)] at different pH values. Results for dendrimers with rigid bonds are shown in panels (a), (c) whereas those for soft-bonded dendrimers in panels (b), (d). The counter-ion distributions obtained by Poisson-Boltzmann theory are shown as dashed lines.

profiles $\rho(r)$ measured with respect to the center of mass \mathbf{r}_c ,

$$\rho(r) = \left\langle \sum_{i=1}^N \delta(\mathbf{r} - \mathbf{r}_i + \mathbf{r}_c) \right\rangle, \quad (2.10)$$

where \mathbf{r}_i denotes the position of the i -th monomer within the dendrimer or, alternatively, could denote the positions of counter-ions or co-ions.

Figure 2.3 shows the radial density profiles for the monomers and the counter-ion distributions for both cases of rigid- and soft-bonded dendrimers. Upon charging, the dendrimers swell due to electrostatic repulsion between the charged monomers. In combination with the connectivity of the monomers, this results in a clear shell-like density profile in the case of rigid bonds, whereas the additional freedom of bond stretching for the soft-bonded dendrimers leads to a less structured density profile. The space within the dendrimer that has been freed by the swelling becomes partially occupied by the counter-ions, which can easily diffuse into the core of the dendrimer. This effect is obviously enhanced by an increased overall charge of the dendrimer. Whereas the additional freedom in arranging monomers in the soft-bonded dendrimers due to bond stretching allows the counter-ions to occupy the space throughout the dendrimer, the shell structure maintained by the rigid bonds expels them via the short-range repulsive Lenard–Jones forces from the center of the dendrimer.

The results for the counter-ion distributions from the Poisson-Boltzmann approach based on the measured radial density profiles are also shown in Fig. 2.3(c) and (d). In the case of the soft bonds, this leads to a remarkably good agreement with simulation results. In contrast, for the rigid-bonded dendrimers, there is a significant discrepancy. This is caused by the fact that the Poisson-Boltzmann theory neglects the steric interactions that, in particular for the rigid-bonded dendrimer, expel the counter-ions from the region close to the center of mass, which in the shell-like structure of the dendrimer lies close to the central monomer pair on average. For the dendrimer with soft bonds, the radial density profiles are much less structured, which does not require the near coincidence of the center of mass and the center of the dendrimer, i.e., the location of the $g = 0$ generation. Only in the case of the fully charged dendrimer does the Coulomb attraction of the central monomers lead

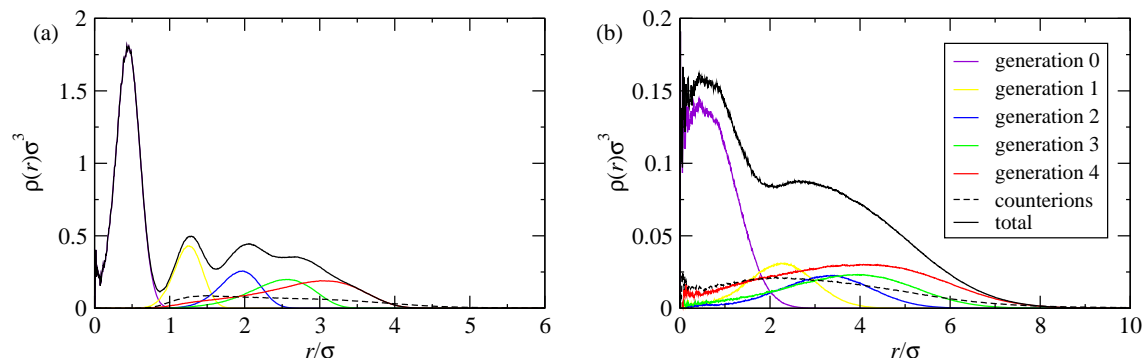


Figure 2.4: Radial density profiles of the monomers of end-charged dendrimers: (a) in the rigid bonds; (b) soft bonds. Also shown is a breakdown in the contributions emerging from each different generation. Partial generation densities are shown in the order of growing generation number from left to right.

to a significant deviation in the core region.

The existence of the shell structure of the dendrimer in the rigid-bonded case, and its absence in the soft-bonded dendrimers, is illustrated in Fig. 2.4, where the contributions to the radial density profiles of the individual generations are shown for dendrimers with only the terminal generation charged. The mutual repulsion of the monomers and restricted bond lengths for the rigid dendrimers push the monomers of the last generation further outwards, enforcing a shell-like structure on the monomers of lower generation, with almost no back-folding present. For the dendrimer with soft bonds, the flexibility gained by stretching not only leads to a much larger size, but also enables the charged monomers to distribute over the whole available space occupied by the dendrimer; it is even possible for them to be found in the core region. The same is true for the monomers of lower generations, with the exception of the central ones, which by construction are close to the center of mass.

In Table 2.3 we list the number N_{in} of absorbed counter-ions as obtained from simulation and theory. Hereby, a counter-ion is assumed to be absorbed if its distance to the center of mass of the dendrimer is less than the maximum distance R_{max} at which a monomer of that dendrimer is found within the simulations. In the case

Z	Rigid		Soft	
	$N_{\text{in}}^{(sim)}$	$N_{\text{in}}^{(th)}$	$N_{\text{in}}^{(sim)}$	$N_{\text{in}}^{(th)}$
62	46	50	46	46
56	40	44	40	42
48	32	36	33	34
32	18	21	18	19

Table 2.3: The number of absorbed counter-ions N_{in} for the salt-free solutions from simulation (*sim*) and Poisson-Boltzmann Theory (*th*).

of the rigid-bonded dendrimers this value $R_{\text{max}} = 4.7\sigma$ is the same for the different kinds of charge distributions, whereas for the soft-bonded dendrimers this increases somewhat with the overall charge and ranges from $R_{\text{max}} = 11\sigma$ to 13σ . Not surprisingly, this number increases with the overall charge Z of the dendrimer but seems to be insensitive to the nature of the bonds. Since the Poisson-Boltzmann theory neglects the steric interactions due to the short-range Lennard–Jones repulsion between monomers, it overestimates the number of absorbed counter-ions. Since, in the case of the rigid bonds, the charged monomers are forced to remain in a smaller enclosed volume, this overestimation is further enhanced.

A way to characterise the internal freedom in the conformation of the dendrimer is to measure the bond angles θ and ϕ averaged over each node. Here θ , associated with a monomer of generation g , is defined as the bond angle between the bond with the joined monomer of the lower generation $g - 1$ and those of each of the joined monomers of the higher generation $g + 1$. Likewise, ϕ , associated with the same monomer of generation g , is defined as the bond angle between the two bonds to both linked monomers of the higher generation $g + 1$. The probability distributions of the bond angles are shown in Fig. 2.5. The steric interactions in the rigid case result in a vanishing of the probability for values of bond-angles smaller than $\pi/3$ [Figs. 2.5(a) and 2.5(c)]. Upon increasing the charge of the dendrimer, this effect becomes less important, since the repulsive Coulomb interactions lead to a natural avoidance of small angles. In the soft-bonded dendrimers, the steric restriction can

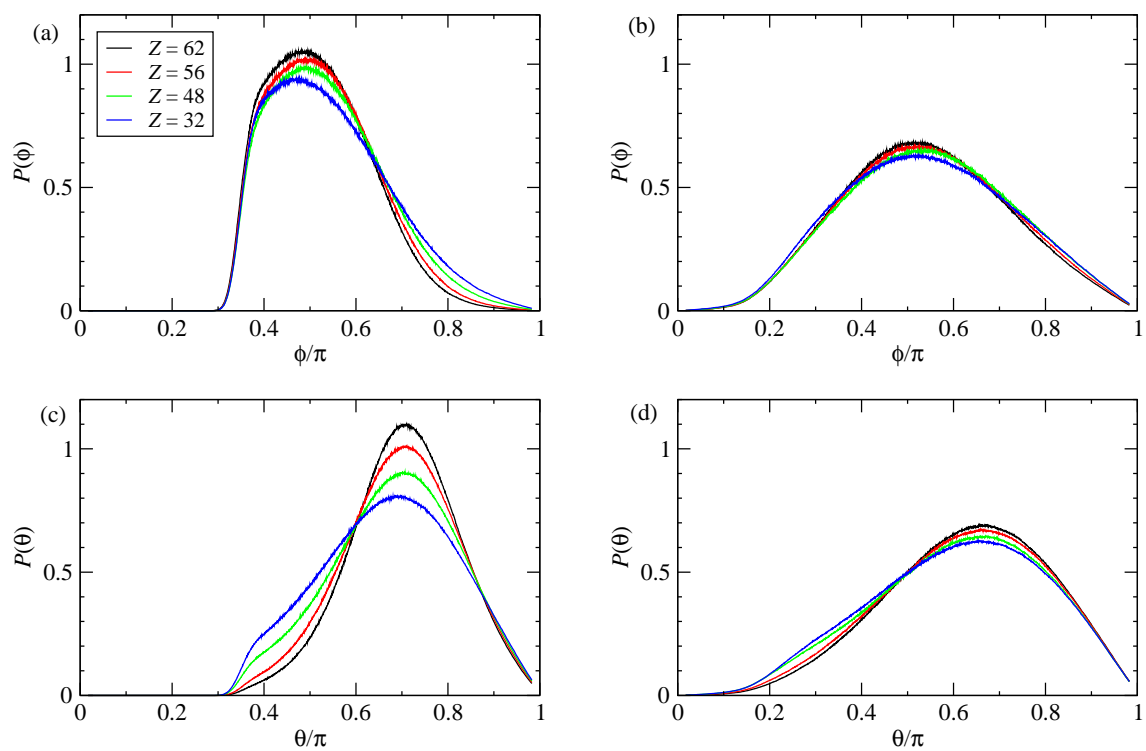


Figure 2.5: Probability distributions of the angles ϕ and θ for all types of dendrimers considered in this work. Panels (a) and (c) show results pertaining to rigid-bonded dendrimers, whereas panels (b) and (d) demonstrate the results for soft-bonded ones.

be bypassed by exploiting the fact that bonds can be stretched, thus allowing for even small angles because of the increased distance between joined monomers. This also causes the angle distributions to be less sensitive to the overall charge of the dendrimer.

For star polymers, it is known that an increase of the salinity of the solution can result in a dramatic collapse of the polymers²⁴. In order to investigate whether a similar behavior can be observed for dendrimers, we performed simulations at three different salt concentrations of monovalent ions. Hereby, we focus on the dendrimers with only the terminal groups charged ($Z = 32$) and both kinds of bonds. For the salinity we chose physiologically relevant concentrations of 10, 50, and 100 mM.

The resulting density profiles are shown in Fig. 2.6 and indicate that, at least for monovalent salt ions, addition of salt at these concentrations has no significant effect on the conformation of the rigid-bonded dendrimers. In the case of the soft-bonded ones, it results in a slightly more compact structure as indicated by change in the radius of gyration in Table 2.4. This is due to a minor increase in the counterion concentration within the dendrimer, which increasingly screens the Coulombic repulsion between the charged dendrimer monomers. At the same time the number of absorbed co-ions, where the same criterion as for the counter-ions is used, for all dendrimers and concentrations remains less than 1. As mentioned before, the results from a Poisson-Boltzmann calculation for the rigid dendrimers are somewhat inaccurate, since it neglects the short-range repulsive steric interactions between monomers and ions, which are amplified in the central region of the rigid-bonded dendrimer. For the soft-bonded dendrimers, a similar, but smaller, discrepancy can be seen as well. In the outer regions and outside the dendrimer, however, Poisson-Boltzmann theory predicts density profiles for counter-ions and co-ions that agree quite well with the simulation data as illustrated in Fig. 2.7.

2.5 Summary and conclusions

We have performed Molecular Dynamic simulations of charged dendrimers of generation 4. In experiments the overall charge can be handled by modifying the pH of the solvent, and the location of the chargeable groups can be controlled by the

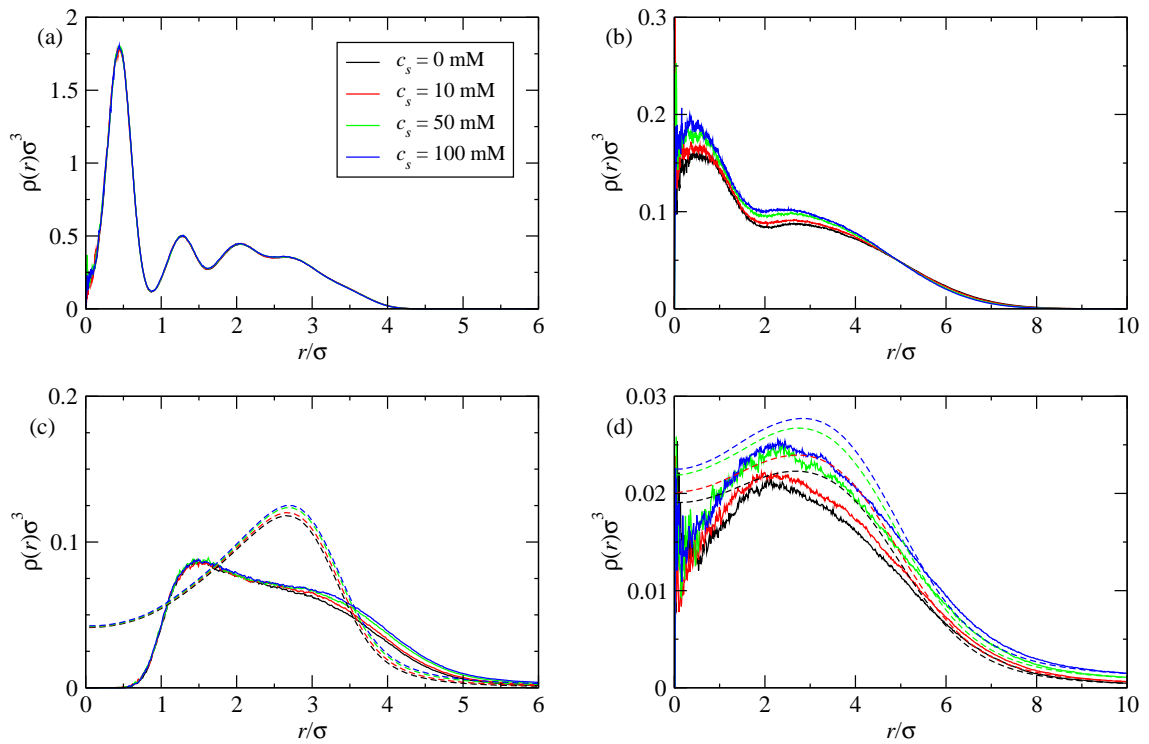


Figure 2.6: Radial density profiles for terminal-group charged (a) rigid and (b) soft dendrimers at varying salt concentrations ranging between 0 and 100 mM. The corresponding counter-ion distributions are shown in panels (c) and (d), respectively. Solid lines: simulations; dashes lines: Poisson-Boltzmann theory. Salt concentrations, as indicated in the legend, decrease from top to bottom.

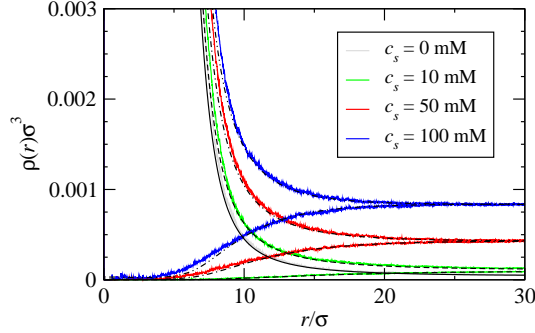


Figure 2.7: A comparison of the simulation data and Poisson-Boltzmann results for the counter-ion and co-ion distribution for the soft, end-group charged dendrimers at the various salt concentrations. The colored lines denote simulation results for the salt concentrations indicated in the legends, whereas the black lines illustrate results from Poisson-Boltzmann theory. For the case of no salt ($c_s = 0$ mM), there is a single curve corresponding to the counter-ions, whereas for finite salt concentrations the monotonically decreasing curves denote counter-ion profiles and the increasing ones those of the co-ions.

c_s [mM]	Rigid bonds			Soft bonds		
	R_g/σ	$N_{\text{in}}^{(sim)}$	$N_{\text{in}}^{(th)}$	R_g/σ	$N_{\text{in}}^{(sim)}$	$N_{\text{in}}^{(th)}$
0	2.70	18	21	4.8	18	19
10	2.70	19	22	4.7	20	21
50	2.70	20	23	4.6	24	25
100	2.69	20	24	4.6	27	28

Table 2.4: The radius of gyration R_g and the number of absorbed counter-ions N_{in} from simulation (*sim*) and Poisson-Boltzmann (*th*) for different salt concentrations c_s . Results are provided, again, for a dendrimer with only the end-groups charged and with either rigid or soft bonds.

appropriate synthesis techniques. We have restricted these investigations, for simplicity, to four different kinds of charge distributions, starting from ones with only chargeable end-groups, to the fully charged dendrimer by successively adding charge to lower generation monomers. In order to investigate the effect of the bond stiffness on the behavior of the dendrimers, we also considered two different varieties: the rigid bonds, which almost keep the bond length fixed, and a soft bond that can be stretched up to almost twice its optimal length.

The Coulomb repulsion of the charged monomers results in an increasing size of the dendrimer of about 10% for our rigid parameters, but almost 50% for the weaker bonds. However, whereas in the rigid case the dendrimer forms a shell-like structure for its monomers of different generation, in the case of the soft bonds the additional stretching allows for a more homogeneous distribution of the monomers and back-folding. The charged monomers draw counter-ions into the dendrimer, compensating roughly 60% - 70% of the overall charge of the dendrimer. The size of the simulation box is here already sufficiently large to guarantee that this number does not change substantially with increasing box size.

The distribution profiles of the counter-ions obtained by the simulations have been compared with predictions of a Poisson-Boltzmann theory based on the monomer profiles from the simulations. For the soft-bonded dendrimers this results in an excellent agreement. For the dendrimers with rigid bonds, however, a significant discrepancy arises, which can be explained by the fact that this theory neglects the short-range repulsive interactions between monomers and counter-ions. Due to the shell-like structure, the central monomer pair on average will be close to the center of mass of the whole dendrimer, thus expelling counter-ions from the core region despite the Coulomb attraction of the counter-ions to the core in the fully charged dendrimers.

The addition of monovalent salt of various concentrations has no substantial effect on the behavior of the dendrimers. It results in a minor increase in size and number of absorbed counter-ions. It is to be expected, however, that the addition of multivalent salt will lead to a collapse similar to that found for polyelectrolyte stars, but this falls outside the scope of the current work and is left for future studies. Finally, future work will address the question of the effect of pH and salinity

of the solvent on the effective interaction between the different dendrimer types. We expect a Gaussian effective interaction potential with stronger repulsion upon charging, where the range of the interaction can be reduced by increasing the salinity of the solvent.

Chapter 3

Conformations of high-generation dendritic polyelectrolytes

We perform monomer-resolved computer simulations of high-generation dendritic molecules, varying the amount of charge and the spacer length between subsequent generations. Charged entities (monomers and counter-ions) are simulated with the explicit Coulomb interaction, employing the Ewald summation technique. We discover considerable stretching of the molecules with increasing generation number and spacer length, whereas the effects of charging are less pronounced on the overall size of the molecule than those of the former two parameters. For large generations and spacer lengths, charging of the molecules leads to both the opening of large voids within the dendrimer and to charge distributions that are nearly uniform along the molecule's extent. These findings suggest both the possible usage of charged dendrimers as efficient encapsulating agents and their character as realizations of model charged colloids with a uniform charge distribution in their interior.

3.1 Introduction

Dendrimers have been the topic of intensive research ever since their discovery, due to their promising role in a large number of possible applications,¹³ which include their roles as solubility enhancement,⁵⁰ as drug-delivery vectors,^{51,52} as nanocarriers,⁵³ and many more. Beyond their technological relevance, research on dendrimers has become very popular in the last three decades also on fundamental grounds. Since their first preparation¹² and steady progress in synthesis techniques,^{29,54} many simulation studies,¹⁵ scattering experiments^{34,35} and self-consistent field calculations^{33,55} have been performed on neutral dendrimers with regard to their conformations and interactions. Chen *et al.*⁵⁶ successfully described the conformational properties of dendrimers of various generations and spacer lengths by the same scaling exponent valid for linear polymers. It has also been shown that neutral dendrimers exhibit a tunable and ultra-soft interaction potential³⁰ with a Gaussian shape,^{17,18} and that salient characteristics of the conformations of dendrimers are insensitive to the details of the microscopic interactions employed.^{19,30} Therefore a certain type of universality⁵⁷⁻⁵⁹ as in case of star polymers¹¹ holds for dendrimers as well, and also appears to generalize to non-equilibrium situations.^{60,61}

One of the reasons for the long debate about the conformation of dendrimers has been the finding of a dense-shell structure in one of the first theoretical treatments.⁵⁵ Now, almost three decades later, the dense-core structure is a well-accepted fact for neutral dendrimers in good solvents,^{15,31,32,62,63} yielding a monomer density profile that is high close to the center of the dendrimer, and which falls off on approaching the periphery.⁶⁴ Lescanec *et al.*⁶⁵ showed by means of a computational study that back-folding is a common process in such cases and that the end-groups are distributed throughout the whole volume of the dendrimer. In further studies of particularly the conformational properties of dendrimers up to the ninth generation³⁰ or with tunable stiffness,^{18,19} the dense core conformation and their sphericity³⁵ has also been confirmed.

With increasing order of complexity of the versatile kind of dendrimer structures synthesized, novel questions arise. For instance, it is pertinent and useful to understand how the introduction of charge through, e.g., variation of pH, influences

the shape of the dendrimer²⁶ and under which conditions screening effects become important, bringing about a reduction of swelling.⁶⁶ Linear polyelectrolytes and polyelectrolyte stars stretch upon the onset of charge, which induces a transition from coiled to rod-like conformations.^{24,67} The existence of a similar stretching, and possibly opening, of the dendrimer structure would allow the absorption of smaller molecules into a hollow “host”. In a contrast variation SANS experiment by Li *et al.*,⁴² the intramolecular space of neutral PAMAM dendrimers was investigated. It was found that the overall available internal cavity grows with increasing generation number from four to six, a result in agreement with findings of the current work. Other studies focused on changes of pH and salinity for fixed model interactions both in implicit^{36,37,68} and explicit solvent.^{69,70} Quantitative SANS data experiments and recent simulations have shown that the radius of gyration depends only weakly on changes of the pH^{26,38,39,41} and generation number.³⁹ The first experimental evidence for an intramolecular structure change has been reported by Porcar *et al.*⁴⁰ for G4 PAMAM dendrimers in aqueous solutions, as was already suggested by computer simulations.^{44,71}

In the present work we focus on the question of how the conformational properties of dendrimers depend on the generation G , the different number of spacer segments P , and on the pH of the solution. To this end, we employ monomer-resolved Molecular Dynamics (MD) simulations^{7,8} for dendrimers with up to $P = 6$ segments and generations $G = 4 - 7$. Dendrimers can be synthesized in such a way, so that by changing the pH of the solvent, various groups in the dendrimer become protonated.¹⁵ We use this to model the pH indirectly, by assuming that the pH value of the implicit solvent leads to three different types dendrimers: neutral dendrimers, fully charged ones, and dendrimers for which only the end groups are charged, whereby the charges are restricted to the nodes only, whilst the spacer-particles remain neutral. In Sec. 3.2 we introduce the model and the simulation method. The results are presented in Sec. 3.3, where we investigate the conformational properties of the various dendrimers by focusing on the radius of gyration, the bond-lengths within the dendrimer, and density profiles of nodes, monomers, and counter-ions. Finally, in Sec. 3.4 we conclude with a discussion of the main results and perspectives for future work.

3.2 Simulation model

We performed monomer-resolved MD-simulations of dendrimers with different generations G and number of spacer segments P in solutions of varying pH. We employ a bead-spring model for the dendrimers. The core of the dendrimer, generation 0, is formed by a chain of $P + 1$ monomers, the two ends being functional nodes for the growth of generation 1. A new shell or generation is set up by connecting two additional monomers to each site of the highest generation only. Since the g -th shell contains 2^{g+1} monomers, the total number of nodes of a dendrimer of generation G generations is $N(G) = 2^{G+2} - 2$. This is only the “skeleton” of the dendrimer, i.e., the arrangement of the nodes or a dendrimer with $P = 1$. A dendrimer with $P > 1$ spacer segments is formed by inserting a linked chain of $p = P - 1$ neutral monomers between each pair of the connected nodes, and consists therefore of $PN(G) - P + 1$ monomers. In order to explore the dependence on the different parameters available, we restrict ourselves to dendrimers of generations $G = 4 - 7$ and the number of spacer segments from $P = 1$ up to $P = 6$, i.e., the chains connecting nodes consist of $p = 0$ up to $p = 5$ monomers. The bonds between chemically connected monomers are rather rigid. It seems however plausible that the usage of an intermediate spacer results in an effective, much weaker, bond between nodes in the dendrimer.⁷¹ In order to examine the validity of such a coarse-graining, we also consider dendrimers without spacers but with soft-bonded interactions between the nodes.

Dendrimers can be synthesized in such a fashion that the monomer units are neutral at high pH values, but become ionized at low pH.¹⁵ By the choice of appropriate functional groups as monomeric units, such as secondary and tertiary amines, only the end-groups become ionized at intermediate pH values. We therefore assume that the effect of the pH of the implicit solvent on the dendrimers can be modeled indirectly by different charge distributions within the dendrimer. For this purpose, we focus on three different possibilities, the neutral dendrimer, the fully charged dendrimer, and an intermediate case for which only the end-groups are charged. It should be noted that only the nodes of the dendrimer will carry a single elementary charge and that all spacer-monomers remain neutral. Consequently we consider dendrimers with an overall charge number of $Z = 0$, $Z = 2^{G+1}$, and $Z = N(G)$ for

the various generations G .

To prevent monomers from coming arbitrary close, each pair of monomers at a relative distance r interacts via the purely repulsive, truncated and shifted Lennard-Jones⁴⁵ potential:

$$V_{\text{LJ}}(r) = \begin{cases} 4\epsilon \left[\left(\frac{\sigma}{r}\right)^{12} - \left(\frac{\sigma}{r}\right)^6 + \frac{1}{4} \right] & r \leq 2^{1/6}\sigma \\ 0 & r > 2^{1/6}\sigma, \end{cases} \quad (3.1)$$

where the interaction strength ϵ fixes our unit of energy and the diameter σ our unit of length. The connectivity in the dendrimer, which is typically a covalent chemical bond, can be described by the so-called finite extensible nonlinear elastic (FENE) potential⁷²:

$$V_{\text{FENE}}(r) = \begin{cases} -U_0 \left(\frac{R_0}{\sigma}\right)^2 \ln \left[1 - \left(\frac{r}{R_0}\right)^2 \right] & r \leq R_0 \\ \infty & r > R_0. \end{cases} \quad (3.2)$$

Here, U_0 is a measure for the bond strength and R_0 is the maximal bond-length between two monomers. For the normal, rigid bonds we used $U_0 = 15\epsilon$ and $R_0 = 1.5\sigma$, whereas the soft bonds are modeled by $U_0 = \epsilon$ and $R_0 = 10\sigma$. Due to the short-range repulsive interaction between the monomers, the unphysical crossing of bonds does not occur for these rigid bonds.⁴⁸ In the case of the soft-bonded dendrimer, however, this self-correcting mechanism is lacking. Consequently, the crossing of bonds can be observed and will affect some dynamical properties. For the static properties of these dendrimers, however, it is evident that such crossings are irrelevant because they lead to allowed configurations anyway; thus, we can examine whether the soft-bonded model serves as a good approximation for a flexible spacer of rigid bonds despite the existence of unphysical moves in the simulation of the former.

The simulations were performed using the Ewald summation method for the long-range Coulomb interactions between charged particles, given by

$$V_{\text{Coulomb}}(r) = k_{\text{B}}T\lambda_{\text{B}} \frac{Z_i Z_j}{r} \quad (3.3)$$

with Z_i and Z_j being the valencies of the charged units, k_{B} the Boltzmann constant,

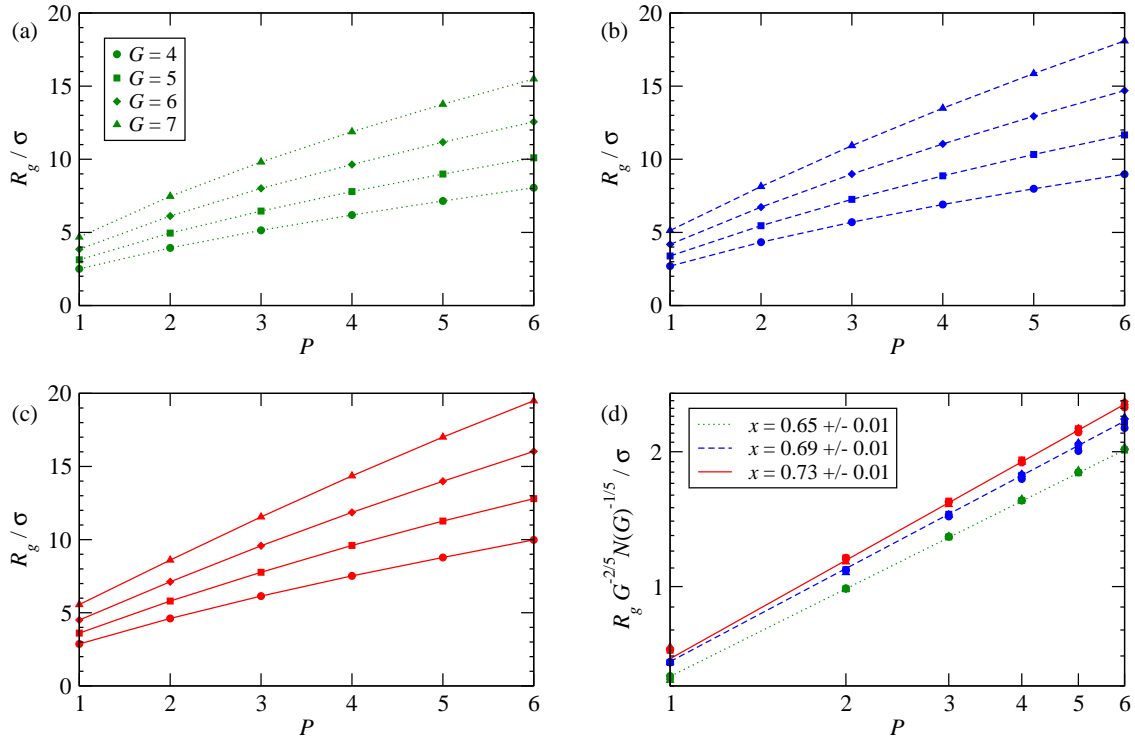


Figure 3.1: The radius of gyration R_g in units of the monomer diameter σ for (a) neutral, (b) end-group charged and (c) fully charged dendrimers, as a function of the number of segments P between the nodes. The symbols correspond to different generations G of the dendrimers. Panel (d) shows a double-logarithmic plot of the scaled radius of gyration R_g versus the spacer length P , with the lines being linear fits corresponding to increasing dendrimer charge from bottom to top. The quoted values of x are the exponents stemming from linear fits. The error bars (not shown) are smaller than the symbol size.

T the temperature and λ_B the Bjerrum length

$$\lambda_B = \frac{e^2}{\epsilon_r k_B T}, \quad (3.4)$$

where ϵ_r is the relative permittivity of the solvent. The monomers are chosen to be either neutral or monovalently charged. Counter-ions with opposite charge, which behave otherwise as normal monomers, are added to the system in order to maintain overall charge-neutrality.

Water at room temperature is chosen for the solvent and is simulated in an implicit fashion by imposing $\epsilon_r = 80$ and a temperature of $k_B T = 1.2\epsilon$, which is maintained via an Andersen thermostat. The corresponding Bjerrum length $\lambda_B = 0.714$ nm is obtained by choosing $\lambda_B = 3\sigma$, which results in a monomer diameter $\sigma = 0.238$ nm typical for the van-der-Waals radii of atoms and the persistence length as used in the framework of a bead-spring model for polymer molecules^{3,46}. The simulation box is chosen to be cubical with sides in the range $L = 60\sigma$ to $L = 120\sigma$. Time is measured in units of $\tau = \sqrt{m\sigma^2/\epsilon}$ and time-steps of $\delta t = 0.002\tau$ have been used to integrate the MD equations of motion. Initial configurations have been allowed to relax sufficiently long, enabling the counter-ions to diffuse into the core of the dendrimer and reach a steady state for the in- and out-flux, followed by up to 5×10^6 time-steps to obtain good statistics for the measurements.

3.3 Results

To examine the effects of generation, spacer length, and pH of the solvent on the conformation of the dendrimers, we focus on three essential quantities: the dendrimer's overall size, the bond lengths and the density distributions. The overall size of the dendrimer can be characterized by the radius of gyration, a quantity that also is accessible in experiments. It is experimentally much more complicated to obtain information on the internal structure of dendrimers, a quantity which is however directly accessible in computer simulations. Although the chemical bonds within the dendrimer are all identical, the extension of the same is not. In general the internal bonds between connected monomers are stretched more than those on the outside of the dendrimer, which is caused by the repulsive interactions of the monomers

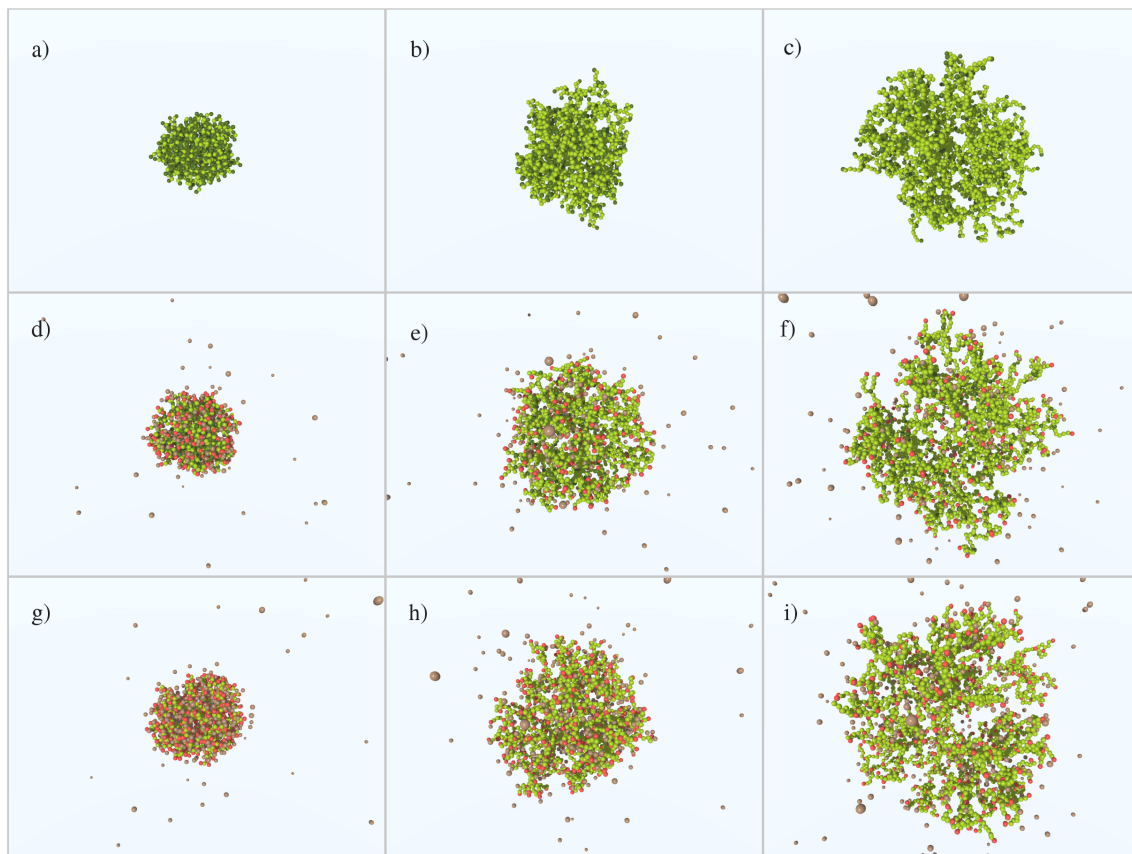


Figure 3.2: Snapshots from simulations of dendrimers with generation $G = 7$ for neutral dendrimers [(a),(b),(c)], dendrimers with charged end-groups [(d),(e),(f)], and fully charged dendrimer [(g),(h),(i)]. The number of spacer segments is $P = 2$ [(a),(d),(g)], $P = 4$ [(b),(e),(h)] and $P = 6$ [(c),(f),(i)]. Neutral monomers are green, charged monomers are red, and counter-ions are colored brown.

that propagate to the core region via the connectivity of the dendrimer structure. Finally, the dense-core structure of the dendrimer, the phenomenon of back-folding of terminal groups towards the center, and the adsorption of counter-ions by the charged dendrimers can be analyzed with the aid of various density profiles arising from the simulations.

3.3.1 The radius of gyration

The size of dendrimers can be measured by SANS-, X-Ray- or static-light scattering experiments and can be characterised by the radius of gyration R_g :

$$R_g^2 = \left\langle \frac{1}{N} \sum_{i=1}^N (\mathbf{r}_i - \mathbf{r}_c)^2 \right\rangle \quad (3.5)$$

where N is the number of monomers and \mathbf{r}_c position vector of the center of mass of the dendrimer. The simulation results are shown in Fig. 3.1, where the radius of gyration is plotted versus the number of spacer segments P for the different charge distributions and generations of the dendrimers. The size of the neutral dendrimers, shown in Fig. 3.1(a), is mainly determined by the steric interactions and increases monotonically with both increasing spacer length and generation. The presence of additional charged monomers in the end-group charged and fully charged dendrimers, depicted in Figs. 3.1(b) and 3.1(c) respectively, results in an additional swelling due to the repulsive Coulomb forces.

For a neutral dendrimers, it has been argued⁵⁶ that the radius of gyration scales with the generation G , the number of spacer segments P , and the number of monomers n according to $R_g \sim (PG)^{2/5}n^{1/5}$. Since $n \approx N(G)P$, this results in $R_g \sim G^{2/5}N(G)^{1/5}P^{3/5}$. The validity of this relation is examined in Fig. 3.1(d), where the quantity $R_g G^{-2/5}N(G)^{-1/5}$ is plotted against P in a double-logarithmic fashion. It can be seen there, that by using this scaling relation, the rescaled data for different generations coincide. The exponent of the number of segments obtained from a linear fit however is 0.65, which is somewhat higher than the expected value of 0.6. This is still surprisingly good, considering that with $P \leq 7$ and an average monomer-monomer distance $r_0 = 0.97\sigma$ this is not in the true scaling regime.

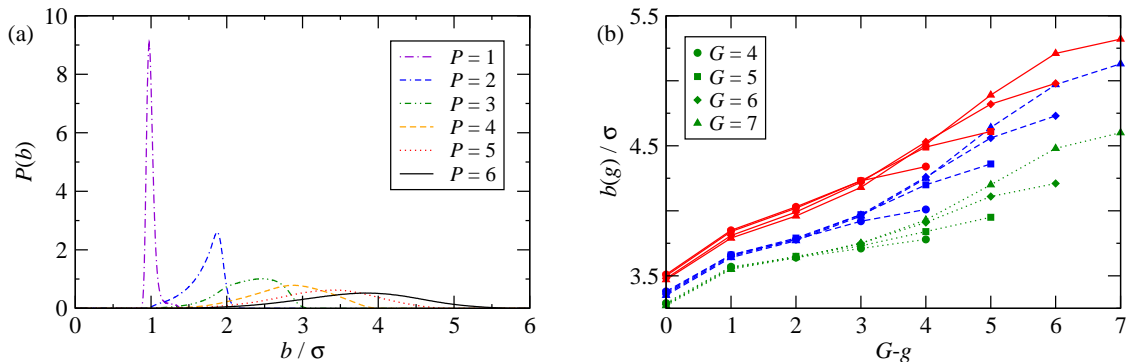


Figure 3.3: (a) Bond length probability distribution $P(b)$ as a function of the bond length b for a fully charged dendrimer of generation $G = 7$ and different numbers of spacer segments P . (b) Generation resolved bond lengths for dendrimers with $P = 6$ as a function of $G - g$ for the different generations $G = 4$ (\bullet), $G = 5$ (\blacksquare), $G = 6$ (\blacklozenge), $G = 7$ (\blacktriangle) and neutral (green), end-group charged (blue), and fully charged (red). The connected points correspond to bonds belonging to the same dendrimer.

Although the scaling argument used has been proposed *only* for neutral dendrimers, also the appropriately rescaled data for the various generations of the *charged* dendrimers collapse on top of each other, yielding however somewhat larger exponents. This indicates that the swelling due to the repulsive electrostatic interactions is almost independent of the generation of the monomers and increases with spacer length from 8 – 16% in the case of the dendrimers with only end-groups charged, and 14 – 28% for the fully charged dendrimers, to be compared with an increase of factor 2 upon going from $G = 4$ to $G = 7$ and almost factor 4 in going from $P = 1$ to $P = 6$. Thus, it can be stated that although charging does have a stretching effect on dendrimers, this is quantitatively much weaker than the corresponding one from adding a new generation or increasing the spacer length.

The growth in the size of the dendrimers upon increasing overall charge and spacer length is qualitatively illustrated in Fig. 3.2, where representative snapshots are shown for generation $G = 7$ dendrimers, for the three different charge distributions, and the number of spacer segments $P = 2$, $P = 4$, and $P = 6$. Already from these figures it can be recognized that the increase in spacer-length has not

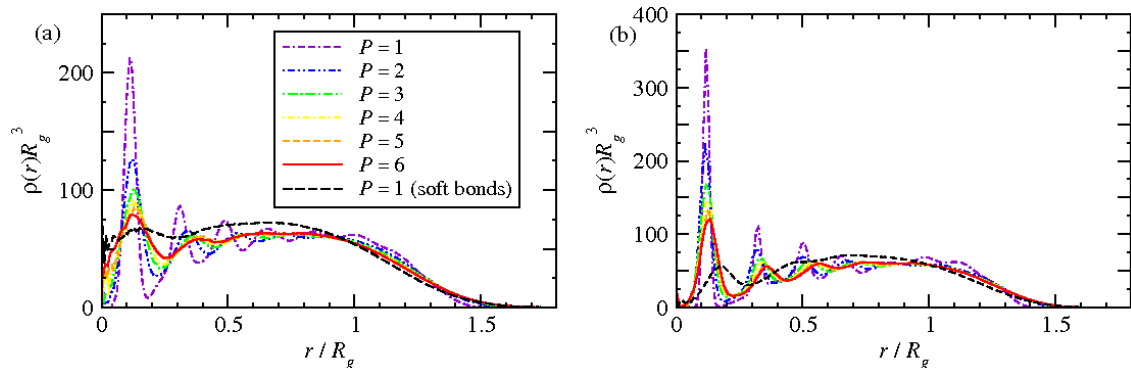


Figure 3.4: Radial density profiles for the nodes of generation $G = 7$ dendrimers in the cases of (a) neutral dendrimers and (b) fully charged ones for different number of spacer segments P . The black dashed lines correspond to dendrimers without spacer particles, but with soft-bonds. The distance is measured in terms of radius of gyration R_g .

only an enormous effect on the size of the dendrimers, but also on its internal structure, which changes from a compact, almost sphere-like to a blob-like structure with empty pockets of various sizes. With reference to Fig. 3.2(i) in particular, we can see that the dendrimer fluctuations for $G = 7$, $P = 6$ and full charge lead to the appearance of sizable voids within the molecule, an issue to which we will return shortly.

3.3.2 The bond lengths

In this section we will focus on the effective bond-lengths between nodes, rather than those between directly bonded monomers. In Fig. 3.3(a), an example of the probability $P(b)$ of finding a node-node distance b is shown for a dendrimer of generation $G = 7$, with all its nodes charged and for different spacer lengths. Not surprisingly, the average bond-length increases with a growing number of spacer segments. The asymmetry in these bond length distributions, is also present in the neutral dendrimer, but becomes more pronounced upon increasing the total dendrimer charge. For increasing number of spacer segments, this asymmetry becomes less apparent.

Götze and Likos showed that for neutral dendrimers, the central bond becomes more stretched upon increasing the generation.³⁰ Also for charged dendrimers, it has been observed that the bonds between connected monomers near the center of the dendrimer are more stretched than those in the outer region.^{44,71} This can easily be understood, since the energy cost of stretching the single bond in the center of the dendrimer, is compensated by the gain of energy caused by the resulting increase in distance between the outer monomers of the different branches and the additional entropy arising from this redistribution. Also in the present case where there are additional spacer particles, this argument can be exploited, and hence the asymmetry observed in the bond-length distribution can partially be explained by the fact that there are fewer central, stretched bonds, than more condensed bonds near the outer regions of the dendrimers.

To illustrate this we introduce the node-node distance $b(g)$ between a node of generation g and its parent node of generation $g - 1$. To facilitate the comparison between dendrimers of different generation, which produce an additional stretching, the average node-node distance is shown in Fig. 3.3(b) as a function of $G - g$ for all dendrimers with $P = 6$ spacer-segments. From this plot, one can directly observe that on increasing the value $G - g$, i.e. going from the outside of the dendrimer inwards, the node-node distances increase. It is remarkable that for the neutral dendrimer the bond-lengths of the outermost 3-4 generations almost coincide, irrespective of G : adding new generations causes increased stretching of the *inner bonds only*, leaving the outermost unchanged. The same finding carries over to dendrimers with charged end-groups and, to a lesser extent, the fully charged ones. The average bond-lengths also grow with increasing dendrimer charge. This partially explains the related swelling, observed in the radius of gyration and caused by the additional electrostatic repulsive interactions. It should be noted that the increasing bond-length of the core bonds for larger generation dendrimers will be terminated as is indicated by the leveling-off of the curves at larger values of $G - g$. This is caused by the fact that there is an upper limit to the bond-length formed by the number of spacer-segments and the maximum monomer-monomer distance R_0 stemming from the FENE potential, Eq. (3.2).

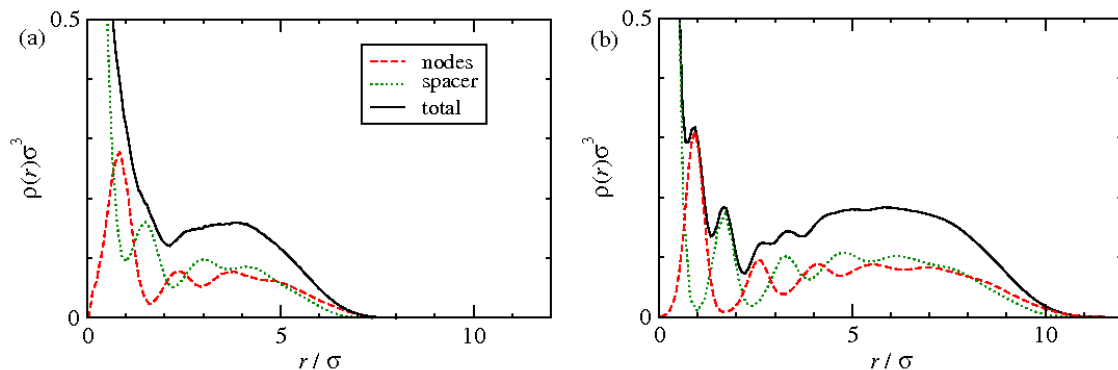


Figure 3.5: Radial density profiles of monomers for (a) $G = 4$ and (b) $G = 6$ dendrimers with all nodes charged and $P = 2$ spacer segments. The contributions from the nodes and spacer-particles are also indicated.

3.3.3 The Radial Density Distribution

More detailed information about the internal structure of the dendrimer can be obtained by considering how the monomers and counter-ions are distributed within and around the dendrimer. To this end radial density profiles $\rho(r)$ have been measured with respect to the center of mass \mathbf{r}_c ,

$$\rho(r) = \left\langle \sum_{i=1}^N \delta(\mathbf{r} - \mathbf{r}_i + \mathbf{r}_c) \right\rangle \quad (3.6)$$

where \mathbf{r}_i denotes the position of the i -th particle from the total number of particles N , which can be either monomers, nodes, or counter-ions.

In Fig. 3.4, the radial density profiles for the nodes of a generation $G = 7$ dendrimer are shown for the cases of neutral and fully charged dendrimers. To facilitate the comparison between different spacer lengths, the distance is measured in terms of the radius of gyration. For the neutral dendrimer, the steric interactions, caused by the exponentially growing number of monomers with each generation shell, enforce a shell-like structure. This is clearly visible for the shorter spacer lengths, where one can easily identify the peaks corresponding to the nodes of the first few generations. For the case $P = 1$ even a depletion zone can be observed between the first and second peak. Further away from the central region, the monomers

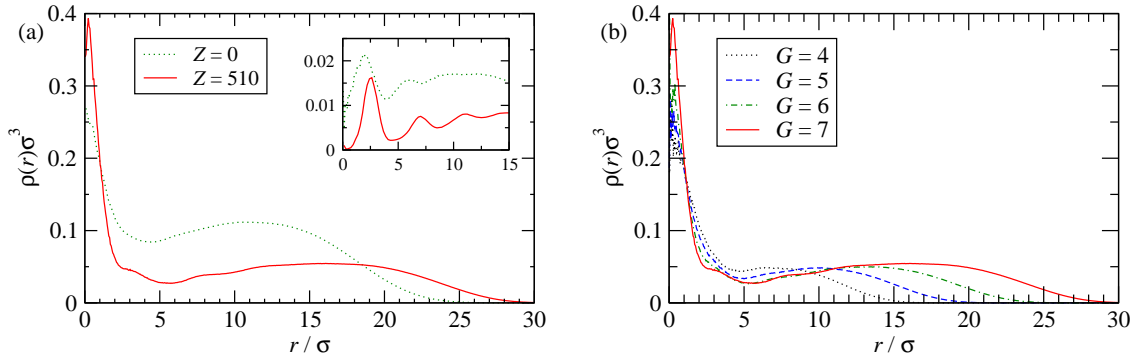


Figure 3.6: Radial density profiles of monomers for dendrimers with $P = 6$ spacer segments. (a) Neutral and fully charged dendrimers of generation $G = 7$ [The inset shows the density profiles of the nodes only]. (b) Fully charged dendrimers for different generations.

can distribute themselves better over the available volume by partially back-folding, which leads to a more homogeneous density profile.

On increasing the number of spacer segments, the shell signature diminishes, but even for $P = 6$ one can still identify some structure, which approaches the profile of a simulated dendrimer with soft-bonds also shown in Fig. 3.4. The effective soft-bonds caused by spacers or those that are modeled directly, enable the nodes to distribute more homogeneously throughout the accessible range of the dendrimer, including the area near the center of mass.

In the case of a fully charged dendrimer, shown in Fig. 3.4(b), the structure becomes even more apparent and is maintained for dendrimers with more spacer segments. This is not surprising, since the repulsive Coulomb interactions do not only stretch the individual node-node distances, as shown in Fig. 3.3, but also attempt to stretch the complete branches of the dendrimer by directing the bonds radially outwards. As a result, the center of mass of the dendrimer remains closer to the geometrical center of the dendrimer structure and voids between the nodes as can be seen by the density profile for small distances. In addition, the structure of the dendrimer becomes more open, as was illustrated by the snapshots shown in Fig. 3.2. The structure stabilizing effect of the dendrimer charge, suggests that

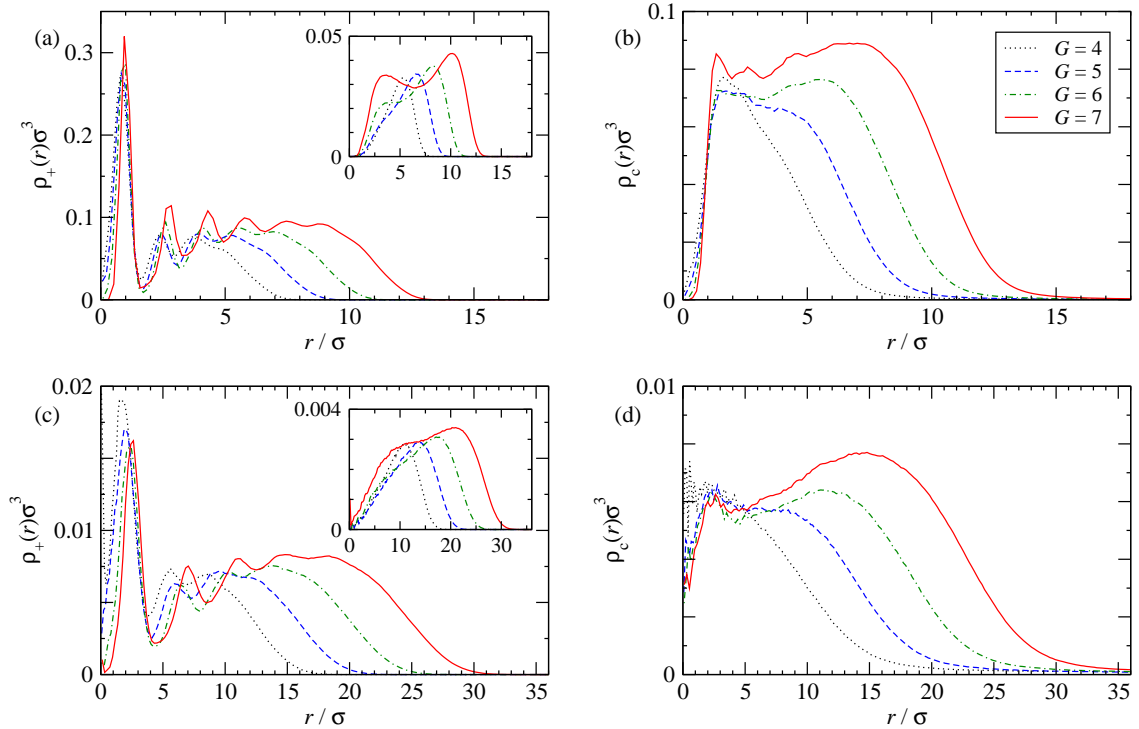


Figure 3.7: Radial charge-density profiles for fully charged dendrimers with (a) $P = 2$ and (c) $P = 6$, and their corresponding counter-ion distributions, (b) and (d), respectively. The insets show the contribution of the end-groups only.

longer spacers would be required to obtain a dendrimer that can be well described by the parameters of the soft-bonded dendrimer used here.

The structure observed in the density profiles shown in Fig. 3.4 is a consequence of focusing on the nodes of the dendrimer only. If one considers the density profiles of all monomers much of this structure is washed away as can be seen in Fig. 3.5 where the monomer density profiles are shown for fully charged dendrimers of generation $G = 4$ and $G = 6$ with $P = 2$ spacer segments. Whereas the separate density profiles of the nodes and spacer particles still show sufficient structure, their sum, i.e., the profiles for all monomers, becomes more featureless. This can be understood if one looks at the probability distribution of finding a specific monomer at a given distance from the center of mass. Since there is only a limited amount of space in

the center and the connectivity of the dendrimer puts an upper limit to its distance, these distributions have an optimal value. This preferred distance shifts to larger values if a monomer is considered that is further away from the center measured along the network of the dendrimer. The increasing number of bonds between the center and the monomer will also lead to an increasing width of the probability distribution of distances. Therefore, the total density profile of all monomers, is a sum over increasingly wider, somewhat shifted distributions which will “wash out” the underlying structure. In Fig. 3.5 this can be recognized in the alternating peaks in the density profiles of nodes and spacer particles. In the case of the higher generation, $G = 6$, the characteristic peaks are enhanced by the more extreme stretching of bonds near the center and remain still visible in the overall density profile.

In Fig. 3.6 the monomer densities profiles are shown for dendrimers with $P = 6$ spacer segments. In the case of neutral and fully charged dendrimers of generation $G = 7$ the underlying structure, as can be seen in the inset of Fig. 3.6(a), has almost completely disappeared. The remaining curves show a more or less homogeneous distribution of monomers within the volume of the dendrimer. Only for the charged dendrimer some weak features are still visible, but those are a consequence of the stronger ordering due to the stretched bonds caused by the high generation, which for lower generation dendrimer is absent, as can be seen in Fig. 3.6(b). It also shows that the more or less homogeneous density of monomers is nearly independent of the generation of the dendrimer. Another interesting effect visible in particular for the $G = 7$, $P = 6$ dendrimer, Fig. 3.6(a), is the emergence of a depression in the total monomer density in a region around $r = 5\sigma$, which has a rather large width, $w \cong 5\sigma$. This has to be compared with the existence of voids, i.e., regions of low monomer density, seen, e.g., in Fig. 3.2(i). Since the long spacer between the generations allows for more free space in which the terminal monomers can move, backfolding is less strong in this case. Not all of the dendrimer’s branches have to fold back to the center, a conformation that is energetically unfavorable due to the high charge concentration it would cause there. Concomitantly, the molecule goes over to a conformation that has, apart from a locally dense core, also a dense shell with a depression in-between, see Figs. 3.6(a) and 3.6(b). Such molecules are good

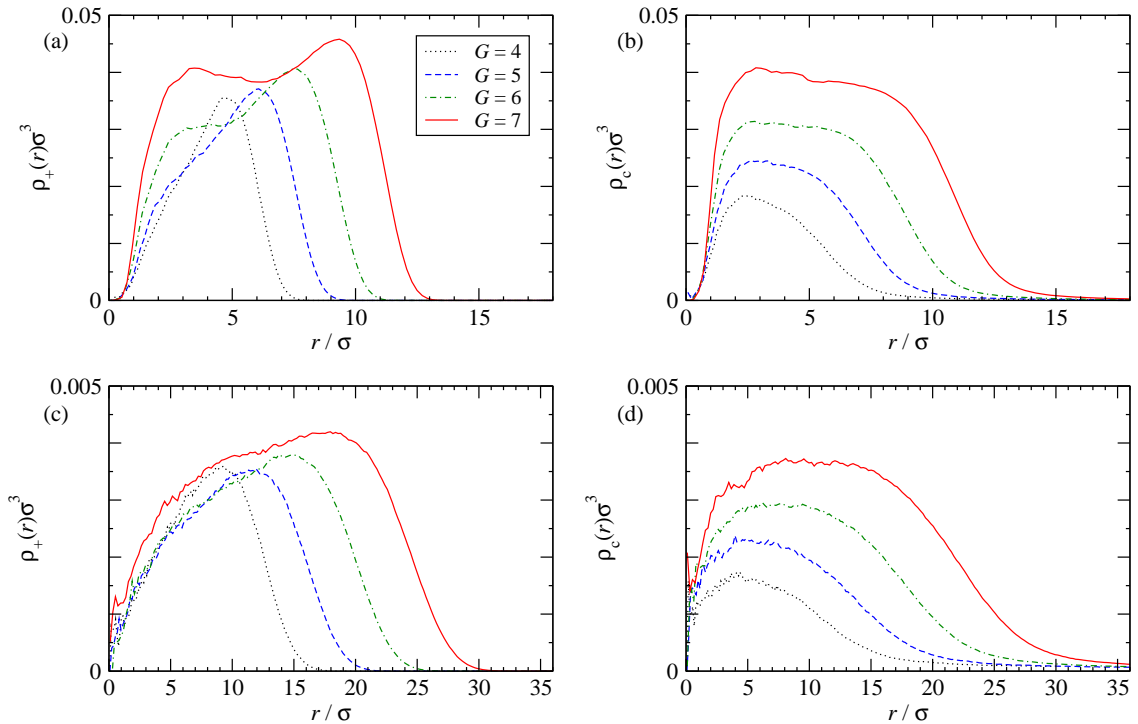


Figure 3.8: Radial charge-density profiles of dendrimers with only their end-groups charged for (a) $P = 2$ and (c) $P = 6$, and their corresponding counter ion-distributions, (b) and (d), respectively.

candidates to serve as carrier vehicles for smaller entities that can be encapsulated in their interior.

Though it is tempting to attribute the different peaks in the the density profiles of the nodes to particles of a given generation shell, this is not entirely correct. In Fig. 3.7 the density profiles of the charged monomers and the counter-ions with respect to the center of mass of the dendrimer are shown for fully charged dendrimers with $P = 2$ and $P = 6$ spacer segments and different generations. As already mentioned before, the structure in the profiles is more pronounced for the shorter spacer lengths. What can also be observed is the shifting of the peaks to larger distances from the center of mass for increasing generation G , which can be attributed to the increase in effective bond lengths between the nodes.

Further, the plots in Fig. 3.7 demonstrate that the charge density in the outer

regions increases with the generation. The limitations in the bond-distance between connected monomers and effective bonds between nodes, require that the additional monomers of higher generation need to be distributed over a volume that does not grow fast enough to allow for a constant density, hence its increase. This problem is even enhanced by the presence of counter-ions that diffuse into the dendrimer. For the shorter spacer lengths, this packing constraint can be noticed already for lower generation dendrimers, and leads to a situation where monomers of the outer generation shells are not necessarily further away from the center of mass than those of lower generation. This can be seen in the insets of Fig. 3.7(a), where the contribution to the profiles of only the end-groups is shown. For the increasing generation the range over which they are distributed becomes wider and even bimodal for generation $G = 7$. This indicates that there is a substantial amount of back-folding of the end-groups, which therefore also contribute to the first peaks in the density profiles. Since the counter-ions that get adsorbed by the dendrimer are free to move, they can distribute more homogeneously over the extent of the dendrimer.

For the larger spacer length $P = 6$, the same arguments apply. Here, however, the flexibility available to the spacers, can be exploited to stretch the node-node distance up to larger generations and the effect of back-folding, although present, is not as strong yet. This also results in a situation where the local charge density for higher generation dendrimers in the central region is lower than at the rim, which is copied by the counter-ions as can be seen in Figs. 3.7(c) and 3.7(d).

Thus far, we have not discussed the effects of generation and spacer length on dendrimers with *only* their terminal nodes being charged. The simulation results for the density profiles of the charged endgroups, for dendrimers with short spacers ($P = 2$) and the counter ion distributions are found in Figs. 3.8(a) and 3.8(b), respectively. The corresponding curves belonging to the dendrimers with long spacer chains ($P = 6$) are shown in Figs. 3.8(c) and 3.8(d). The distributions of end-monomers, which are the only ones that carry charge, behave in a very similar fashion as compared to the end-monomer distributions of the dendrimers with all their nodes charged [cf. insets of Figs. 3.7(a) and 3.7(c)]. With growing number of generations, the monomers of the highest generation are distributed in the outer region. However, a dense shell configuration is the more unfavorable the higher

the charge density. The electrostatic repulsion between the monomers therefore results into a stronger degree of backfolding. This can be seen for the dendrimer of generation $G = 7$, where the relative height of the two different density peaks is decreased when only end-monomers carry charges [cf. Fig. 3.7(a), inset]. For long spacer chains [cf. Fig. 3.8(c)], the difference in the distribution between dendrimers with all nodes charged and end-monomers charged is less due to the larger available space as compared to the case of short spacer chains.

Regarding the counter ion distributions [Figs. 3.8(b) and 3.8(d)], these do not only increase their range with growing number of generations, they also show a broad and flat distribution, especially for the short spacer dendrimers. In the latter case, for the $G = 7$ dendrimer, the substructure present in the dendrimer with all nodes charged [Fig. 3.7(b)] is almost completely lost. Therefore it is not necessary for them to preferentially assemble at the periphery of the dendrimer building a local maximum there, because it is easier for them to enter the core region. More generally, it is remarkable that end-charged dendrimers with large spacer lengths bring about density profiles that are almost uniform throughout the extent of the molecule, both as far as the charged monomers and as far as the corresponding counter-ions are concerned. Therefore, these molecules are physical realizations of an oft-used model in charged colloidal science, in which model colloids are considered as uniformly charged spheres.⁷³

3.4 Conclusions

We studied dendrimers of varying generation, spacer length and pH values of the solution. A comparison of the dendrimers without spacer but with soft interacting nodes to the dendrimers with long spacers resulted in very good agreement. For dendrimers with rigid bonds but with spacer monomers between the nodes ranging from 0 to 5, a change from terminally charged nodes to fully charged nodes changes neither the size nor the internal structure of the dendrimer considerably. The radii of gyration for a given pH value of the solution were found to collapse for all generations and spacer lengths upon application of the scaling law for neutral dendrimers proposed by Chen *et al.*⁵⁶ As compared to the neutral case, the dendrimers make a

transition towards a more open and stretched configuration. We have investigated this effect for different number of generation and number of spacer monomers. For dendrimers with long spacer chains, the increase of the number of generations has the effect to stretch the central bonds up to their maximum extent at a certain generation, thereby reducing the energy of the system. For further increase of generation, the terminal groups begin to enhance backfolding and spread out the more over the whole dendrimer to prevent a too high charge density in the outer region. We therefore expect that for dendrimers with even higher generations than studied here, a more dense structure would be obtained, thereby leading to smaller holes again, unless the spacer length is further increased.

In the case of charged dendrimers, backfolding is a common process but it is both diminished and overshadowed by other effects for long spacer chains, with the result that the dendrimer assumes a configuration that looks rather like dense-shell than like dense core. This is in agreement with the finding of a maximum transfection efficiency of dendrimers of generation 6 found in gene delivery experiments with PAMAM dendrimers.⁷⁴ It would now be interesting to quantify the size of the arising voids and to figure out the effect of added colloids which could be seen as a model for, e.g., drug molecules. Another application is gene delivery, where many dendrimers complexate with a larger DNA-molecule. The void structure is relevant also for this case, since the empty spaces are prime candidates for a gene to locally dock inside the dendrimer.

All results presented here were for the case of salt-free solutions. Effects of salinity for low-generation dendrimers and $P = 1$ have been recently presented elsewhere,^{43,71} finding that the effects of added salt to such relatively compact molecules are minor. This has to be opposed to the case of star polymers, for which an increase of salinity leads to a collapse of the star.²⁴ Finally, a subject of current investigation pertains to the effective interaction between charged dendrimers. Here, the effect of charges will be to increase the strength of the force, whereas the increase of spacer chain length will soften the interaction potential. The general shape of the latter is well-approximated by a Gaussian,⁷⁵ in similarity to the case of neutral dendrimers.^{18,19}

Chapter 4

Explicit vs. implicit water simulations of charged dendrimers

We have performed MD simulations of fully charged dendrimers and hydrophobic dendrimers with charged end-groups without and with spacer. The solvent is considered both implicitly and explicitly by employing the SPC/E model in the latter case. The electrostatic interaction dominates over solvent induced attractions. For the fully charged dendrimer excellent agreement of the conformation is found between implicitly and explicitly simulated water molecules. In contrast, the charge terminated dendrimers with hydrophobic interior show a reduction of the swelling with regard to the implicitly simulated dendrimers.

4.1 Introduction

Dendrimers^{12,13} are very versatile macromolecules with a large number of technical and pharmaceutical applications. Dendrimers are of great technological importance due to their role in gene-delivery experiments,⁷⁶ cancer treatment,⁷⁷ or their use as contrast agents in biomedical imaging,⁷⁸ to name only a few. Moreover dendrimers are interesting for fundamental research.^{20,34,35,47,79} Their compactness and flexibility can be tuned by changing generation number or spacer length which makes them an ideal model system, capable of bridging the gap between flexible polymers and hard spheres.¹⁵

Advances in synthesis techniques have lead to a large number of dendritic architectures with many different key structural features making a systematic nomenclature inevitable.¹⁴ Nowadays, the most commonly studied dendrimers are of the poly(amidoamine) (PAMAM) or poly(propyleneimine) (PPI) kind. Dendrimers with acidic functional groups, synthesized by Newkome *et. al.* were the first, where large size changes with pH variance have been discovered for three generational (G3) dendrimers.¹⁴ The change of the solution's pH value induces dissociation of ions into the solution thereby charging the molecule, which in turn leads to electrostatic swelling. In a more systematic study, Young *et. al.*, compared dendrimers with acidic, neutral or basic terminal functionality.²⁵ By means of diffusion ordered spectroscopy experiments they reported a maximum swelling of the hydrodynamic radius of 35% for the carboxylic acid- and amine-terminated dendrimers. However, alcohol-terminated dendrimers displayed no swelling or shrinking under pH change at all. Their results are consistent with the supposition, that size variation arises from coulombic repulsions between the charged monomers. Furthermore, they concluded that the findings of size variation as a function of pH should be general, provided the interior branches of the dendrimers are relatively flexible.²⁵ The afore mentioned discoveries formed the basis for experimental and simulation studies regarding the conformation of charged dendrimers and their possible use as encapsulation agents. It is known for polyelectrolyte chains and stars that a charging leads to dramatic changes in size and conformations.^{3,15,24} On the other hand some controversy arose regarding the electrostatic swelling of high-generation dendrimers. Nisato *et. al.* found in

small angle neutron scattering (SANS) experiments that the size of a G8 PAMAM dendrimer is independent of charge density and ionic strength.²⁶ On the contrary, Chen *et. al.* found in their experiments on G6 dendrimers clear evidence for conformational changes and attributed the size invariance found by Nisato *et. al.* to the dense packing of the G8 dendrimer.⁸⁰ Moreover, a pioneering simulation studies of dendrimers under varying ionic strength predicted a conformational change from dense-core to dense-shell.²⁷ These contradictory observations lead to many conjectures and debates whether a charge induced dendrimer swelling is completely absent or only diminished due to the very high steric crowding.^{15,26,40,41,43,44,69,80,81} A recent combined SANS and X-ray scattering experiments study performed by Liu *et. al.* shed light on the microscopic picture on charged polyelectrolyte dendrimers.³⁸ They provided conclusive evidence of high-generation PAMAM dendrimers to undergo electrostatic swelling and conformational changes towards a denser-shell conformation upon protonation. Almost simultaneously, a MD-simulation study of stiff and flexible dendritic polyelectrolytes not only confirmed their observation, but also showed that the flexibility of the dendrimer is of crucial importance.⁸² In line with this observation is the common use in gene delivery experiments to make high generational PAMAM dendrimers more flexible by hydrolytic removal of some of their branches, which is necessary to maximize transfection efficiency.⁷⁶

The size of the dendrimers, being of the order of a few nm, is much smaller as compared to that of typical colloids. Their building blocks, the monomeric units, consisting of e.g. hydrocarbons, are of the same order of magnitude than water, which makes a theoretical treatment very time-consuming since a large number of water molecules is involved. However, the granular nature of the solvent might possibly not be neglected since the formation of hydrogen bonds, the electrostatic repulsions and attractions vs. hydrophobic attractions between non-polar molecules can lead to non-trivial effects. For example, Dzubiella *et. al.* pointed out that taking into account the water molecules explicitly can lead to like-charge attractions between otherwise hydrophobic solute molecules.⁸³ A direct comparison of explicit vs implicit water simulation of dendrimers at different pH conditions is missing up to now. In this work we want to address the question which effect explicitly simulated water molecules have on the conformational properties of a G4 dendrimer. We

employ MD-simulations with the SPC/E model for water at ambient conditions and compare the results with the simulations of dendrimers, where the water is treated in an implicit fashion by adjusting the Bjerrum length. The Simulation Model is described in Sec. 4.2. We present our results in Sec. 4.3 for dendrimers with and without spacer monomers between their branching nodes as a means of tuning their flexibility. A direct comparison shows that for charged dendrimers essentially the same behavior can be seen for implicit and explicit water. We summarize and draw our conclusions in Sec. 4.4.

4.2 Simulation Model

We examine the conformations of 4-th generation G4-dendrimer and number of spacer segments P in solvents of varying pH by means of monomer-resolved MD simulations.^{7,8} A bead-spring model is used for the dendrimers and the monomers are modeled as beads in a united-atom approximation. The dendrimer model used in this work consists of two central beads that form the core, the so called generation 0. By repeatedly linking two beads at each site a new generation is formed. A dendrimer constructed this way has thus 2^{g+1} monomers or nodes per generation g and no spacer monomers between the nodes, i.e. $P = 1$ spacer segments. When one spacer monomer is inserted between each of the nodes of the dendrimer, the number of spacer segments is $P = 2$. A G4-dendrimer has therefore 32 terminal monomers and a total of 62 nodes. If a dendrimer with $P = 2$ spacer segments is considered, the total number of monomers adds up to 123.

A dendrimer can be synthesized in such a fashion that the nodes become ionized at low pH values of the solution and neutral at high pH.¹⁵ Furthermore, when monomeric units like primary and secondary amines are used, a dendrimer can be obtained which has only its terminal beads charged at intermediate pH values.⁸⁴ Therefore, a change of the pH value of the solution is modeled by charging the dendrimers in two different ways. We restrict our work to end-group charged dendrimers, $Z = 32$, and fully charged dendrimers, $Z = 62$.

By assuming athermal solvent conditions for the monomers of the dendrimer, we employ a model of inter monomer interactions in which each pair of beads at a

relative distance r interacts via the purely repulsive, truncated and shifted Lennard-Jones⁴⁵ potential:

$$V_{\text{LJ}}(r) = \begin{cases} 4\epsilon \left[\left(\frac{\sigma}{r}\right)^{12} - \left(\frac{\sigma}{r}\right)^6 + \frac{1}{4} \right] & r \leq 2^{1/6}\sigma \\ 0 & r > 2^{1/6}\sigma, \end{cases} \quad (4.1)$$

where the interaction strength ϵ fixes the unit of energy and the diameter σ the unit of length. A value of $\sigma = 4 \text{ \AA}$ has been chosen for the monomer diameter and $\epsilon = 0.8 \text{ kJ mol}^{-1}$ for the interaction parameter which are reasonable values for hydrocarbons in a united-atom approximation for the monomers.^{17,85}

The connectivity in the dendrimer, which is typically a covalent chemical bond, can be described by the so-called finite extensible nonlinear elastic (FENE) potential:⁷²

$$V_{\text{FENE}}(r) = \begin{cases} -U_0 \left(\frac{R_0}{\sigma}\right)^2 \ln \left[1 - \left(\frac{r}{R_0}\right)^2 \right] & r \leq R_0 \\ \infty & r > R_0. \end{cases} \quad (4.2)$$

Here, U_0 is a measure for the spring constant and R_0 is the maximal bond-length between two monomers. The bonds are modeled by $U_0 = 15\epsilon$ and $R_0 = 1.5\sigma$.

The simulations were performed using the Ewald summation method for the long-range Coulomb interactions between charged particles, given by

$$V_{\text{Coulomb}}(r) = \frac{e^2}{\epsilon_r} \frac{Z_i Z_j}{r} \quad (4.3)$$

with Z_i and Z_j the charge numbers, e the elementary charge, and ϵ_r the relative permittivity of the solvent. The monomers are chosen to be either neutral or with monovalent charges. Overall charge neutrality is guaranteed by adding oppositely charged counterions to the solution, which otherwise behave as neutral monomers.

Water at room temperature is chosen for the solvent and is simulated in an implicit and explicit fashion by imposing $\epsilon_r = 80$ and $\epsilon_r = 1$, respectively. In the latter case the extended simple point charge (SPC/E) model for water⁸⁶ has been employed with the parameter set of Ferguson.⁸⁷ For bulk water properties at room temperature and normal pressure the non-polarizable SPC/E model can be compared in accuracy to other very good rigid and more complex models.^{88,89} Simulation studies of polarizable water models have shown that polarization effects are of secondary

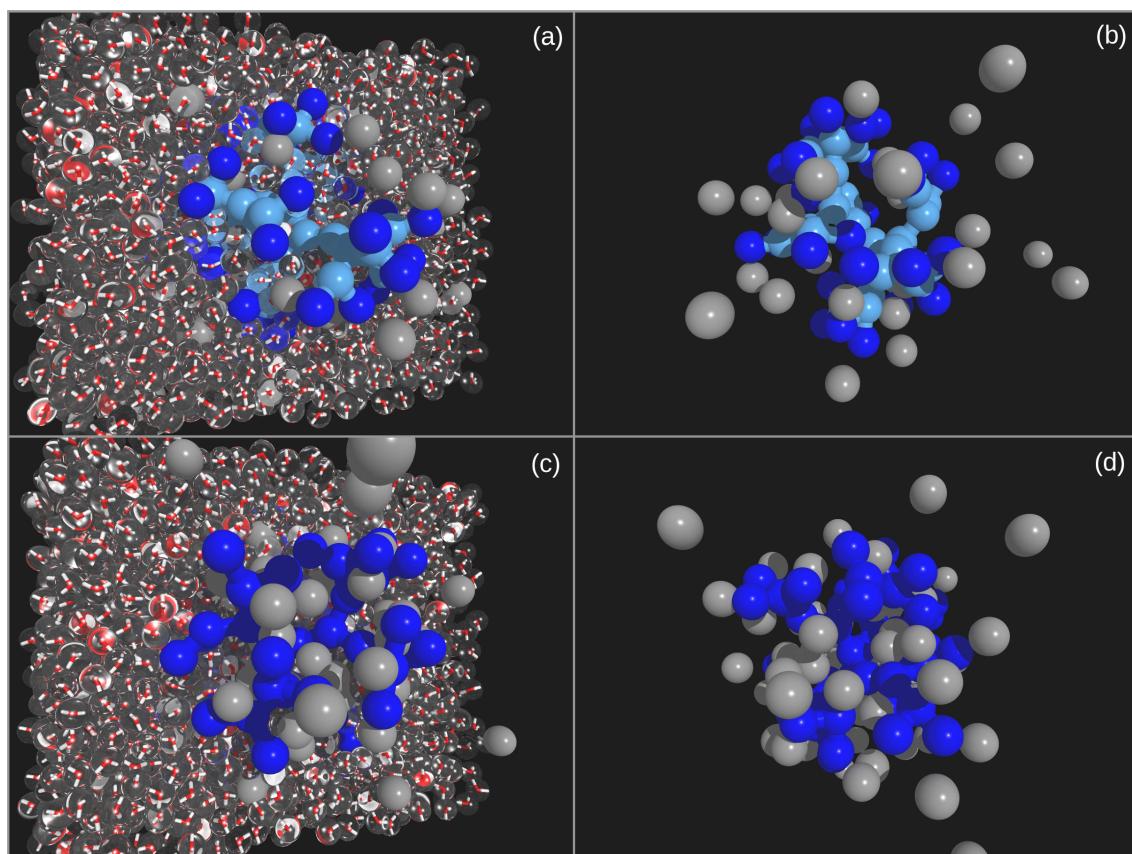


Figure 4.1: Snapshots from simulations of $P = 1$ dendrimers with $Z = 32$ [(a),(b)], and $Z = 62$ [(c),(d)] in explicitly and implicitly simulated water, respectively. Charged monomers of the dendrimer are shown in dark blue, neutral monomers in light blue and counterions in gray color. The water molecules are shown as transparent spheres, where the oxygen position is indicated by red and that of the hydrogens by white colors.

importance at hydrophobic and other surfaces.⁹⁰⁻⁹² For the mutual interaction between oxygen atoms and monomers a Lennard-Jones potential has been employed, for which the parameters were estimated by means of the Lorentz-Berthelot mixing rules. A temperature of $T = 293\text{K}$ has been maintained by applying the Berendsen thermostat⁸⁶ to the solvent only, in order to avoid artifacts like the hot-solvent/cold-solute problem.⁹³ For implicit solvent the Andersen thermostat⁹⁴ has been used. The simulation box is cubical with sides of the length $L = 48\text{\AA}$. The MD equations of motions were integrated with a timestep of $\delta t = 1.25$ fs. Initial configuration have been equilibrated for about 400 ps, which is sufficiently long for the counterions to diffuse into the core of the dendrimer and to reach a steady state for the inward and outward flux. The simulations were run for 1.25 ns to obtain good statistics for the measurements.

4.3 Results

Hydrocarbons in aqueous solution are subject to the hydrophobic effect, which is manifested in the segregation of polar water molecules from non-polar ones. Hydrophobicity plays an important role in many technical and biological processes, e.g., protein folding, which are yet not fully understood. The hydrogen-bond structure of water is modified with respect to the bulk around hydrophobic solutes.⁹⁵ A water molecule in the bulk can at most build four bonds with its neighbors, two at the oxygen and one at each hydrogen site. The water molecules tend to increase the number of hydrogen bonds, which can be done in this case by minimizing the interface with the molecule.⁹⁶ Due to poor water solubility, many effective drugs can either not be used or have harmful side effects, which can in principle be circumvented by encapsulation of these drugs in bio compatible dendrimers.⁹⁷ It should be noted, that when nano-particles are envisioned to be taken up by biological cells, a detailed understanding of the cytotoxic mechanism is of high importance and a topic of current investigations.⁹⁸ A dendrimer entirely composed of hydrophobic molecules would therefore be insoluble in a polar solvent like water. An example of a host-guest system is realized by so called core-shell dendrimers, that consist of a hydrophobic core and a hydrophilic shell.⁹⁹ The hydrophobic core of the dendrimers

facilitates the solubilization of a hydrophobic drug at high pH values of the aqueous solution. However, charging of the dendrimer by lowering the pH leads to a release of the drug. The experiments on core-shell dendrimers⁹⁹ have shown, that a certain fraction of soluble constituents to the dendrimer is necessary in order to be soluble as a whole. The solubility of a dendrimer-capsule complex in water can be enhanced by building polar groups like carboxylates into the molecule. Water molecules are then found within the structure, because partial charges on the carboxylates allow for hydrogen bonds. Charging of an otherwise hydrophobic solute can bring about a strong reduction of the hydrophobic attraction.⁸³ Due to the small size of dendrimers we consider the granular nature of the water by simulating it explicitly.

Simulation snapshots of $P = 1$ dendrimers with charged end-groups, $Z = 32$, and with all nodes charged, $Z = 62$, are shown in Fig. 4.1(a)-(d) for explicitly and implicitly simulated water. The end-group charged dendrimer in implicitly simulated water, Fig. 4.1(b) has an open conformation, which is mainly due to the Coulomb repulsion between the charged monomers. At the same time, counterions are attracted into the dendrimer's core screening the electrostatic repulsion to some extent. Although the same fraction of particles in the dendrimer is non-polar, the dendrimer is soluble in aqueous solution as can be seen from Fig. 4.1(a), where the water molecules are considered explicitly. This can be understood as follows. Water molecules near non-polar and non-adsorbing interfaces are predominantly aligned parallel to the surface, thereby maximizing the number of hydrogen bonds, since breaking them costs energy.⁹⁶ When the dendrimer's terminal moieties carry charges, they allow for more hydrogen bonds, than water molecules in the bulk. Thereby the water density at their periphery is increased with regard to hydrophobic solutes.⁸³ This effect leads to an enlarged separation between the charged monomers in addition to the electrostatic repulsion, because more water molecules are involved in hydrogen bonding this way. Similar considerations hold for the fully charged dendrimer, shown in Fig. 4.1(c), (d) for explicitly and implicitly simulated water, respectively. Here, no hydrophobic interaction is involved, since all monomers are charged. With regard to the conformations, no difference can be seen from the snapshots. Information about the size changes can be obtained by considering the radius of gyration, R_g , of the dendrimers, which can be measured by SANS-, X-Ray-

or static-light scattering experiments directly:

$$R_g^2 = \left\langle \frac{1}{N} \sum_{i=1}^N (\mathbf{r}_i - \mathbf{r}_c)^2 \right\rangle, \quad (4.4)$$

where N is the number of monomers and \mathbf{r}_c the position vector of the center of mass of the dendrimer. Simulation results are shown in Tab. 4.1. The size of the $P = 1$ dendrimers increases for explicitly simulated water for both, the end-group charged and fully charged, dendrimers. When spacer monomers are added between the dendrimer, the number of neutral monomers is larger in case of the end-group charged dendrimer, which can explain its smaller size with regard to the dendrimer that is simulated in implicit water. The relative size increase of the dendrimers upon pH change, e.g. from intermediate to low pH values, is in good quantitative agreement with experiments.^{14,25,38,40} It is remarkable, even though our model is not atomistic it generates correctly the essential features necessary to understand the conformational properties of dendrimers.

Z	explicit water		implicit water	
	$P = 1$	$P = 2$	$P = 1$	$P = 2$
32	2.80	3.87	2.72	4.14
62	3.23	4.57	2.95	4.44

Table 4.1: Radius of gyration, R_g , measured in units of the monomer diameter σ for dendrimers with $P = 1$ and $P = 2$ spacer segments in explicitly and implicitly simulated water.

In order to gain a better understanding of the intramolecular structure the density profiles of the node monomers and of the counterions have been measured with respect to the center of mass \mathbf{r}_c ,

$$\rho(r) = \left\langle \sum_{i=1}^N \delta(\mathbf{r} - \mathbf{r}_i + \mathbf{r}_c) \right\rangle \quad (4.5)$$

where \mathbf{r}_i denotes the position of the i -th particle from the total number of particles N , which can be either nodes, or counterions.

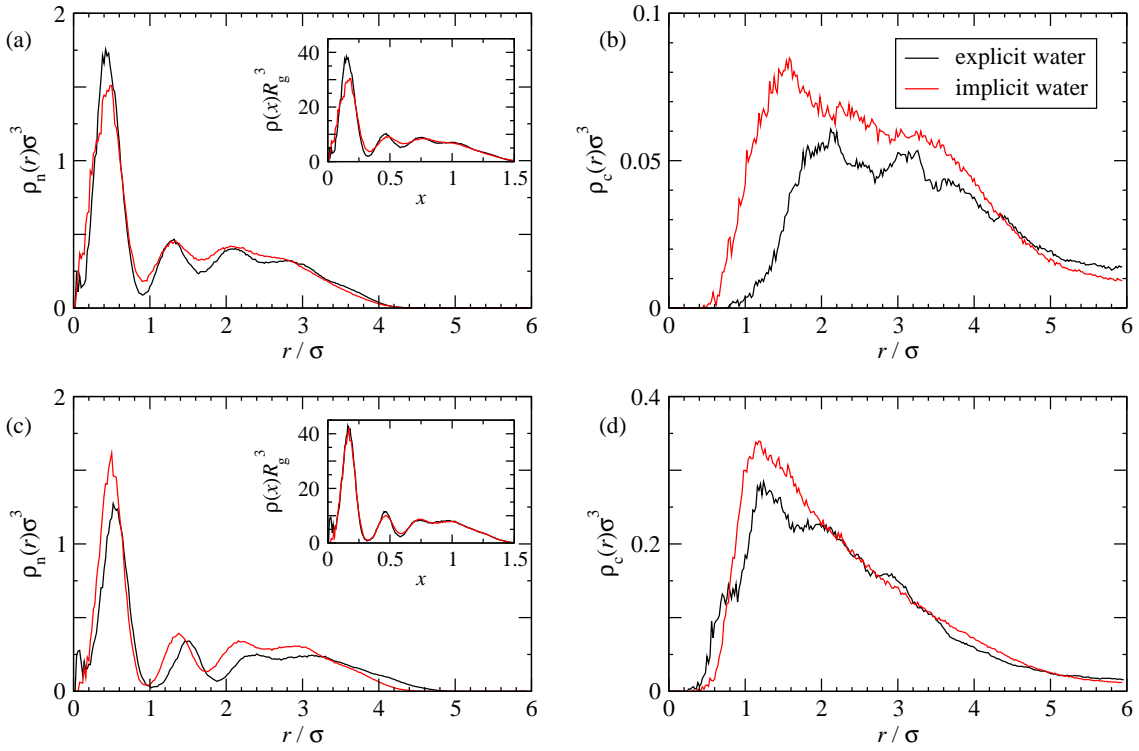


Figure 4.2: Radial density distribution of node monomers, $\rho_n(r)$, [(a),(c)] and counterions, $\rho_c(r)$, [(b),(d)] as a function of the distance, r , from the center of mass for the $P = 1$ dendrimer. The dendrimer's and counterion's total charge is $Z = 32$ [(a),(b)] and $Z = 62$ [(c),(d)]. The insets show the distribution of node monomers but with the radius of gyration, R_G , as the reference length scale.

The density profiles of the node monomers, $\rho_n(r)$, and of the counterions, $\rho_c(r)$, are shown in Fig. 4.2(a)-(d) for the $P = 1$ dendrimer. When the terminal groups are charged, see Fig. 4.2(a), the density distributions of the dendrimers with explicitly and implicitly simulated water almost coincide. However, the shell structure of the dendrimer emerges more, when the water molecules are included in the simulation. When the water molecules are within the dendrimer, they also restrict the movement of the monomers and therefore decrease the entropy of the dendrimer. In Fig. 4.2(c) the density distribution of the fully charged dendrimers are shown. Also here is the shell structure more pronounced but additionally the peaks are shifted farther outwards with respect to the implicit water case. This can only be explained by an increased amount of water, absorbed into the dendrimer. Thus both, charging the dendrimer and the absorbed water have a stabilizing effect on the dendrimer structure. The counterion distributions are shown in Fig. 4.2(b), (c) for the end-group and fully charged dendrimers, respectively. Firstly, the density profiles of the counterions are more structured when the water molecules are simulated explicitly, since these also occupy some of the space inside the dendrimer. The peripheral groups of the $Z = 32$ dendrimer are more back folded leading to a less structured density profile in the implicit case. Whereas the effect of water is to increase the separation between the charged monomers. Therefore the counterions are also distributed closer to the periphery. The counterions around the $Z = 62$ dendrimer are attracted more deeply into the interior, because all monomers are charged and the dendrimers are more stretched in both cases. Especially the bonds between the innermost generations are stretched the most in order to minimize the electrostatic energy leading to a maximum of the counterion distribution there. A coarse-grained view the picture can be obtained by choosing the radius of gyration, R_g as the reference length scale. Thus, the density distributions are plotted as a function of $x = r/R_g$ in the insets. The density profile of the fully charged dendrimers collapse onto the same curve. It is surprising that explicitly simulated water brings about essentially the same conformation as implicitly simulated water. This shows that the implicit model is sufficient to reproduce the salient characteristics of charged dendrimers.

The measured density distribution of node monomers and counterions of the

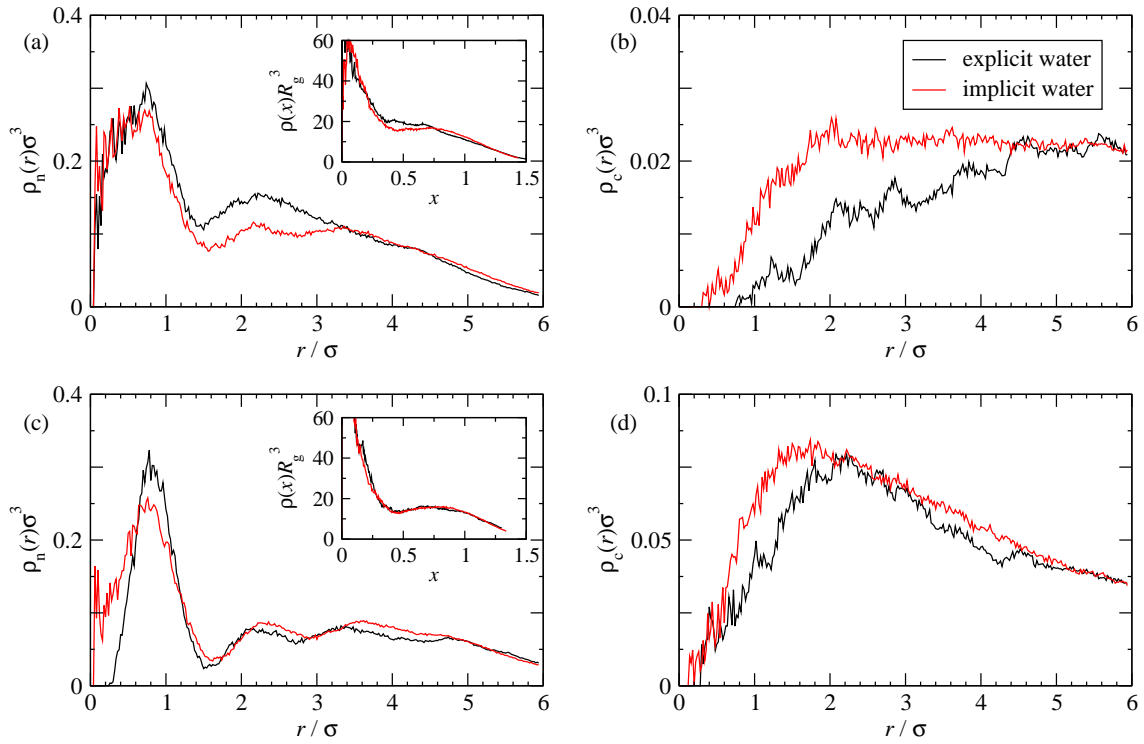


Figure 4.3: Radial density distribution of node monomers, $\rho_n(r)$, [(a),(c)] and counterions, $\rho_c(r)$, [(b),(d)] as a function of the distance, r , from the center of mass for the $P = 2$ dendrimer. The dendrimer's and counterion's total charge is $Z = 32$ [(a),(b)] and $Z = 62$ [(c),(d)]. The insets show the distribution of node monomers but with the radius of gyration, R_G , as the reference length scale.

$P = 2$ dendrimer are shown in Fig. 4.3(a)-(d). The dendrimer with charged end-groups in Fig. 4.3(a) is more compact in explicit water, which is due to the hydrophobically induced attraction between the neutral monomers of the lower generations. The charged monomers repel each other which is further enhanced by the water. However, here the hydrophobicity of the monomers masks this effect to a large extent. This can also be seen from the distribution of counterions in Fig. 4.3(b), which are much more expelled from the dendrimer's interior for explicit water. The nodes of the fully charged dendrimer, Fig. 4.3(c), show good agreement between explicit and implicit water both with respect of the position of the peaks and their height. But the structure stabilizing effect of the water, absorbed into the dendrimer is clearly visible here, as indicated by the absence of oscillations in the density profile at small separations. The counterions, Fig. 4.3(d), show a similar behavior than for the dendrimer without spacer, and their maximum lies in the center, because the bonds are stretched the most there and give way to the counterions. The density of the dendrimers and counterions is smaller in this case, which shows that the counterions have more free volume at their disposal. This explains why the distributions are less structured as compared to the dendrimer without spacer. The combined density profiles of node monomers and spacer are shown in the insets with the radius of gyration as the reference length scale. The effect of the non-polar spacer monomers is small when the fully charged dendrimer is considered. The same trend as for the $P = 1$ dendrimer can be seen here, which is a much better agreement between explicitly and implicitly simulated water, when the dendrimer is fully charged.

A quantity measurable in experiments is the water intake by the dendrimers.⁴² The water distributions, $\rho_w(r)$, of the $P = 1$ and $P = 2$ dendrimers are shown in Fig. 4.4(a) and (b), respectively. In both cases much more water is absorbed the higher the charge of the dendrimers. The shell structure of the dendrimer without spacer is imposed on the water distribution in Fig. 4.4(a), when fully charged. Water can predominantly be found between the shells, where the dendrimer's density is lower. This shows that the amount of free space is very limited and the degrees of freedom of the dendrimers are reduced by the water, leading to the more stretched conformation with respect to the implicit simulation. Moreover, the fact that water density is higher in the fully charged case confirms that the presence

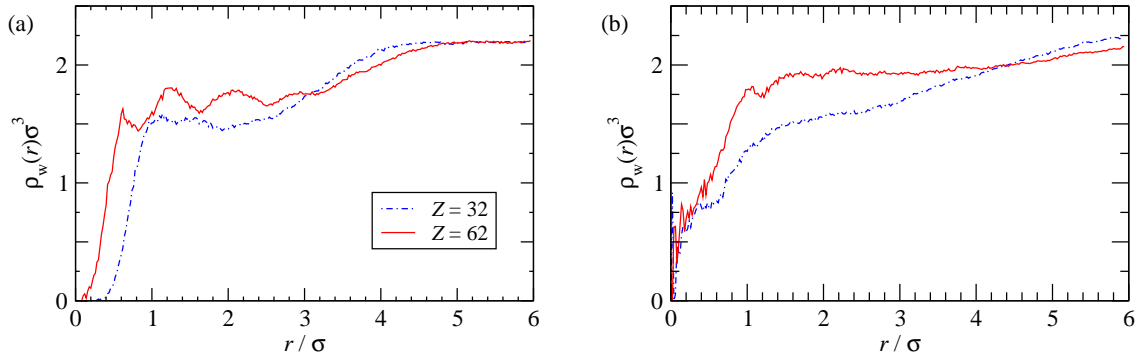


Figure 4.4: Radial distribution of water molecules, $\rho_w(r)$, as a function of the distance, r , from the center of mass for dendrimers with (a) $P = 1$ and (b) $P = 2$ spacer segments.

of charged monomers tends to minimize the energy associated with the hydrogen bonds between monomers and water molecules with respect to bulk water-water bonds. The hydrogen bonds between charged monomers and water are energetically favorable with regard to water-water hydrogen bonds, because the monomer's charge is larger than the partial charges on the water molecules. The water within the $P = 2$ dendrimer, Fig. 4.4(b) is distributed within the whole dendrimer and is not excluded from the region around the center of mass as for the $P = 1$ dendrimer. Due to the spacer monomers, the dendrimer becomes more flexible thus allowing the center of mass to lie maybe close but not exactly between the monomers of the innermost generation. Also here the dendrimer's structure is imposed on the water distribution, yet to a much lesser extent than for the dendrimer without spacer. It should be noted that the peak positions of the water coincide with the peaks of the charged nodes, which reflects the fact, that the water density is higher close to charged surfaces with respect to the bulk.⁸³

In order to quantify the amount of absorbed water the number of water molecules within a sphere of radius R_g around the center of mass have been measured, see Tab. 4.2. There it can be seen that the amount of absorbed water is almost doubled upon going from a end-group to a fully charged dendrimer. This observation is the almost the same independent of the spacer length considered in this work and thus

Z	$P = 1$	$P = 2$
32	137	412
62	242	779

Table 4.2: Water intake obtained by integrating the radial water distribution up to R_g .

of the flexibility of the dendrimer. Again it can be said, that the water intake is strongly correlated with the total charge of the dendrimer. However due to the relatively small amount of free space within the $P = 1$ dendrimer the density of water is lower than that of the dendrimer with $P = 2$ spacer segments.

4.4 Conclusions

Electrostatic interactions between charged monomers constitute the main contribution to the conformation of the dendrimers in all studied cases. Considering the water molecules explicitly is only of secondary importance if weakly charged dendrimers without or with only few hydrophobic monomers are considered. In this case, the assumption of athermal solvents brings about a model that suits well for the description of watersoluble dendrimers. We have seen, that the water intake does only lead to a small reduction of the degrees of freedom of the dendrimer. When dendrimers with polar groups are considered, this work can be extended to a similar comparison of neutral dendrimers.

Chapter 5

Effective interactions between charged dendrimers

We perform monomer-resolved computer simulations of fourth-generation charged dendrimers at various conditions of charging (full, terminal and neutral) and for different values of the spacer length P connecting the branching nodes, from $P = 1$ to $P = 6$. We examine the sizes, overlaps and effective forces between the centers of mass of the dendrimers with and without added monovalent and divalent salt. For neutral dendrimers, we find that all effective interactions for the various spacer lengths can be scaled on a universal curve. Adding charge to the dendrimers leads to increased repulsions between the same, which can be tuned by the spacer length P , becoming softer as the latter increases. Addition of monovalent salt of various concentrations leads to no visible effects on the effective interaction, in contrast to divalent salts, which cause a dramatic reduction of the effective repulsion as the salinity increases.

5.1 Introduction

Complex fluids render a conspicuous part of our daily life and have a high relevance in a vast number of applications in the chemical, pharmaceutical and food industries¹. They are generally characterized by the mesoscopic length scale of the dissolved macromolecular aggregates, and the concomitant macroscopic softness of the system. New exciting phenomena, phases and structures are challenges for a theoretical treatment of soft matter systems, such as, e.g., the currently topical issue of predicting block-copolymer self-assembly and properties¹⁰⁰. A well-established tool in statistical soft matter physics, allowing us to examine how to tune and control material properties in a particular way by adjusting the microscopic parameters of the system, is the concept of the effective Hamiltonian. It can be employed to describe the interaction between large macromolecules in a sea of small solvent molecules, and the results obtained allow for direct contact with experiment³. Coarse-graining, or equivalently, tracing out the degrees of freedom of the smaller particles results in a simplified effective one-component system and the standard tools of liquid state theory can be applied to bridge the scales to macroscopic properties. In this way, star polymers^{11,101}, star-branched polyelectrolytes^{23,24} as well as star-linear mixtures¹⁰²⁻¹⁰⁴ have been successfully described, yielding excellent agreement between theory and experiment³.

One of the most prevalent macromolecules to be found in nature are polyelectrolytes, an important building block of complex matter. Steady progress of synthesis techniques and chemical modifications of biological macromolecules have led to an abundant supply of constituents which are now under investigation^{3,11,15,81,98,105}. Due to their biological and technical relevance, they have been the topic of intensive research¹⁰⁶⁻¹⁰⁸. Another class of charged macromolecular architectures are polyelectrolyte dendrimers, which have become very interesting for experimental and theoretical research¹⁰⁹. This is not only due to their role in applications such as solubility enhancement, drug-delivery vectors or nanocarriers⁵⁰⁻⁵³ but also from a fundamental point of view. They combine properties of colloidal and polymeric systems¹⁵, they possess an interaction potential with Gaussian shape^{17,18} when they are uncharged, and can be regarded as homogeneously charged spheres when only their

end-groups carry charges⁸². Accordingly, dendrimers^{12,13,29,54} play a prominent role in soft matter research^{34,35,39–42,47,79}. Most of the research to-date has focused on conformations, interactions and phase behavior of neutral dendrimers in dilute and concentrated solutions^{16,19–21}. On the contrary, relatively little is known about the effective interaction between polyelectrolyte dendrimers.

When dissolved in water the ionizable groups of the polyelectrolyte dissociate leaving behind a charged molecule and oppositely charged counterions in the solution, which can bring about a swelling of the dendrimer^{26,66}. Also the addition of salt, a change of the pH of the solution or the addition of spacer segments between the nodes of the dendrimer go along with conformational changes^{44,68,71}. It is therefore not surprising, that charged dendrimers are challenging, because they combine the complexities of polymer physics in the form of chain connectivity, self avoidance and long range Coulomb interactions. In this work, we address the question how the dendrimer charge, regulated by the solution's pH value, as well as the salinity influence the interaction between dendrimers of varying spacer length. By modifying the pH value of the aqueous solution, charges can be induced on the dendrimers. For this purpose, monomer-resolved Molecular Dynamics (MD) simulations using the Ewald summation technique to treat the electrostatic interactions were employed. We find a stronger repulsion the more the dendrimers are charged. The effect of increasing the salinity is to reduce the effective force down to values of neutral dendrimers, provided divalent salts are employed.

The rest of the paper is organized as follows. In Sec. 5.2 we present the simulation model. In Sec. 5.3 the effect that explicitly simulated spacer monomers have on the interactions are examined. It is shown that the effective force between neutral dendrimers with different spacer lengths can be scaled appropriately to collapse onto a single curve. The change of the pH of the solution is modeled in an implicit fashion by charging the dendrimers, and the charge distributions inside and between the dendrimers are studied. The effective interactions under these conditions are presented in Sec. 5.4. The effect of salinity of the solution, for the cases monovalent and divalent salt molecules, is treated in Sec. 5.5, and in Sec. 5.6 we summarize and draw our conclusions.

5.2 Simulation Model

In order to examine the behavior of interacting pH-responsive dendrimers we performed monomer-resolved MD-simulations^{7,8} of two dendrimers with generation G and number of spacer segments P in aqueous solution. A bead-spring model is used for the dendrimers to model the covalent bonds. The arrangement of the nodes of a dendrimer with generation G is set up as follows: a single pair of monomers forms the core of the dendrimer, generation 0. A new shell is formed iteratively by connecting two additional monomers to each site of the previous generation. Thus, the g -th shell consists of 2^{g+1} monomers. Since we consider dendrimers with generation $G = 4$ only, the total number of nodes in this case is 62. By inserting a linked chain of $P - 1$ monomers between each pair of the connected nodes, a dendrimer with $P > 1$ spacer segments is formed, containing a total number of $N(P) = 61P + 1$ monomers. In order to explore the dependence of the effective interaction on the number of spacer segments, only dendrimers of generation $G = 4$ with $P = 1$ up to $P = 6$ spacer segments are considered, i.e., the chains connecting nodes consist of 0 up to 5 monomers.

Polyelectrolyte dendrimers can be obtained by synthesizing the dendrimers in such a fashion that the monomer units are neutral at high pH values, but become ionized at low ones¹⁵. The choice of appropriate functional groups, such as secondary and tertiary amines, as monomeric units opens the way to new dendritic structures. Of particular interest is the case where only the end-groups become ionized at intermediate pH values. The effect of a change in pH value of the solution is modeled indirectly by a different distribution of the charges within the dendrimers. For this purpose, we focus on three different possibilities, the neutral dendrimer, the fully charged dendrimer, and an intermediate case for which only the end-groups are charged. Accordingly, single elementary charges are placed only on the nodes of the dendrimer and all spacer-monomers remain neutral. Consequently we consider dendrimers with an overall charge number of $Z = 0$, $Z = 32$, and $Z = 62$.

By assuming athermal solvent conditions for the monomers of the dendrimer, we employ a model of intermonomer interactions in which each pair of beads at a relative distance r interacts via the purely repulsive, truncated and shifted Lennard-

Jones⁴⁵ potential:

$$V_{\text{LJ}}(r) = \begin{cases} 4\epsilon \left[\left(\frac{\sigma}{r}\right)^{12} - \left(\frac{\sigma}{r}\right)^6 + \frac{1}{4} \right] & r \leq 2^{1/6}\sigma \\ 0 & r > 2^{1/6}\sigma, \end{cases} \quad (5.1)$$

where the interaction strength ϵ fixes the unit of energy and the diameter σ the unit of length. The connectivity in the dendrimer, which is typically a covalent chemical bond, can be described by the so-called finite extensible nonlinear elastic (FENE) potential⁷²:

$$V_{\text{FENE}}(r) = \begin{cases} -U_0 \left(\frac{R_0}{\sigma}\right)^2 \ln \left[1 - \left(\frac{r}{R_0}\right)^2 \right] & r \leq R_0 \\ \infty & r > R_0. \end{cases} \quad (5.2)$$

Here, U_0 is a measure for the spring constant and R_0 is the maximal bond-length between two monomers. The bonds are modeled by $U_0 = 15\epsilon$ and $R_0 = 1.5\sigma$. This parameter choice guarantees that the unphysical crossing of bonds does not occur⁴⁸.

The simulations were performed using the Ewald summation method for the long-range Coulomb interactions between charged particles, given by

$$V_{\text{Coulomb}}(r) = k_{\text{B}}T\lambda_{\text{B}} \frac{Z_i Z_j}{r} \quad (5.3)$$

with Z_i and Z_j the charge numbers, k_{B} the Boltzmann constant, T the temperature and λ_{B} the Bjerrum length

$$\lambda_{\text{B}} = \frac{e^2}{\epsilon_{\text{r}}k_{\text{B}}T}, \quad (5.4)$$

where ϵ_{r} is the relative permittivity. The monomers are chosen to be either neutral or monovalently charged. Counter-ions with opposite charge, which behave otherwise as normal monomers, are added to the system in order to maintain overall charge-neutrality. The effect of salt on the effective interaction between the charged dendrimers is examined by adding monovalent and divalent salt-ions at concentrations of 0.05, 0.10 and 0.50 mol/l.

Water at room temperature is chosen as solvent, and it is simulated in an implicit fashion by imposing $\epsilon_{\text{r}} = 80$ and a temperature of $k_{\text{B}}T = 1.2\epsilon$, which is maintained via an Andersen thermostat. The corresponding Bjerrum length $\lambda_{\text{B}} = 0.714$ nm is obtained by choosing $\lambda_{\text{B}} = 3\sigma$, which results in a monomer diameter $\sigma = 0.238$ nm

typical for the van-der-Waals radii of atoms that can be used in the framework of a bead-spring model for polymer molecules^{3,46}. The simulation box is chosen to be a cube with sides of length $L \cong 11R_{g,\infty}$, where $R_{g,\infty}$ denotes the radius of gyration of a single dendrimer with typical values of 2.86σ or 4.55σ for $P = 1$ or $P = 2$ dendrimers, respectively. The centers of mass, $\mathbf{R}_1, \mathbf{R}_2$, of the two dendrimers are kept fixed by external force fields. Rather than measuring the effective interaction potential, $V_{\text{eff}}(D)$, as a function of the distance $D = |\mathbf{R}_1 - \mathbf{R}_2|$ between the centers of mass, we consider in this work the effective force, which can be measured directly in MD-simulations. It is related to the effective interaction $V_{\text{eff}}(D)$ via:

$$\mathbf{F}_\alpha = -\nabla_{\mathbf{R}_\alpha} V_{\text{eff}}(D), \quad (5.5)$$

where the index $\alpha = 1, 2$ denotes the dendrimer under consideration. The total force acting on the dendrimer α is the sum of all forces on each of its monomers,

$$\mathbf{F}_\alpha = \left\langle \sum_{i=1}^N \mathbf{F}_{i\alpha} \right\rangle. \quad (5.6)$$

The distance between the centers of mass of the dendrimer was varied between $D = 0$ and $D = 5R_g$. Due to the actio-reactio principle, we omit the index α in what follows and write $F = \mathbf{F}_\alpha \cdot \hat{\mathbf{D}}_\alpha$, where $\hat{\mathbf{D}}_\alpha$ is the unit vector along the connecting line pointing to dendrimer α . Time is measured in units of $\tau = \sqrt{m\sigma^2/\epsilon}$ and time-steps of $\delta t = 0.002\tau$ have been used. Initial configurations have been allowed to relax sufficiently long, to enable the counter-ions to diffuse into the core of the dendrimer and reach a steady state for the in- and out-flux, followed by up to 10^7 time-steps to obtain good statistics for the measurements.

5.3 Effect of Spacer

The possibility to tune the interactions between molecules in complex fluids makes the study of their effective interaction a topic of particular interest. The many different types of interactions lead to a large variety of phases of the systems. Neutral dendrimers possess an interaction potential that has a Gaussian shape if they are uncharged and dissolved in athermal solvents^{17,18}. The dependence of the effective

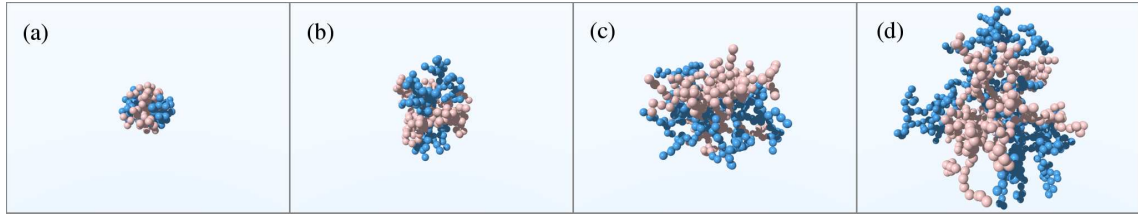


Figure 5.1: Snapshots from simulations of neutral dendrimers with (a) $P = 1$, (b) $P = 2$, (c) $P = 4$, and (d) $P = 6$ spacer segments. The distance between the centers of mass is $D = 0$ in all four cases.

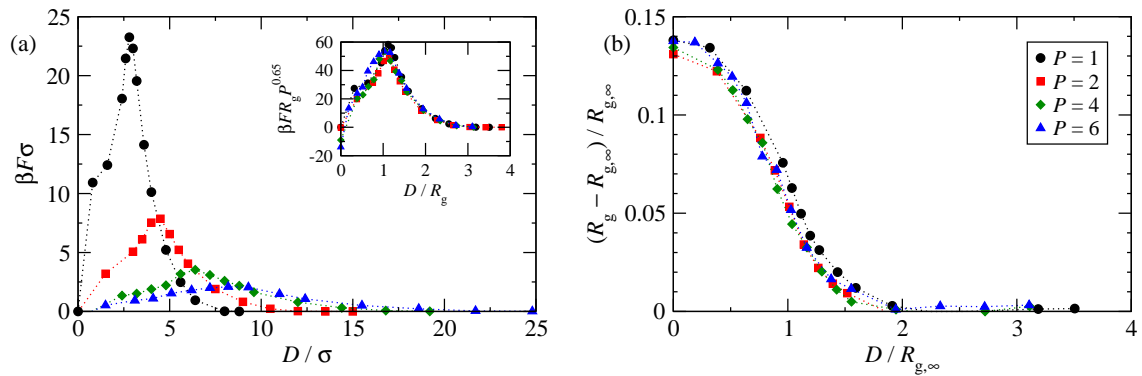


Figure 5.2: (a) Effective force, F , between two neutral dendrimers with number of spacer segments P plotted against the distance D between their centers of mass. The inset illustrates that the data collapse when scaled appropriately. (b) Relative deviation of the radius of gyration, R_g , from its value at infinite dilution, $R_{g,\infty}$, as a function of center of mass distance D between two neutral dendrimers with varying number of segments P .

interaction on generation number and spacer length between the branching points offers a way to tune range and strength of the interaction potential. In a previous simulation study by Götze *et. al.*¹⁹, the spacer length has been modified by altering the softness of the interaction between the nodes of the dendrimers. When comparing dendrimers with explicitly modeled spacer monomers to those with soft interacting nodes⁸², the scaling law for the radius of gyration of neutral dendrimers, $R_g \propto P^{3/5}$, could be confirmed for fixed generation G . Moreover, the density profiles of the nodes can be scaled to collapse onto a master-curve. To examine whether such a scaling exists for the interaction as well, a model of dendrimers with explicit monomers between their branching points is employed.

Simulation snapshots of two neutral dendrimers whose centers of mass coincide are shown in Figs. 5.1(a)-(d) for increasing number of spacer monomers. For all spacer lengths the monomers of the two different dendrimers are segregated into separate regions rather than being intermixed. The dendrimers seem to be folded around each other when they are forced to have coinciding centers of mass. A reduction of the branching density by elongating the spacer chains results in a larger flexibility of the dendrimers. The number of possible conformations increases as the monomers have more free volume at their disposal, thus the forces are correspondingly weaker. Therefore the interaction becomes softer and increases its range, which can be seen from Fig. 5.2(a) for dendrimers of varying number of spacer segments, P . Here, the effective force is shown which has been measured as a function of the distance, D , between the centers of mass of the dendrimers. The softening with increasing spacer length is obviously non-linear; for instance, the drop of the maximum of the force when going from $P = 1$ to $P = 2$ is more significant than increasing the spacer length further.

An interesting point is the collapse of the forces upon scaling, as can be seen in the inset of Fig. 5.2(a). We have used the radius of gyration, R_g , as the reference length scale and obtain $P^{-0.65}$ as the scaling factor for the interaction potential making a quantification of the softening possible. When scaled in such a fashion, the shape of the force becomes independent of the spacer length. As the two dendrimers approach each other, the crowding together of the monomers increases the effective force between the dendrimers. At a separation of the order of their radius of gyration

the force attains its maximum value, before it drops down to zero, when the centers of mass coincide. The force reduces at close approaches because the monomers of the one dendrimer reach the opposite site of the other dendrimer, i.e. they reach farther out than the center of mass of the other. Therefore, the dendrimers are somewhat pushed together due to the pressure of the monomers on the outward side. In addition, upon approaching each other, the dendrimers get stretched. In Fig. 5.2(b), we plot the relative increase of the radius of gyration, R_g , at a distance D of the centers of mass with respect to its value at infinite separation, i.e., for a single dendrimer, $R_{g,\infty}$. Again, the curves collapse and R_g increases by up to 15% at $D = 0$ independently of the spacer length. The dendrimers obtain a conformation that is more swollen than at larger separations. This can easily be understood, since the presence of the second dendrimer restricts the degrees of freedom of the first and vice versa. Moreover, the inner bonds of the dendrimers stretch in order to enlarge the space accessible to the monomers.

5.4 Effect of pH

In this section, we analyze the effect of pH value of the solvent on the effective interaction between dendrimers. By the choice of appropriate functional groups for the monomeric units, it is possible to synthesize a dendrimer that has all its node-monomers and end-groups protonated at low pH values but is neutral at high pH values of the solvent. The pH value of the aqueous solution can therefore be modeled implicitly by modifying the charge carried at certain units of the macromolecule. We accordingly employ three types of dendrimer models, which differ only in the way their nodes and/or end-groups are charged. The fully charged dendrimer thus has valency $Z = 62$ and the neutral dendrimer $Z = 0$; without loss of generality, we assume that the dendrimer carries positive charge. When primary or secondary amines are chosen as monomer units, a dendrimer can be synthesized in which only the end-groups are charged, resulting in a valency $Z = 32$.

The effect of the pH value of the solution on two interacting $G = 4$ dendrimers with $P = 4$ spacer segments and charges $Z = 0, 32, 62$ is illustrated in Figs. 5.3(a)-(f). The dendrimers swell monotonically upon charging, due to the electrostatic

repulsion between charged monomers, which in turn allows the counterions to move more freely through the hollow regions between the monomers of the dendrimer, thereby screening the electrostatic repulsions to some extent⁷¹. At the same time, the number of possible conformations of each dendrimer is reduced both by the presence of the counterions and of course by the presence of the other charged dendrimer. The dendrimers are considerably stretched and they become intertwined with one another as they approach, rather than simply interpenetrating. This can be seen from Figs. 5.3(a) and 5.3(b), where the fully charged dendrimers are shown for coinciding centers of mass ($D = 0$) and at a distance $D \cong R_g$, respectively. The interacting dendrimers at intermediate pH values, Figs. 5.3(c),(d) are considerably stretched as well, and the charged beads are able to back-fold into the dendrimers interior more easily. This is in line with our studies on the conformations of single dendrimers, where it was found charging of only the end-groups leads to a uniform charge distributions along the molecule's extent⁸². The neutral dendrimers, Figs. 5.3(e),(f), are much less swollen than their charged counterparts, but also in this case, they show the same type of folding as for the charged cases.

As can be seen from the snapshots, charged dendrimers are much more stretched than their neutral counterparts. This is expected to have consequences on the way in which two dendrimers engage with one other, in particular at center-to-center distances $D \lesssim R_g$. In order to quantify the interpenetration/intertwining of two dendrimers, we employ the following definition of the *overlap* $O(D)$ as a function of the distance D between the centers of mass of dendrimers with P spacer segments. When a monomer of a dendrimer crosses the plane perpendicular to the connection line between the dendrimer's centers of mass, it is counted as an overlapping one. The associated overlap function, $O(D)$, is defined as twice the fraction of overlapping monomers over the total number of monomers within a dendrimer. To facilitate a quantification of the overlap, we compare the results from simulations with the overlap of two homogeneous spheres of radius R_g , given by

$$O(D) = \begin{cases} \frac{1}{16}(4 + D/R_g)(2 - D/R_g)^2 & D \leq 2R_g \\ 0 & D > 2R_g. \end{cases} \quad (5.7)$$

which is the dimensionless sphere-sphere intersection volume.

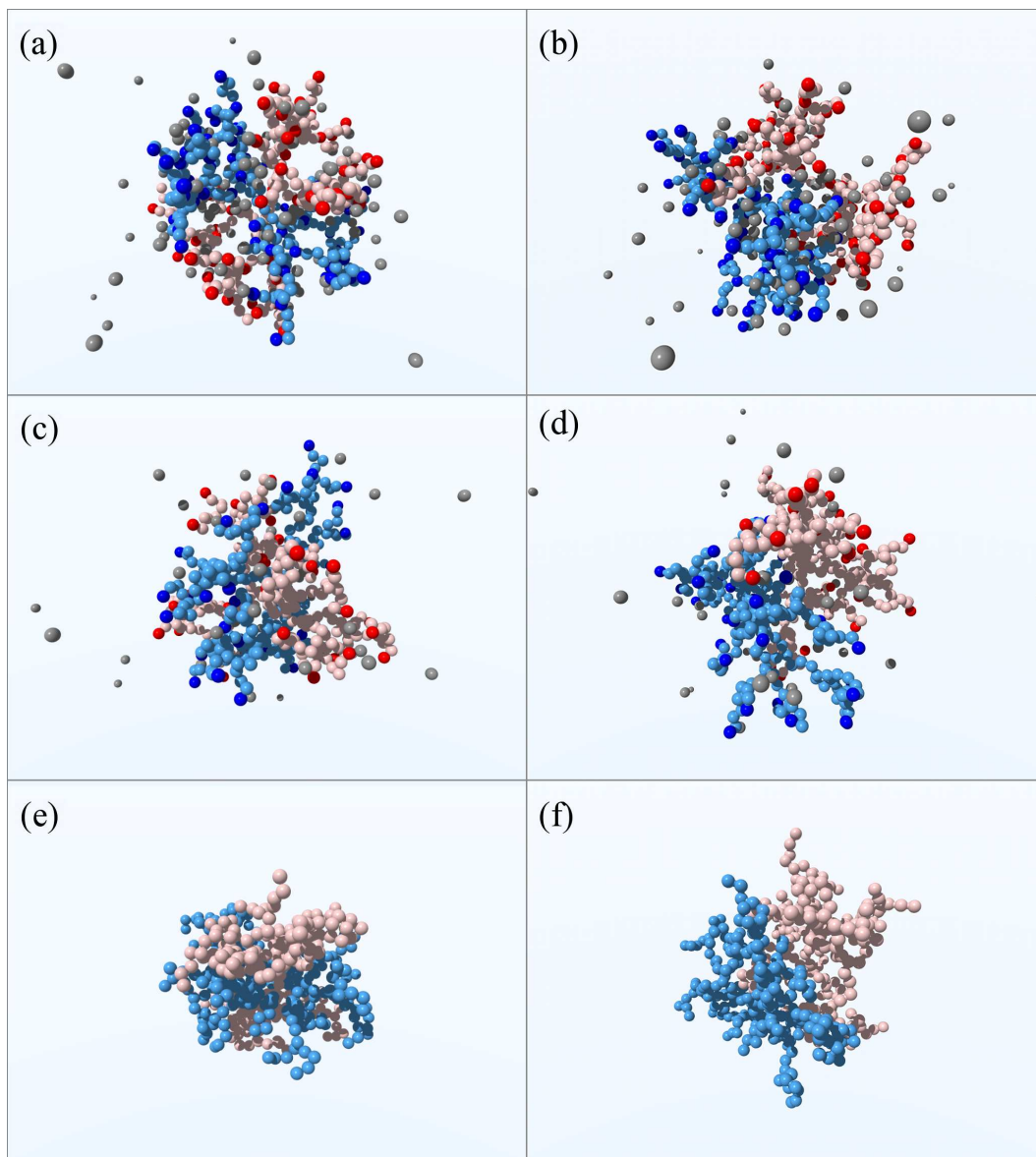


Figure 5.3: Snapshots from simulations of dendrimers with $G = 4$ and $P = 4$ at distance $D = 0\sigma$ for different pH values of the solvent: (a),(b) fully charged dendrimers, (c),(d) dendrimers with end-groups charged, and (e),(f) neutral dendrimers. The dendrimer's centers of mass either coincide, (a),(c),(e) or are separated at a distance $D \cong R_g$, (b),(d),(f). Counterions are gray, neutral monomers are shown in pale colors, and charged monomers in dark colors.

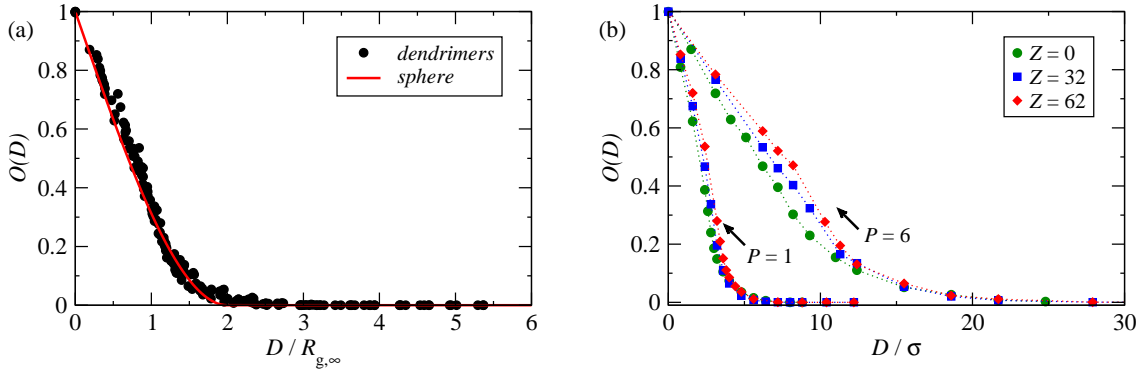


Figure 5.4: (a) Overlap as a function of the center of mass distance D in units of the radius of gyration for all dendrimer types considered in this work. The overlap of two homogeneous spheres is shown for comparison. (b) Overlap for $P = 1$ and $P = 6$ dendrimers vs. distance D in units of the monomer diameter σ for three different pH values of the solution.

The overlaps $O(D)$ for all types of dendrimer types considered in this work, i.e., $P = 1, 2, 4, 6$ and $Z = 0, 32, 64$, are shown in Fig. 5.4(a) using the radius of gyration at infinite dilution, $R_{g,\infty}$, as the reference length scale. The overlap as obtained from the intersection volume of two spheres, Eq. (5.7), is shown for comparison in the same figure. When the monomers of one dendrimer do not cross the plane lying perpendicular to the connecting-axis at half the distance between the centers of mass, the two dendrimers are fully separated. Upon reducing the distance, $O(D)$ increases to unity at full center-of-mass coincidence. The agreement between the behavior of two spheres and the simulation results is surprisingly good, which suggests the assumption to be valid that the types of dendrimers considered here can be viewed as homogeneously (charged) spheres from a coarse grained point of view. The dendrimers do not retreat when they approach each other because their monomers are still distributed homogeneously within a sphere around the center of mass. However, when other macromolecules are considered, for example high-functionality neutral and charged star polymers²⁴, where the centers of mass are not allowed to coincide, the monomers of those molecules do retreat, resulting in a value of the overlap less than one for small distances – the so-called *no interdigitation*

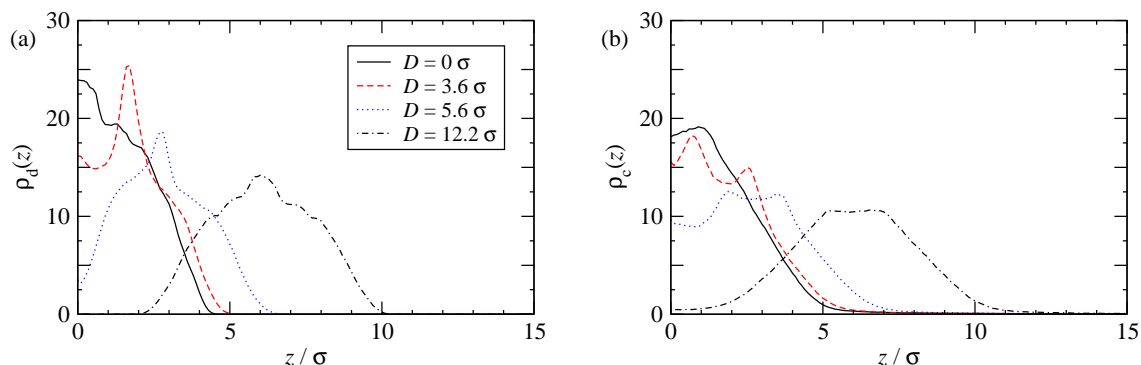


Figure 5.5: (a) Density of charged dendrimer monomers, $\rho_d(z)$, measured within a cylinder of radius 7σ along the box-diagonal (z -axis) for three different center of mass distances D for fully charged $P = 1$ dendrimers. (b) Density of charged counterions, $\rho_c(z)$, distributed around the dendrimers shown in (a).

condition.

In Fig. 5.4(b), the unscaled version of the overlap is shown for dendrimers with $P = 1$ and $P = 6$ at three different chargings, $Z = 0, 32, 62$. Clearly the effect of longer spacer chains is to increase the range over which the overlap attains its smallest value. This is not surprising, because the larger molecule has also a larger extent. However, when the nodes carry charges, the deviation of the overlap from the neutral case is larger for the dendrimer with long spacer chains: when holding the distance fixed one can see that the neutral dendrimer has less overlap than a dendrimer with higher charge Z . This is reasonable, because the charged dendrimers are more stretched and are able to reach the other side of the plane at $z = 0$ at an earlier stage due to their increased size. The opening of voids upon charging alleviates the penetration further. The dendrimers stretch when they approach each other [see Fig. 5.2(b)] but remain roughly spherical.

When the nodes of the dendrimers are protonated at low pH values of the solution, the dissociated counterions are attracted to the charge sites, thereby influencing not only the internal structure but also the interaction between the dendrimers. The charge distributions can give us more detailed information about the system, and moreover they might serve as input parameters for a theoretical derivation of the

effective force⁷³. We have measured the counterion density, $\rho_i(z)$, of species i inside slices of thickness $dz = 0.1\sigma$ and radius $R_c = 7\sigma$, which is about twice the typical value of the radius of gyration⁸². The species index $i = d, c$ denote either the dendrimer ions or counterions, respectively. The dendrimers were placed oppositely at a distance $z = \pm D/2$ from the midpoint of the simulation box, where the z -axis lies along the body diagonal of the simulation box having $z = 0$ at its geometrical center. The charge distribution of fully charged dendrimer ions are shown in Fig. 5.5(a) and their counterions in Fig. 5.5(b) for a selection of distances D between their centers of mass. For the largest distance shown, $D = 12.2\sigma$, the charges are equally distributed to both sides of the dendrimer with its center of mass lying at $z = 6.1\sigma$ supporting the picture of the dendrimer as a densely packed object. The shell structure emerges to some extent, but the cylindrical symmetry of the profiles makes a clear assignment of monomers to each of the shells difficult. The influence of the other dendrimer is very weak here, leading to only a small asymmetry in the counterion distribution. At smaller distances, the dendrimer's monomers and counterions are asymmetrically distributed around its center of mass. The counterions are found in-between and inside the two dendrimers, thereby screening the electrostatic force between the charged sites. When the dendrimers are placed at a distance of $D = 3.6\sigma$ the monomer distribution is peaked more narrowly around the center of mass of the individual dendrimers. A combination of steric and Coulombic interactions expel the counterions from the central region at $z = 0$ leading to the appearance of two peaks around the dendrimers center of mass. At the overlap distance the range of the monomer distribution becomes maximal corresponding to an increase of the radius of gyration by about 15%, which means that the dendrimer is further stretched than at large separations. This is in line with the same effect that has been observed for neutral dendrimers, see Fig. 5.2(b).

In Fig. 5.6(a), the distribution of the charged monomers for the interacting end-group charged dendrimers, i.e., $Z = 32$, are shown. Also here at large separations, the monomers are distributed symmetrically around the center of mass of the dendrimer. The increase in range of the distributions on approaching of the dendrimers, indicates that the macromolecules are being stretched. It can also be observed that at a distance of $D = 3.2\sigma$, the number of charged sites found in the slice at $z = 0$

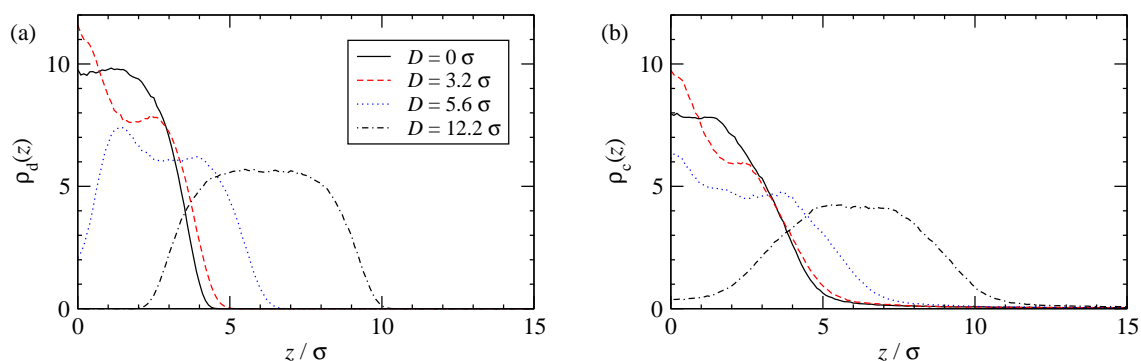


Figure 5.6: (a) Density of charged dendrimer monomers, $\rho_d(z)$, measured within a cylinder of radius 7σ along the box-diagonal (z -axis) for three different center of mass distances D for $P = 1$ dendrimers with end-groups charged. (b) Density of charged counterions, $\rho_c(z)$, distributed around the dendrimers shown in (a).

has increased to twice its value in the plateau found at a distance of $D = 12.2\sigma$, which is due to the fact that now monomers of both dendrimers are measured. The charged end-groups of the dendrimers, as well as the counterions are distributed symmetrically around the centers of mass, when the latter coincide. Further, the counterion distribution depicted in Fig. 5.6(b) shows that the counterions are not depleted from the central slice. Thus, they are able to compensate the charges of the terminal beads of the dendrimer to a larger extent than for the fully charged dendrimers. At the same time the particles are less restricted in their movement, due to the smaller amount of counterions involved.

To study the effect of pH on the effective interaction between the dendrimers, the effective force acting on the center of mass has been measured according to Eq. (5.6). We examined dendrimers of varying spacer length under different pH values of the solvent. The effective force between dendrimers with $P = 1$ spacer segment between the nodes is shown in Fig. 5.7(a). The shape of the force indicates that the underlying potential is of Gaussian shape, in agreement with other work published on this topic¹⁷⁻¹⁹. Upon raising the charge Z of the dendrimers from $Z = 0$ to $Z = 62$, the effective force increases monotonically attaining twice to three times the value of the force between the neutral dendrimers at its maximum, depending on

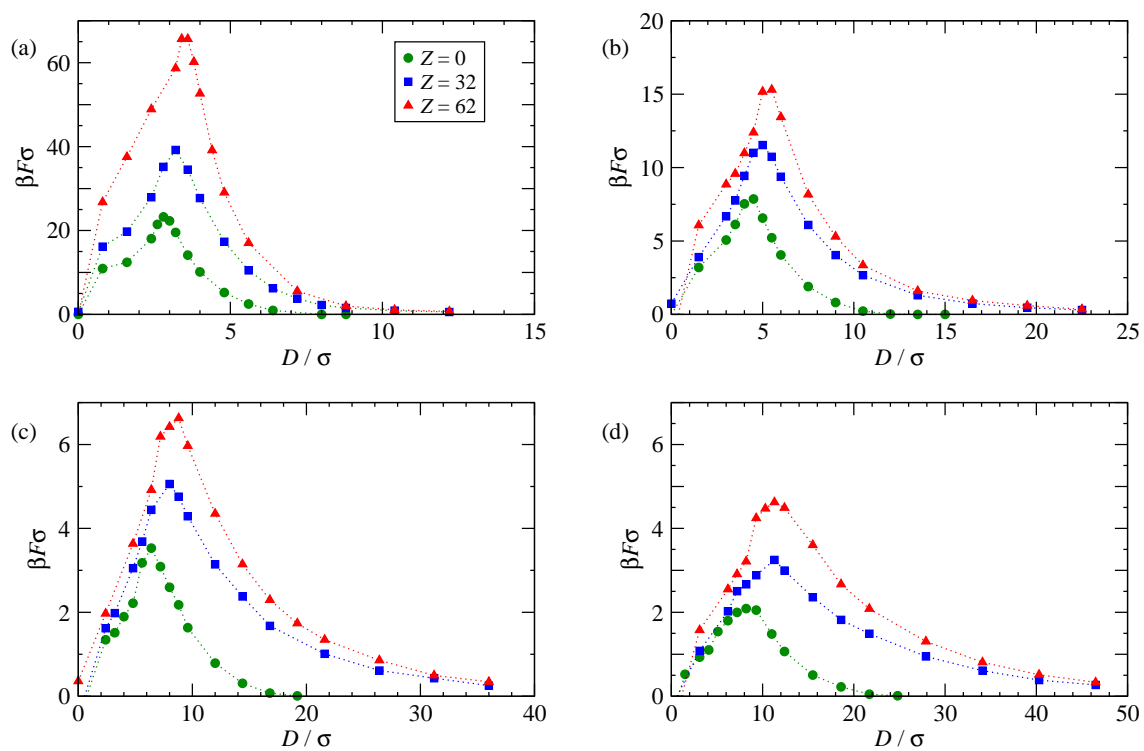


Figure 5.7: The effective force, F , between $G = 4$ dendrimers with number of spacer segments (a) $P = 1$, (b) $P = 2$, (c) $P = 4$, and (d) $P = 6$ at different pH values of the solvent. The total charge of a dendrimer is denoted by Z .

P . At the same time its range is enhanced, since the whole molecule grows. At large distances, where the monomers do not overlap, the force is governed by a Yukawa-like decay for the charged dendrimers which is caused by the screening of the charged sites of the dendrimers by the oppositely charged counterions. At a distance of about $D \cong 1.2R_g$ the forces attain their largest value and drop to zero independently of their charge Z at $D = 0$. This might sound counterintuitive, because there are no attractive forces acting between the monomers of the dendrimers that would compensate the steric and electrostatic repulsive interactions. However, it should be noted that there is no preferred direction at $D = 0$, and hence the effective force vanishes for reasons of symmetry.

When the number of neutral spacer monomers between the nodes of the dendrimer is increased up to $P = 6$ [see Figs. 5.4(a)-(d)], the range of the force increases due to the larger size. The strength of the force is lower the higher the number of spacer segments P between the nodes, because the branching density is reduced allowing for a larger amount of free space. It should be noted that on larger distances where the dendrimers are fully separated the force has the same order of magnitude independently of P .

5.5 Effect of Salt

In this section, we extend the studies to the effective interaction between dendrimers with $P = 1$ and $P = 2$ spacer segments to varying concentrations of monovalent and divalent salt. Whereas for charged star polymers an increase of the salt concentration can lead to a dramatic collapse,²⁴ we have not seen this effect for dendrimers with $P = 1$ spacer segments⁷¹. However, for dendrimers with long spacer chains, it has been found that their properties start resembling those of the star- and linear-counterparts more and more as P grows. We consider anew the number density of charges within slices of $d = 0.1\sigma$ in a cylinder of radius $R_c = 7\sigma$ along the box diagonal (z -axis), measuring their distributions in the same fashion as in Sec. 5.4. The number of charges of the fully charged dendrimers with $Z = 62$ and $P = 1$ at a distance of $D = 3.6\sigma$, where the force is maximal, is depicted in Fig. 5.8(a). By increasing the salinity of the solution, the charge distribution of the dendrimers

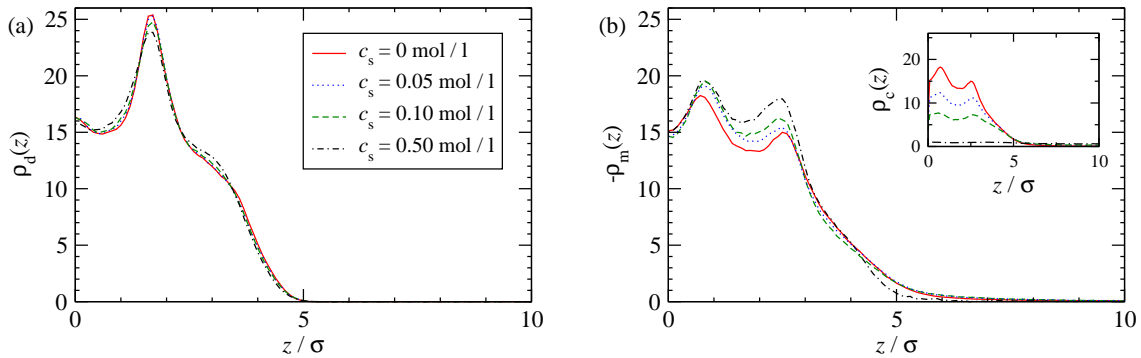


Figure 5.8: (a) The density of $P = 1$ charged dendrimer-monomers, $\rho_d(z)$, measured within a cylinder of radius 7σ along the box-diagonal (z -axis) for different divalent salt concentrations. (b) The total mobile charge density $\rho_m(z)$ of monovalent counterions and divalent salt counter- and co-ions belonging to the dendrimers. The inset shows the charge density of counterions only.

remains practically unaltered. The distribution of the total mobile charges $\rho_m(z)$ belonging to the dendrimers mentioned above is shown in Fig. 5.8(b), whereas the inset shows the distributions of the monovalent counterions only. Upon increasing the salt concentrations up to very large values of $c_s = 0.50$ mol/l, the total mobile charge density around and between the dendrimers is increased. However, from the inset we can see that at the same time the monovalent counterions are expelled from the dendrimer's interior, forming a uniform gas at the larger salt concentrations. Since the salt ions carry twice the charge of the counterions, this exchange results in gain of entropy for the released dendrimer counterions without loss of Coulomb energy; at the same time, it creates more free space inside the dendrimer, since one needs only half the number of salt counterions to compensate the same charge as is required for the counterions. This exchange is expected to have considerable impact on the effective interaction, and we therefore compare the influence of salinity of the solution for monovalent salt with divalent salt for two of our dendrimer types, namely the fully charged dendrimers with $P = 1$ and $P = 2$.

The effective force for various salt concentrations of monovalent salt is shown in Figs. 5.9(a) and 5.9(b) for the dendrimers with $P = 1$ and $P = 2$ spacer segments,

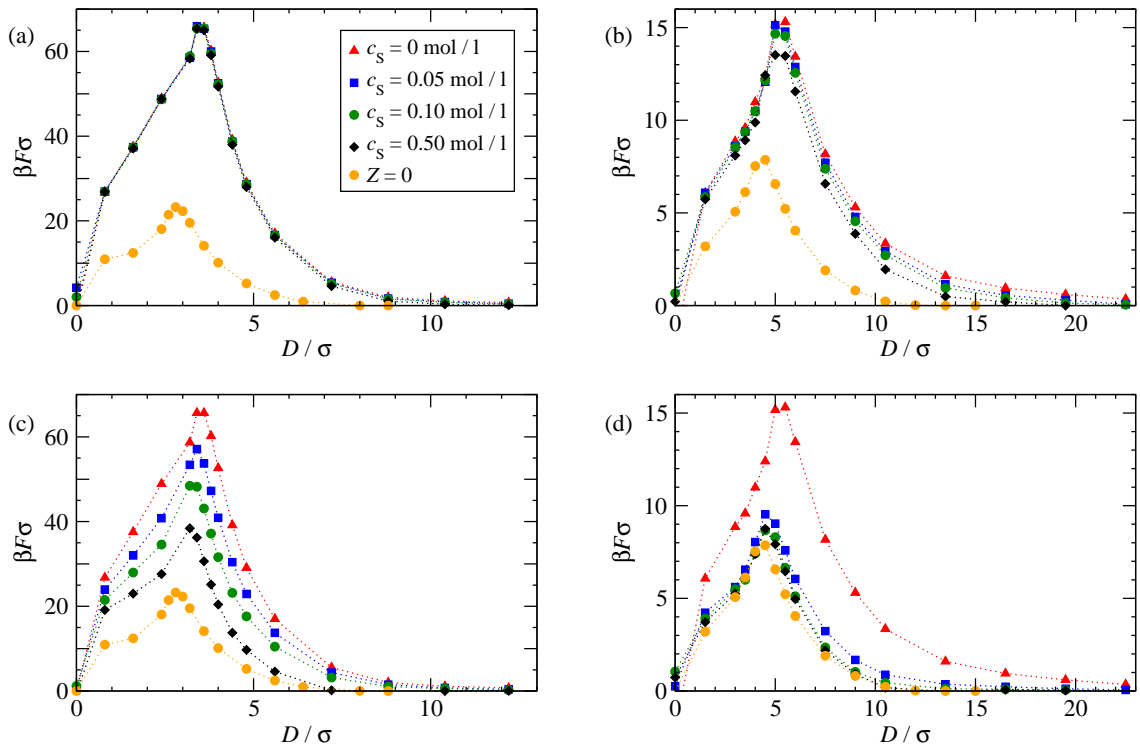


Figure 5.9: The effective force, F , between fully charged dendrimers with number of spacer segments $P = 1$ [(a),(c)] and $P = 2$ [(b),(d)] at different salt concentrations c_s , where the salt ions are either monovalently charged [(a),(b)] or divalently charged [(c),(d)]. The forces for neutral dendrimers without salt are shown for comparison.

respectively. The increase of concentration of monovalent salt has only a minor effect on the effective force for both cases of $P = 1$ and $P = 2$. These results are in line with our observations on the conformations regarding dendrimers with rigid and soft bonds⁷¹. The effect seems to be a bit more pronounced for $P = 2$ than for $P = 1$, pointing to the importance of the free space available in the interior of the dendrimer and the deformability of the whole molecule. For the stiff, $P = 1$ dendrimer, the amount of counterions in its interior can hardly be increased by adding salt and the osmotic pressure exerted from the salt outside it is not sufficiently strong to deform and shrink the molecule. Accordingly, the force for overlapping dendrimers is hardly affected by the addition of salt and only for *nonoverlapping* distances a small decrease can be discerned, which can be attributed to an increase of the Debye screening length κ_D^{-1} due to the additional salt.

On the contrary, when divalent salt is added to the solution, two features become immediately apparent in Figs. 5.9(c) and 5.9(d). First, the divalent salt has clear effects on the effective force and second these are different for $P = 1$ and $P = 2$ dendrimers. Adsorption of divalent salt counterions is now favorable according to the exchange mechanism explained above. Since this mechanism creates new space inside the dendrimer, the effective force for overlapping molecules can be reduced on two accounts: first because the net charge of the dendrimer and enclosed counterions is reduced and second because the entropic penalty of squeezing together the counterions of two interacting dendrimers drops as well. Upon raising the concentration of divalent salt molecules the negative charge density inside the dendrimers increases, thereby expelling more monovalent counterions. This not only leads to a stronger screening of the Coulombic repulsion between the charged dendrimer monomers but raises the entropy of the dendrimer as well, because the monomers have a larger amount of free space at their disposal. However, this comes to an end when the number of salt molecules that can be absorbed by the dendrimer reaches its limit which is caused by the steric repulsion between the monomers and salt molecules. This is evident for the case $P = 1$, where it can be seen that addition of divalent salt leads to a step-by-step reduction of the repulsive forces, though it does not bring the same as low as the effective forces between neutral dendrimers. The reason lies in the limited free space $P = 1$ -dendrimers have in their interior and a concomi-

tant saturation of the amount of counterions they can absorb. Concomitantly, the screening of the Coulomb repulsion between the dendrimer monomers by the salt molecules is not strong enough to neutralize the effective force acting on the centers of mass of the dendrimers, although the number of salt molecules is large enough to facilitate a neutralization. At very high salt concentrations of $c_s = 0.50\text{mol/l}$ the total charge of all $N_s = 147$ divalent salt molecules clearly can compensate the charge of the dendrimers, each carrying $Z = 62$ elementary charges. For the lower concentrations in the given simulation box size, this is not the case.

Things are different for the $P = 2$ dendrimers, as testified by the picture emerging from Fig. 5.9(d). To make a fair comparison, we first point out that, since these are larger than their $P = 1$ counterparts, we had to employ bigger simulation boxes in this case, so that the same value of c_s for $P = 1$ and $P = 2$ does not imply the same amount of salt ions: there are more of them in the box in the second case. Already at a salt concentration of just $c_s = 0.05\text{mol/l}$, there exist in the box $N_s = 51$ divalently charged salt counterions, bringing up a charge of $Z_c = 102$ that can almost neutralize the dendrimers' own charge. Since there is sufficient space within the dendrimers for these counterions to absorb, the resulting effective force is almost at the values of that of neutral dendrimers. Here, due to the larger available free space, the salt ions are able to explore the whole dendrimer leading to a more effective screening than for the more densely packed $P = 1$ dendrimer. For even larger salt concentrations the effective force, is screened so strongly that it attains the values measured between neutral dendrimers.

5.6 Conclusions

We have studied the effective interaction between dendrimers with explicitly modeled short and long spacer chains between successive generations under varying pH values of the aqueous solvent. The effect of the pH value has been modeled implicitly, by adapting the degree of charging of the dendrimers. By increasing the salinity of the solution with divalent salt molecules the interaction coincides with that of neutral dendrimers, when the spacer chains are sufficiently long, whereas monovalent salt hardly affects the effective interaction. The observed softening of

the interaction of neutral dendrimers with elongated spacer chains is in line with general observations in other polymeric systems, such as polymer brushes, where a decreasing grafting density leads to similar results³. It is possible to rationalize the softening by scaling the effective force onto a master-curve, where the shape of the interaction is independent of spacer length for neutral dendrimers. We have been able to quantify the overlap of two interacting dendrimers and found very good agreement with the overlap as obtained from the intersection of two spheres. This further supports a coarse grained picture of dendrimers as charged, penetrable spheres. We therefore expect the effective force to be a valid approximation for dendrimer solutions up to the overlap concentration, because many body contributions to the force are negligible¹⁶.

It has been demonstrated how the interaction can be tuned by a change of the pH. When the dendrimers become fully charged, the force increases to about twice its value as compared to the neutral case. Thus, by choosing an appropriate spacer chain length the interaction can be modified in such a way as to design a trap-and-release system. The dendrimers can be brought in contact with large, polyvalent objects ('drug molecules'), which will be absorbed into their interior, expelling the dendrimers' own counterions. Upon changing the pH-value of the solution and therefore neutralizing their nodes, the dendrimers should collapse, releasing the encapsulated molecule back into the solution. In line with this observation, continuing research could focus on the dendrimer-drug complexation and the dependence of the efficiency of the mechanism on size and charge asymmetry, as well as on spacer length.

Chapter 6

Osmotic shrinkage in star/linear polymer mixtures

Multiarm star polymers were used as model grafted colloidal particles with long hairs, to study their size variation due to osmotic forces arising from added linear homopolymers of smaller size. This is the origin of the depletion phenomenon that has been exploited in the past as a means to melt soft colloidal glasses by adding linear chains and analyzed using dynamic light scattering experiments¹ and an effective interactions analysis yielding the depletion potential. Shrinkage is a generic phenomenon for hairy particles, which affects macroscopic properties and state transitions at high concentrations. In this work we present a small-angle neutron scattering study of star/linear polymer mixtures with different size ratios (varying the linear polymer molar mass) and confirm the depletion picture, i.e., osmotic star shrinkage. Moreover, we find that as the linear/star polymer size ratio increases for the same effective linear volume fraction (c/c^* with c^* the overlapping concentration), the star shrinkage is reduced whereas the onset of shrinkage appears to take place at higher linear polymer volume fractions. A theoretical description of the force

¹The entire set of experimental results showed in this chapter was acquired by A. Wilk, E. Stiakakis, J. Kohlbrecher, D. Vlassopoulos, G. Meier, J.K.G. Dhont, G. Petekidis, and R. Vavrin at the Forschungszentrum Jülich and FORTH Crete.

balance on a star polymer in solution, accounting for the classic Flory contributions, i.e. elastic and excluded volume, as well as the osmotic force due to the linear chains, accurately predicts the experimental findings of reduced star size as a function of linear polymer concentration. This is done in a parameter-free fashion, in which the size of the cavity created by the star, and from which the chains are excluded, is related to the radius of the former from first principles.

6.1 Introduction

Star polymers with high functionality have emerged as a novel class of ultrasoft colloidal particles, characterized by interactions that feature Yukawa-type repulsions at long distances and logarithmic repulsions at short distances.³ They are representative of a large class of long hairy particles, including block copolymer micelles and grafted colloids, where the polymeric nature of the hairs has a stabilizing effect and determines to a large extent their macroscopic behavior.¹¹⁰ At high volume fraction, achieved at different number densities through manipulation of the effective grafted layer thickness in conditions of varying solvent quality, these systems exhibit a glasslike transition.^{111–113} Its main features are an enhanced frequency-independent storage modulus (G') in rheology, which is much larger than the loss modulus (G''), and a non-ergodic plateau in the intermediate scattering function.^{112,113} Recently, it was observed that small amounts of added linear homopolymer with smaller size compared to the star leads to glass melting due to depletion.^{102,112–114} This osmotic phenomenon¹¹⁵ is akin to that known in hard colloid-polymer mixtures^{116–118} but bears an important difference: the colloidal star is a soft and deformable particle, and thus the osmotic force due to the added polymers can squeeze it, which leads to a shrinkage of its size; for high concentrations eventually star aggregation and possibly phase separation takes place.^{112,119} Our previous investigations addressed the depletion problem partly, via dynamic light scattering (DLS) and some limited small-angle neutron scattering (SANS) studies, which were complemented by calculations based on an effectiveinteractions approach.^{102,112,114,119} However, DLS provided the hydrodynamic radius, whereas the radius of gyration had to be ob-

tained via extrapolation due to the small size of the stars. On the other hand, very limited SANS data are available and there is no systematic study yet on the effect of concentration of added linear chains. Moreover, an important question that has not been addressed is the effect of the linear-to-star polymer size ratio. Last but not least, whereas the depletion effect was unambiguously confirmed with SANS (and rheological) studies, which conformed to the reduced repulsion of the effective pair interaction potential,^{102,112,120–122} no theoretical rationalization for the single-particle shrinkage from first principles is yet available. Yet, this behavior appears to be generic in soft deformable particles,^{110,119–123} and a fundamental understanding is needed. Hence, in this work we attempt at complementing our earlier studies by measuring the form factor of single stars in a sea of linear homopolymers of different molar masses, and give a theoretical description of the observed osmotic star shrinkage.

6.2 Experimental

6.2.1 Materials

We used a model 1,4-polybutadiene star (coded as h-12880, where 128 stands for the nominal star functionality f , and 80 for the nominal arm molar mass in kg/mol) with $f = 114$ arms and weight-average arm molar mass 72 kg/mol, synthesized via hydrosilation anionic chemistry¹²⁴ and provided by J. Roovers (NRC, Canada). Three deuterated linear 1,4-polybutadienes were used with weight-average molar masses 100, 210 and 900 kg/mol. They were coded as d-100, d-210 and d-900, respectively. The d-100 sample was kindly provided by L. Wilner (Forschungszentrum Jülich, Germany) and the other two were obtained from Polymer Source, Canada. We also employed two protonated 1,4-polybutadienes of 165 kg/mol (coded as h-165) and 356 kg/mol (h-356), obtained by J. Roovers and Polymer Source, respectively. All samples were nearly monodisperse (the ratio of weight to number-average molar mass was below 1.1). Solutions in d-cyclohexane, an essentially athermal solvent, were prepared at given concentrations by first preparing a dilute star solution (less than 0.1 wt%) and then adding the needed amount of linear polymer under gentle

Sample code	R_h (nm)	R_g (nm)	c_h^* (wt%)
d-100	9.67	13.6	4.92
h-165	13.8	19.5	2.78
d-210	15.0	21.1	2.77
h-356	21.9	30.8	1.49
d-900	35.0	49.9	0.93
h-12880(star)	66.8	41.0	1.27

Table 6.1: List of samples used in this work along with the hydrodynamic radii, radii of gyration and hydrodynamic overlapping concentration.

stirring for a few hours. The samples were left to equilibrate for 24 hours before use. A small amount (about 0.1 wt%) of antioxidant (4-methyl-2,6-di-tert -butylphenol) was added to reduce the risk of degradation. The radii (hydrodynamic and gyration) of the samples used and the respective hydrodynamic overlapping concentrations c_h^* are listed in Tab. 6.1.

6.2.2 SANS

In all measurements the star concentration was kept low (well below its overlapping value c^*) to ensure conditions for single-particle form factor measurements. Samples were placed in mm thick quartz Hellma cuvettes in the thermostated sample holder (accuracy $\pm 0.1\%$). Data were taken at 3 different detector distances (1.6, 4.5 and 18 m) and $\lambda = 1.20 \pm 0.06\text{nm}$, which allows for a variation of the scattering vector q in the range $0.01 < q[(\text{nm})^{-1}] < 1$, which is sufficient to follow both the radius of gyration and blob size changes. Note that the scattering length densities of the deuterated solvent and the deuterated linear chains are almost identical (6.7×10^{10} and $6.8 \times 10^{10}\text{cm}^{-2}$, respectively), whereas this is not the case for the protonated linear chains. This is in fact the reason why, for all solution compositions, careful measurement of the background (i.e., solution of deuterated cyclohexane and linear chains of the same kind and concentration as in the main sample) was performed. After all necessary corrections for background, transmission, and detector efficiency,

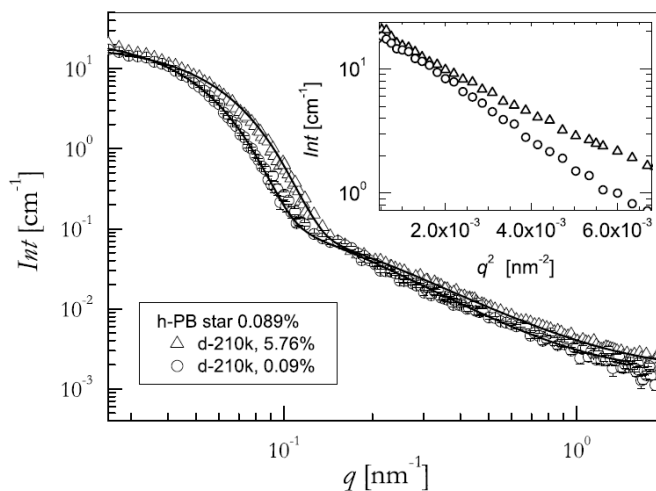


Figure 6.1: Exemplary form factors of protonated colloidal star h-12880 in dilute solution (0.09 wt%) in two deuterated solvents, measured by SANS. The solvents consist of linear polybutadiene d-210 in d-cyclohexane: 0.09 wt% (circles) and 5.76 wt% (triangles). The solid lines are the Dozier fits (see text). The shrinkage of the star at higher linear polymer concentration is reflected at the low- q values, whereas a slight difference at high- q values reflects the blob size variation. Inset: Guinier plot of the low- q region.

the raw data were converted into absolute intensities using water as a standard. The background intensity arising from the linear polymers was measured from their solutions without the stars at the experimental conditions set for the samples at the same concentration as for the main sample.¹²⁵ Consequently, the scattered intensity depicted in figures discussed below results purely from the stars.

6.3 Results and discussion

6.3.1 SANS data

Figure 6.1 depicts typical form factors of the single colloidal star h-12880, measured by SANS. In this particular case, the linear homopolymer was d-210 at two concen-

trations of 0.09 and 5.76 wt%. The data exhibit the typical scattering behavior of multiarm stars,^{10,126–128} with two distinct contributions at small and large scattering wave vector (q) values. The low- q part reflects the “form factor” P , due to scattering from the overall polymer density profile. The inset of Fig. 6.1 depicts the Guinier representation of the data to show the concentration-dependent radii of gyration. The high- q part is dominated by the polymer-solvent fluctuations (blob term) G . This leads to the representation of the SANS intensity by two independent contributions^{10,126–128} and was justified by Marques *et. al.*¹²⁹ using the Daoud-Cotton model⁹

$$I(q) = I_0 \frac{1}{f} [(f - 1) P(qR_g) + G(q\xi)], \quad (6.1)$$

where f is the functionality of the star, R_g is the radius of gyration and ξ is a correlation length (blob size). Note that the functionality of the star is proportional to the weight-average star volume. The scattering contribution from the single star is proportional to $f(f - 1)P(qR_g)$ and the contribution from the blob term to $fG(q\xi)$.¹³⁰ The above representation in Eq. (6.1) leads to the desired normalisation of the forward intensity $I(q = 0) = I_0$, when $P(qR_g)$ and $G(q\xi)$ are equal to one for $q = 0$. The simplest expression for the form factor is a Guinier type¹³¹

$$P(q) = \exp(-q^2 R_g^2 / 3). \quad (6.2)$$

The high- q limit $G(q\xi)$ term in Eq. (6.1) is approximated by¹⁰

$$G(q\xi) = \frac{\Gamma(\mu) \sin[\mu \tan^{-1}(q\xi)]}{q\xi [1 + q^2 \xi^2]^{\mu/2}}, \quad (6.3)$$

where $\mu = \frac{1}{\nu} - 1$ ($\nu = 3/5$ is the Flory exponent), and Γ denotes the gamma function. Since the relative contributions of the form factor and the blob contribution are not known, Γ will be treated in this analysis as an adjustable parameter, along with R_g and ξ . The combined fit of Fig. 6.1 confirms, despite the weak intensity in the high- q regime, the quality of the data and also their good representation with this approach. The same conclusions hold for all measured samples. We note that, despite the very low star concentration (far below the overlapping concentration,

c^*), we have performed a few measurements as a function of concentration to ensure that intermolecular correlation effects are negligible. Indeed, within the range examined no effect was observed. Hence, the approach followed above to describe the scattering curves purely with the star form factor is justified.

The extracted R_g values are normalized to the radius of gyration in pure d-cyclohexane, R_{g0} and are compiled in Fig. 6.2, where they are plotted against the concentration (a) and the effective volume fraction (b) of the added linear homopolymers, the latter being simply the ratio c/c_{lin}^* .¹³² A few remarks are in order. First, in this plot we used the hydrodynamic volume fraction (c_{lin}^* based on R_h) because it has been measured consistently for all samples, and it allows direct comparison with earlier studies.¹¹² Given the fact that the ratio of the radius of gyration to the hydrodynamic radius is constant for a polymer-solvent system at fixed temperature, this representation is justified. Furthermore, considering the mixture of h-12880 star and h-165 linear homopolymer, it is encouraging that the SANS and light scattering data are virtually identical. This confirms the accuracy of the data and the earlier findings with this mixture.¹¹² Moreover, the reduction of R_g/R_{g0} with c/c_{lin}^* reveals the osmotic effect of the added linear homopolymers in reducing the star radius of gyration. This effect is unique for soft and deformable objects.^{114,119–123} The data of Fig. 6.2(a), which are plotted against the weight concentration (or monomer number density), are independent of the linear chain molar mass [Fig. 6.2(a)] for the same isotope composition, since the osmotic pressure of the linear polymer solution scales with number density.¹³³ The latter explains the lower osmotic pressure at the same high c/c_{lin}^* for larger linear molar mass. The plot of Fig. 6.2(b) suggests that, as the molar mass of the polymer increases, the threshold volume fraction at the onset of star shrinkage (where the ratio R_g/R_{g0} becomes about 0.95), increases as well (indicated by vertical arrows in the plot). More specifically, from d-100 to d-210 to d-900, the threshold value appears to shift approximately from 0.3 to 0.8 to 2, respectively. We note here that, whereas the mixtures with linear chains h-165 and h-356 exhibit the same qualitative trend as the other samples, they are very different quantitatively, as demonstrated in figs. 2(a) and (b). In particular, Fig. 6.2(a) is quite revealing as the R_g/R_{g0} data against concentration are clearly separated in two sets; those with deuterated linear chains and those with protonated linear chains.

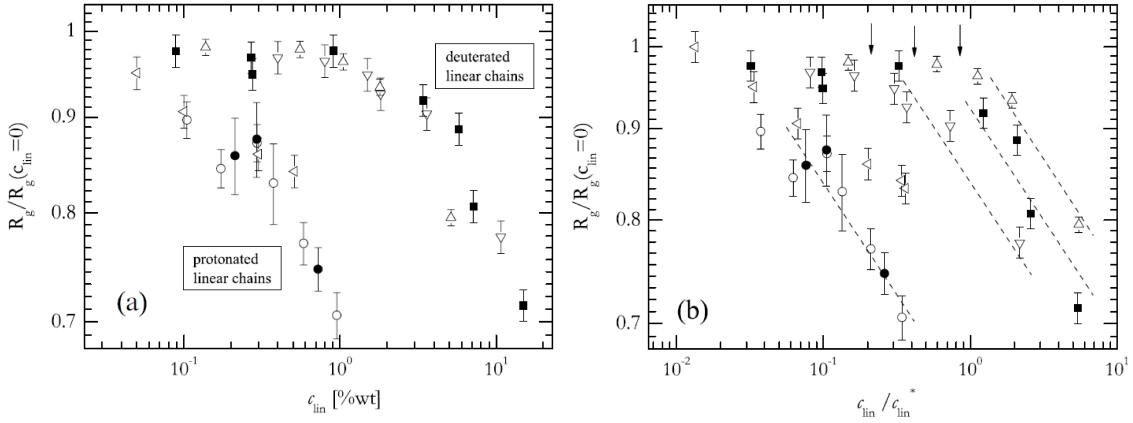


Figure 6.2: Plots of the normalized radius of gyration of the star in the linear homopolymer mixture (to its value in pure solvent d-cyclohexane), R_g/R_{g0} , as a function of the concentration (a) and the effective volume fraction c/c^* (based on R_h) of the polymer (b). SANS data are shown for three linear polybutadienes, d-100 (down triangles), d-210 (filled squares) and d-900 (up triangles). The protonated polybutadiene h-165 (circles) and h-356 (left pointing triangles) data obtained from SANS and light scattering¹¹² (filled circles) are also shown for comparison. Note that the star (h-12880) and linear (h-165) polymers used in ref.¹¹² come from different batches and have slightly different molecular characteristics ($f = 122, 72$ kg/mol per arm and 155 kg/mol, respectively), but these differences are not appreciable, given the small but finite (not exceeding 1.1) polydispersity. The lines with slope -0.125 in (b) are drawn to suggest the shrinking power law behaviour (see text). Also in (b), the vertical arrows indicate the onset star shrinking for the solutions with linear d-100, d-210 and d-900 from left to right, respectively.

We attribute this distinct behaviour to the different type of isotope labelling. Indeed, it makes a difference for SANS whether protonated or deuterated linear chains are mixed with the protonated star in deuterated solvent. It is a well-known effect in polymer physics that the exchange of protons with deuterons in a polymer alters its mixing behaviour with other polymers drastically, which is reflected in the vastly different Flory-Huggins parameters.^{131,134} Therefore, we will compare quantitatively the shrinking of stars in different linear polymer solutions only for samples with the same isotope composition (i.e., both deuterated solvent and deuterated linear polymer). Of course, since shrinking of the stars is a result of the osmotic pressure due to the presence of the added linear chains, the qualitative effect is observed for all star/linear polymer mixtures, and in this respect the star mixtures with h-165 and h-356 are also discussed in this work. Concerning the latter two mixtures, the data confirm the correct qualitative trend, i.e. increasing the molar mass of linear polymer at the same volume fraction reduces the relative shrinking of the star. We note furthermore that the data in Fig. 6.2(b) suggest that the power law exponents characterizing the decrease of R_g/R_{g0} with c/c^* lin appear to be similar for the different samples, and to conform to the exponent of -0.125 governing the shrinkage of linear and star polymers of low functionality above their overlapping concentration.^{3,121,133} Hence, we draw lines with slope -0.125 in this figure, simply for reference. The internal structure of the colloidal stars, which is dominated by f ,^{9,10,135} could affect the magnitude of the shrinkage, but not the asymptotic power law behaviour against linear polymer volume fraction, as discussed below.

6.4 Theoretical analysis

The size of a star polymer in a bath of linear chains can be estimated by employing Flory-type arguments^{3,133} while taking into account the osmotic pressure $\Pi(s)$ exerted on the star due to the presence of the chains. The osmotic pressure depends on the ratio $s \equiv c/c_{lin}^*$ of chain concentration to overlap concentration. The latter is given by $c_{lin}^* = a^{-3}N_c^{-3\nu}$, where N_c denotes the degree of polymerization of the chains, a the length scale of the monomers and $\nu = 3/5$ the Flory parameter. Insertion of a star polymer in a solution of linear chains results into the expulsion of

the latter from a region of size R . The free energy cost for creating such a cavity of radius R in the polymer solution is

$$\beta F_{\text{osm}}(R) = \frac{4\pi}{3} R^3 a^3 \beta \Pi(s), \quad (6.4)$$

where $\beta = 1/kT$, with k being Boltzmann coefficient and R is written in reduced units (the length scale is set by the diameter a of the monomer). It should be noted that R need not coincide with the gyration radius of the star, a quantity that characterizes its size, though it is to be expected that the two are very similar. In contrast to the work on hard colloidal particles in polymer solutions,¹³⁶ we can neglect the surface term here because the transition of the polymer density from the excluded region, in the star interior, to its bulk value is gradual,¹⁰⁴ minimizing thereby the interfacial cost. Associated with a star of radius R_s with functionality f and degree of polymerization N_s is an elastic free energy (F_{el}) and excluded volume or interaction free energy (F_{int}) which are given by

$$\beta F_{\text{el}}(R_s) = \frac{f R_s^2}{2 N_s}, \quad (6.5)$$

$$\beta F_{\text{int}}(R_s) = v \frac{N_s^2 f^2}{2 R_s^3}. \quad (6.6)$$

Again, the star radius R_s and the excluded-volume parameter v are given in reduced units; we employ, for simplicity, $v = 1$ in what follows, which is appropriate for good solvents and maintains the parsimony of the theory in avoiding using several numerical values. The results that follow fall within an order of magnitude, irrespectively of the choice of v . We can already see that the competition between the interaction contribution on the one hand and the osmotic and elastic contribution on the other hand, can only lead to a shrinkage of the star with respect to the chain-free case, since the osmotic free energy grows with R . Concomitantly, the shrinkage of the stars is a direct consequence of the unbalanced osmotic pressure of the chains, which are depleted from the star's interior. Yet, it remains to be seen whether this mechanism alone is capable of bringing about a satisfactory description of the experimental results, which show quite significant shrinkage of the stars in the presence of homopolymer. The size of the star is determined as the value at

which the sum of the free energies Eq. (6.4)-(6.6) reaches a minimum. Regarding the radius R of the cavity in Eq. (6.4) we have to account for the fact that the spatial extent of the region within the star from which the chains are completely excluded (i.e., the cavity), does not necessarily coincide with R_s , the latter being a measure for the radius of gyration of the star. Employing accurate effective potentials between stars and *shorter* chains, Camargo and Likos recently showed¹⁰⁴ that the chains around a star penetrate the latter up to a distance $R = \sigma$ from the star center, where σ is the so-called corona size of the star, at which the logarithmic star repulsion sets in.³ Using the well-known relationship $\sigma = 4/3R_s$, we readily obtain $R = bR_s$, where $b = 1.3$. This numerical factor is practically independent of the size ratio between the chains and the stars, as long as the chains are *smaller* than the star, and increases slightly with it. It can be anticipated, however, that b attains a larger value when the chains are *bigger* than the star, since, in that case, the chain would rather surround the star than penetrate it, an issue to which we will return shortly. Hence, we define in what follows $R = bR_s$, with the previously mentioned value of b . The size ratio δ between a chain and a star is defined as $\delta \equiv \frac{R_c}{R_s}$, where the subscript "c" denotes the chain and "s" the star. From the minimization of the free energy with respect to R_s we obtain the following relation, which can be understood as a balance of forces:

$$\frac{fR_s}{N_s} + b^3 4\pi R_s^2 a^3 \beta \Pi(s) - \frac{3vN_s^2 f^2}{2R_s^4} = 0. \quad (6.7)$$

thin a canonical ensemble renormalization group formalism for a semidilute polymer solution a scaling of the osmotic pressure was found, having the form¹³⁷

$$\frac{\beta \Pi(s)}{c} = 1 + P(s), \quad (6.8)$$

where

$$P(x) = \frac{1}{2}x \exp \left[\frac{1}{4}\epsilon \left(\frac{\lambda}{x} + \left[\frac{\lambda^2}{x^2} \right] \ln \lambda + \left[1 - \frac{\lambda^2}{x^2} \right] \ln [x + \lambda] \right) \right]$$

and

$$x(s) = \frac{1}{2}s\epsilon\pi^2 \left[1 + \epsilon \left(\frac{1}{2} + \ln 2 \right) / 4 \right].$$

Sample code	δ
d-100	0.34
d-210	0.53
d-900	1.25

Table 6.2: Size ratio δ between the chains and the h-12880 star with functionality $f = 114$ and degree of polymerization $N_s = 1393$.

The osmotic pressure of a test chain in the solution is given to the order $\epsilon = 4 - d$, with the spatial dimensionality $d = 3$ in this work and thus $\epsilon = 1$. Further, $\Pi(s)$ depends on the polydispersity, expressed through the index λ for which we have $\lambda = 1$ since we consider a monodisperse system. The results are practically unchanged for $\lambda < 2$. With this information we have $x \cong 6.41s$.

Noting that

$$\begin{aligned} a^3 \beta \Pi(s) &= a^3 c [1 + P(s)] = N_c^{-3\nu} s [1 + P(s)] \\ &= \delta^{-3} N_s^{-3\nu} f^{-3/5} s [1 + P(s)], \end{aligned}$$

where we have used $\delta = \frac{1}{f^{1/5}} \left(\frac{N_c}{N_s} \right)^\nu$, according to scaling theory, the force balance Eq. (6.7) can be rewritten as

$$\frac{f R_s}{N_s} + b^3 4\pi R_s^2 \delta^{-3} N_s^{-3\nu} f^{-3/5} s [1 + P(s)] - \frac{3\nu N_s^2 f^2}{2R_s^4} = 0. \quad (6.9)$$

The values for the various linear/star ratios δ are taken from experiment and are listed in Tab. 6.2.

Typical predictions of the above equation are depicted in Fig. 6.3 in the form of normalized radius of gyration against linear polymer c/c_{in}^* , for two cases: fixed linear/star polymer size ratio $\delta = 0.34$ and a star of (a) varying functionality and fixed arm size to the experimental value ($N_s = 1393$), or (b) varying arm size and fixed functionality to the experimental value ($f = 114$). In both cases the osmotic effect of added linear chains in shrinking the star is demonstrated. We also note the dramatic effect of functionality on shrinkage, where increasing f at fixed volume

fraction reduces the drop of R_g . This is an effect of the star conformation, in agreement with the experimental findings in Fig. 6.2. On the other hand, the effect of arm size is reduced but again, increasing N reduces the shrinkage at fixed c/c_{lin}^* . One can also observe that a drop of the normalized R_g of about 10% is achieved at about $c/c_{lin}^* = 1$, pointing to the fact that the osmotic effect of linear chains is clearly important, but of small intensity as a large concentration is needed to achieve a small (10%) shrinkage. Furthermore, in Fig. 6.3(b) we see that, in agreement with the experimental findings discussed above, the onset of star shrinking shifts to higher c/c_{lin}^* of linear chains as N_s increases.

A quantitative comparison of the experimental results with theoretical predictions is shown in Fig. 6.4 with the values from Tab. 6.2. Again, setting aside the samples with protonated linear chains, which show only qualitative agreement with the theory (which can be made quantitative if a different value of b is employed), the results for deuterated linear chains are satisfactory. For all chains considered experimentally, a quantitative agreement is achieved, and moreover the theory is robust given that b is not a fit parameter but rather takes a value that bears microscopic justification on the basis of effective chain-chain and chain-star interactions.^{104,138} We consider this as an encouraging result that provides predictive power for

this important effect for hairy particles. Interesting is the slight disagreement for the case of the d-900 chains, which are indeed bigger than the stars, and for which a larger value of b must be employed, in agreement with the aforementioned anticipation that these penetrate the stars less than shorter ones. In fact, the same argument can be employed for the h-165 and h-356 chains, for which the value of $b = 1.3$ underestimates the degree of shrinkage in the same fashion as for the d-900 chains shown in the main plot. We should note here that very small chains may be expected to penetrate a star. This could in turn lead to screening of the excluded-volume interactions in its interior, this being a possible additional mechanism for shrinkage. However, such a mechanism is not efficient if present at all. In fact there is no entropic gain in penetrating stars at such low stars concentrations. On the

other hand, recent experiments reported the increase of size of a star when very small linear (much smaller than presently) chains are added, but the system was dispersed in a temperature-dependent solvent.¹¹⁴ Nevertheless, this corroborates the

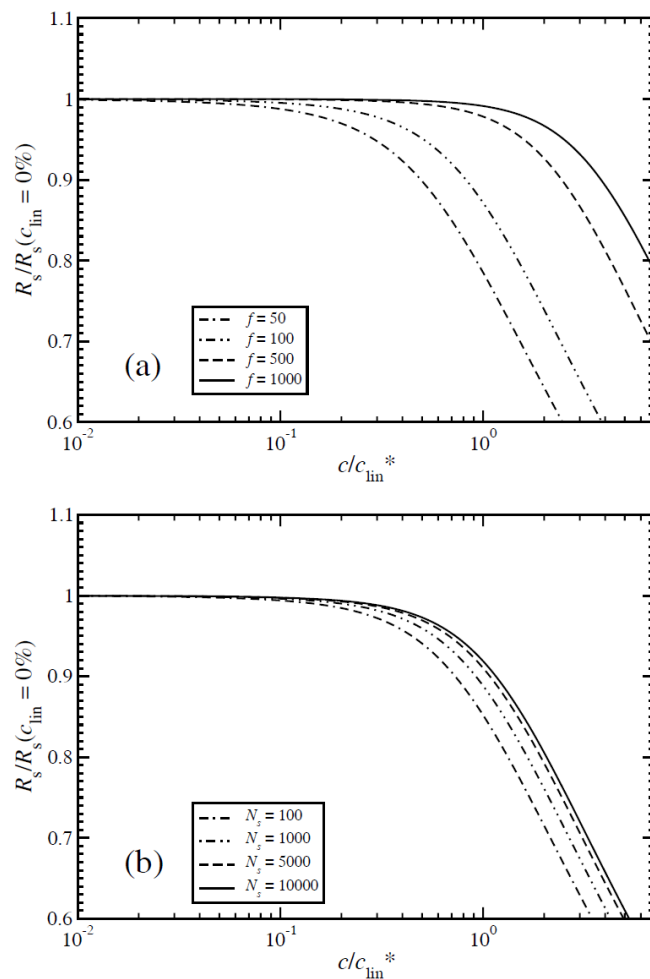


Figure 6.3: Radius of gyration R_g of a star as a function of linear chain concentration c/c_{lin}^* for a star/linear size ratio of $\delta = 0.34$. Shown are the theoretical predictions for (a) fixed degree of polymerization $N_s = 1393$ and varying functionality from $f = 50$ (left curve) to $f = 1000$ (right curve) and (b) for fixed functionality $f = 114$ and varying arm sizes from $N_s = 100$ (left curve) to $N_s = 10000$ (right curve).

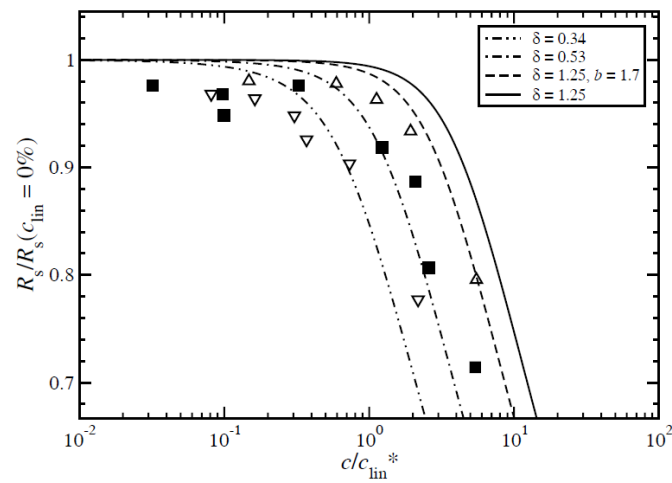


Figure 6.4: Comparison of the theoretical prediction for the degree of shrinkage (lines) with the experimental data for the various linear/size ratios δ from Tab. 6.2. The experimental points are coded as follows: d-100 (down triangles), d-210 (filled squares) and d-900 (up triangles). The theoretical results are shown from $\delta = 0.34$ (left curve) to $\delta = 1.25$ (right curve).

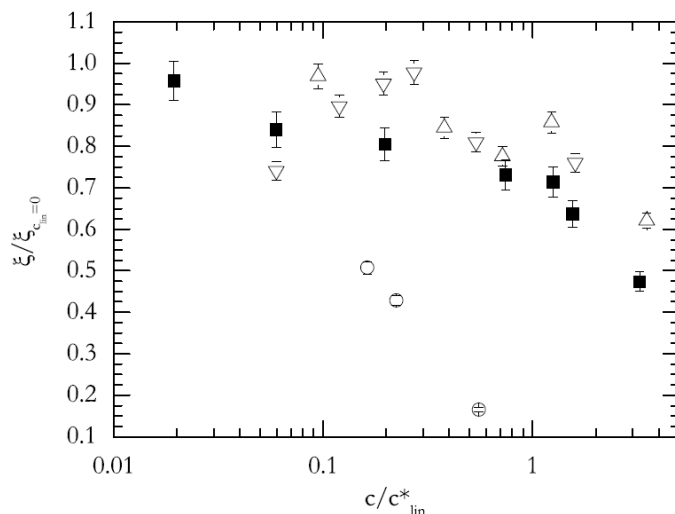


Figure 6.5: Extracted blob size of the h-12880 star in homopolymer solutions (normalized to that of the pure star in the absence of linear chains, ξ_0) as a function of the polymer effective (hydrodynamic) volume fraction. Symbols are the same as in Fig. 6.2.

lack of other mechanisms (than osmotic) for star shrinkage. We also note that similar considerations have been successfully used in other situations, such as describing the shrinkage of polyelectrolyte stars due to added salt, in which case the counter- and co-ions from the outside reduce the star size significantly.²³ Returning to the experiments, the extracted average star blob size ξ (from Eq. (6.3) above) is also found to decrease with increasing concentration of the linear polymer. This is depicted in Fig. 6.5. Determination of the blob size is a very delicate issue since the information is hidden in the high- q regime, which is greatly affected by the accuracy of background subtraction; to this end, the use of the fit model of Eq. (6.1) does not shed much light. Nevertheless, we did find a clear quantitative trend for all solutions measured, and this represents the finding of interest in this work. This result is consistent with the expectation that the star size variations reflect those of their constituent blobs, and in particular those in the excluded-volume regime.^{3,9} We note that, as in the case with the overall star size (R_g), the shrinkage of ξ for the mixture with h-165 differs from that of mixtures

with deuterated linear chains.

6.5 Concluding remarks

The combined experimental and theoretical study of colloidal star/linear homopolymer mixtures in the single star limit, revealed the shrinkage of the former due to the osmotic force exerted by the latter, which is smaller in size. As the linear/star polymer size ratio decreases for the same linear volume fraction, the star shrinkage is enhanced whereas the onset of shrinkage appears to take place at lower linear polymer volume fractions. On the other hand, when plotted against concentration, linear chains of different molar masses give rise to similar star shrinkage due to the same osmotic pressure. Moreover, whereas this osmotic effect is present, its magnitude is rather small, as typically the linear chains have to be brought at about their overlap concentration to achieve a reduction in star size of about 10%. At the same time, the outer blobs follow the same trend, as the reduction of the overall star size is translated into blob size reduction. This phenomenon is generic for soft long hairy particles and provides ways for exploiting depletion as a means for tailoring the state and dynamic behavior of soft colloids. It is also an important molecular parameter that controls macroscopic properties, aside from the stabilizing effect. In closing, we emphasize again the sensitivity of the probed star shrinking behaviour to the different types of isotope labeling of the linear chains. This was observed by comparing the mixture of star with h-165 against the mixtures with deuterated linear chains, and reflected different Flory-Huggins parameters due to different isotope composition of the mixtures.

Chapter 7

Conclusions and outlook

In this Thesis the conformational properties of charged dendrimers in implicit and explicit solvents have been examined. Dendrimers of varying flexibility and generation number have been considered as a function of the charge and for varying salt concentrations. To this end MD simulations were performed and compared to results stemming from Poisson-Boltzmann theory.

In chapter 2 the effect of a change of the pH value of the solution on the conformational properties of a fourth generational dendrimer was examined. By employing functional groups, like, e.g., secondary or tertiary amines, it is possible to synthesize a dendrimer, that is neutral at high and charged at low pH values¹⁵. To model the charging effect of the pH-change, the dendrimers were charged stepwise, beginning with a neutral dendrimer and ending up with a fully charged dendrimer. Intermediate pH values were modeled by charging only the last few generations. The repulsions between the charged monomers lead to a swelling of the dendrimers upon charging. The larger available space created thereby allows for the counterions to diffuse within the dendrimer and screen the repulsion to some extent. In the simulations the charge distributions were measured and only a moderate redistribution of the monomers away from the center of mass is found. However, the swelling of the dendrimer is more pronounced when soft bonds are employed between the nodes instead of rigid ones. The charge distributions of counter-ions and co-ions were compared to the results from Poisson-Boltzmann theory, thereby finding good agreement for the soft bonded dendrimers. Addition of monovalent salt has only a

minor effect on the dendrimers.

In Chapter 3 we showed that the flexibility of the dendrimers is of crucial importance for the conformational properties of the dendrimers. We systematically studied dendrimers of low and high generations with varying flexibility of the spacer and their conformations under varying conditions of the pH value of the solution. The flexibility of the spacer is modeled by inserting monomers between the nodes. We found that good agreement can be obtained between implicitly and explicitly modeled spacer. The increase of the size of neutral dendrimers were compared to the scaling law for dendrimers. Surprisingly good agreement was obtained when the same scaling law has been applied to charged dendrimers. For large generations and spacer lengths an opening of large voids within the dendrimer was observed, which are the prime candidates for a drug molecule to dock inside the dendrimer. It was demonstrated that the conformational changes are more contingent on spacer length and generation number than on the charge of the molecule. Our results are in good agreement with a recent combined SANS and X-ray scattering experiment on charged polyelectrolyte dendrimers, where it was shown that high-generation dendrimers undergo electrostatic swelling upon protonation³⁸. A common practice in gene-delivery experiments is to activate high generational PAMAM dendrimers by hydrolytic removal of some of the branches in order to maximize transfection efficiency of genes in to the cell's nucleus⁷⁶. This further underlines the importance to account for the flexibility within the dendrimer.

Hydrocarbons are typical building blocks used as monomeric units for dendrimers. Their size is of the same order of magnitude as water molecules, which might lead to non-negligible effects. By employing the SPC/E model for water²⁸ we explicitly took into account the granular nature of the aqueous solution in Chapter 4. Terminally and fully charged dendrimers with and without a spacer monomer between the nodes are considered and are compared to the simulations with implicit water. The fully charged dendrimers show very good agreement. However, due to the hydrophobicity of the hydrocarbons a reduction of the swelling of the terminally charged dendrimers can be observed in explicitly simulated water with respect to the implicit case. Thus, the hydrophobic effect needs to be accounted for in an dendrimer model for implicit water.

The effective interaction between two charged dendrimers can be used to make prediction about the phase behavior of dilute solutions by employing standard tools of liquid state theory⁶. In Chapter 5 the effective force has been measured for dendrimers of different spacer lengths. When the dendrimers are neutral, the shape of the force is independent of the flexibility of the molecule, changed by means of the spacer length. Under varying conditions of the pH of the solution the dendrimers become charged, which leads to an increased repulsion between the molecules. The force shows invariance upon addition of monovalent salt, however a reduction of the force can be observed for divalent salt. For larger spacer lengths the force can even drop down to values of neutral dendrimers, due to the larger space inside the molecule.

In Chapter 6 we theoretically analyzed the shrinkage of star polymers due to the osmotic force exerted on them by linear homopolymer chains. By means of a force balance including the elastic and excluded volume contributions as well as the osmotic force due to the linear chains, the reduced star size as a function of linear chain concentration has been calculated yielding accurate agreements with the experimental findings.

Future research on charged dendrimers based on the results from this work can go into the following directions. The phase behavior of charged dendrimers over a broad concentration range can be simulated and compared with experiments. Thereby, the validity of the measured two-body effective force can be tested for concentrated solutions. Moreover the collective effects of dendrimers and the role of counterions in a many body system of charged dendrimers can be examined. The calculation of the effective force can be extended to the case where the solvent molecules are explicitly taken into account. Although our results indicate a weak effect of the solvent on this scale, a dendrimer with hydrophobic core will certainly lead to an attractive contribution. An accurate model to account for this effect needs to be adjusted for this case. The effect of long spacer lengths and larger generations worked out in this Thesis can be utilized to compare different dendrimer-drug complexes and measure the drug-intake. The properties of different dendrimer models can then be compared to develop more effective encapsulation agents.

Another possibility to include screening effects of the solvent in an implicit water

simulation is the introduction of a position-dependent dielectric constant. When the Coulomb interaction between two charges in vacuum is compared to that in a polar solvent, a reduction of the energy must occur at large distances. Whereas at small separations there is no or only a minor reduction of the energy, due to the exclusion of the solvent molecules from the region between the ions. By treating the electrostatic energy between charges in an effective manner with a position-dependent dielectric constant¹³⁹ it would be possible to reproduce solvent effects at small and large distances within a simulation of charged dendrimers^{15,140}. In this way, larger systems can be simulated more efficiently as compared to explicitly simulated water.

Bibliography

- [1] R. J. Hunter, *Foundations of Colloid Science*, Oxford University Press, USA, 2. edition, 2001.
- [2] W. B. Russel, D. A. Saville, and W. R. Schowalter, *Colloidal dispersions*, Cambridge University Press, Cambridge, 1989.
- [3] C. N. Likos, *Physics Reports* **348**, 267 (2001).
- [4] S. A. Safran and N. A. Clark, *Physics of Complex and Supramolecular Fluids*, Wiley Interscience, New York, 1987.
- [5] J.-L. Barrat and J.-P. Hansen, *Basic Concepts of Simple and Complex Liquids*, Cambridge University Press, 2003.
- [6] J.-P. Hansen and I. R. McDonald, *Theory of simple liquids - 3rd ed*, Academic Press, 2006.
- [7] M. P. Allen and D. J. Tildesley, *Computer Simulation of Liquids*, Clarendon Press Oxford, 1989.
- [8] D. Frenkel and B. Smit, *Understanding Molecular Simulation*, Academic Press, San Diego, 1996.
- [9] J. P. C. M. Daoud, *J. Phys. (Paris)* **43**, 531 (1982).
- [10] G. S. Grest, J. S. Huang, L. J. Fetters, and D. Richter, *Adv. Chem. Phys.* **XCIV**, 67 (1996).
- [11] C. N. Likos et al., *Phys. Rev. Lett.* **80**, 4450 (1998).

-
- [12] G. E. Buhleier, W. Wehner, and F. Vögtle, *Synthesis (Stuttgart)* **2**, 155 (1978).
- [13] D. A. Tomalia, A. M. Naylor, and W. A. Goddard, *Angew. Chem. Intl. Engl. Ed.* **29**, 138 (1990).
- [14] G. R. Newkome et al., *Macromolecules* **26**, 2394 (1993).
- [15] M. Ballauff and C. N. Likos, *Angew. Chem. Intl. Engl. Ed.* **43**, 2998 (2004).
- [16] I. O. Götze and C. N. Likos, *J. Phys.: Condens. Matter* **17**, 1777 (2005).
- [17] C. N. Likos et al., *Macromolecules* **34**, 2914 (2001).
- [18] C. N. Likos et al., *J. Chem. Phys.* **117**, 1869 (2002).
- [19] I. O. Götze, H. M. Harreis, and C. N. Likos, *J. Chem. Phys.* **120**, 7761 (2004).
- [20] A. N. Rissanou, I. G. Economou, and A. Z. Panagiotopoulos, *Macromolecules* **39**, 6298 (2006).
- [21] I. O. Götze, A. J. Archer, and C. N. Likos, *J. Chem. Phys.* **124**, 084901 (2006).
- [22] A. K. Patri, J. F. Kukowska-Latallo, and J. R. Baker-Jr., *Adv. Drug Deliv. Rev.* **57**, 2293 (2005).
- [23] A. Jusufi, C. N. Likos, and H. Löwen, *Phys. Rev. Lett.* **88**, 018301 (2002).
- [24] A. Jusufi and C. N. Likos, *Rev. Mod. Phys.* **81**, 1753 (2009).
- [25] J. K. Young, G. R. Baker, G. R. Newkome, K. F. Morris, and C. S. J. Jr., *Macromolecules* **27**, 3464 (1994).
- [26] G. Nisato, R. Ivkov, and E. J. Amis, *Macromolecules* **33**, 4172 (2000).
- [27] P. Welch and M. Muthukumar, *Macromolecules* **31**, 5892 (1998).
- [28] H. J. C. Berendsen, J. R. Grigera, and T. P. Straatsma, *J. Phys. Chem.* **91**, 6269 (1987).

-
- [29] P. Antoni, D. Nystrom, C. J. Hawker, A. Hult, and M. Malkoch, *Chem. Commun.* **22**, 2249 (2007).
- [30] I. O. Götze and C. N. Likos, *Macromolecules* **36**, 8189 (2003).
- [31] S. Rathgeber, M. Monkenbusch, M. Kreitschmann, V. Urban, and A. J. Brulet, *J. Chem. Phys.* **117**, 4047 (2002).
- [32] C. N. Likos, *Soft Matter* **2**, 478 (2006).
- [33] T. C. Zook and G. Pickett, *Phys. Rev. Lett* **90**, 015502 (2003).
- [34] D. Pötschke, M. Ballauff, P. Lindner, M. Fischer, and F. Vögtle, *Macromolecules* **32**, 4079 (1999).
- [35] D. Pötschke, M. Ballauff, P. Lindner, M. Fischer, and F. Vögtle, *Macromol. Chem. Phys.* **201**, 330 (2000).
- [36] W. Tian and Y. Ma, *J. Phys. Chem. B* **113**, 13161 (2009).
- [37] W. Tian and Y. Ma, *Soft Matter* **6**, 1308 (2010).
- [38] Y. Liu et al., *J. Phys. Chem. Lett.* **1**, 2020 (2010).
- [39] L. Porcar et al., *J. Phys. Chem. B* **112**, 14772 (2008).
- [40] L. Porcar et al., *J. Phys. Chem. B* **114**, 1751 (2010).
- [41] W.-R. Chen, L. Porcar, Y. Liu, P. D. Butler, and L. J. Magid, *Macromolecules* **40**, 5887 (2007).
- [42] T. K. Li et al., *Macromolecules* **41**, 8916 (2008).
- [43] G. Giupponi, D. M. A. Buzzza, and D. B. Adolf, *Macromolecules* **40**, 5959 (2007).
- [44] R. Blaak, S. Lehmann, and C. N. Likos, *Macromolecules* **41**, 4452 (2008).
- [45] J. Weeks, D. Chandler, and H. Andersen, *J. Chem. Phys.* **54**, 5237 (1971).

-
- [46] J. des Cloizeaux and G. Jannink, *Polymers in Solution*, The Clarendon Press, Oxford, 1990.
- [47] H. M. Harreis, C. N. Likos, and M. Ballauff, *J. Chem. Phys.* **118**, 1979 (2003).
- [48] G. S. Grest and K. Kremer, *Phys. Rev. A* **33**, 3628 (1986).
- [49] J. D. Jackson, *Classical Electrodynamics - 3rd ed.*, Wiley, New York, 1999.
- [50] U. Gupta, H. B. Agashe, A. Asthana, and N. K. Jain, *Biomacromolecules* **7**, 649 (2006).
- [51] A. D'Emanuele and D. Attwood, *Adv. Drug Deliv. Rev.* **57**, 2147 (2005).
- [52] N. G. Portney and M. Ozkan, *Anal. Bioanal. Chem.* **384**, 620 (2006).
- [53] R. W. J. Scott, O. M. Wilson, and R. M. Crooks, *Journal of Physical Chemistry B* **109**, 692 (2005).
- [54] J. Haensler and F. C. Szoka, *Bioconjugate Chem.* **4**, 372 (1993).
- [55] P. G. Degennes and H. Hervet, *Journal De Physique Lettres* **44**, L351 (1983).
- [56] Z. Y. Chen and S.-M. Cui, *Macromolecules* **29**, 7943 (1996).
- [57] M. Doi and S. F. Edwards, *The Theory of Polymer Dynamics - 1st ed.*, Clarendon Press, Oxford, 1986.
- [58] P. G. de Gennes, *Scaling Concepts in Polymer Physics*, Cornell University Press, Ithaca and London, 1979.
- [59] P. Flory, *Principles of Polymer Chemistry*, Cornell University Press, Ithaca, 1953.
- [60] A. Nikoubashman and C. N. Likos, *Macromolecules* **43**, 1610 (2010).
- [61] A. Nikoubashman and C. N. Likos, *J. Chem. Phys.* **133**, 074901 (2010).
- [62] M. L. Mansfield and L. I. Klushin, *Macromolecules* **26**, 4262 (1993).

- [63] M. Murat and G. S. Grest, *Macromolecules* **29**, 1278 (1996).
- [64] D. Boris and M. Rubinstein, *Macromolecules* **29**, 7251 (1996).
- [65] R. L. Lescanec and M. Muthukumar, *Macromolecules* **23**, 2280 (1990).
- [66] A. A. Gurtovenko, S. V. Lyulin, M. Karttunen, and I. Vattulainen, *J. Chem. Phys.* **124**, 8 (2006).
- [67] R. B. C. N. Likos and A. Wynveen, *J. Phys.: Condens. Matter* **20**, 494221 (2008).
- [68] J. S. Klos and J.-U. Sommer, *Macromolecules* **43**, 4418 (2010).
- [69] Y. Liu, V. S. Bryantsev, M. S. Diallo, and W. A. G. III, *J. Am. Chem. Soc.* **131**, 2798 (2009).
- [70] P. K. Maiti and W. A. Goddard, *J. Phys. Chem. B* **110**, 25628 (2006).
- [71] S. Huißmann, A. Wynveen, C. N. Likos, and R. Blaak, *J. Phys.: Condens. Matter* **22**, 232101 (2010).
- [72] G. S. Grest, K. Kremer, and T. A. Witten, *Macromolecules* **20**, 1376 (1987).
- [73] A. R. Denton, *Phys. Rev. E* **67**, 011804 (2003).
- [74] J. Dennig and E. Duncan, *Rev. Mol. Biotechnol.* **90**, 339 (2002).
- [75] S. Huißmann, A. Wynveen, C. N. Likos, and R. Blaak, in preparation (2010).
- [76] J. Dennig, Gene transfer in eukaryotic cells using activated dendrimers, in *Dendrimers V*, volume 228, pages 621–672, Springer Berlin / Heidelberg, 2003.
- [77] Y. S. Choi, T. Thomas, A. Kotlyar, M. T. Islam, and J. R. Baker, *Chem. Biol.* **12**, 35 (2005).
- [78] S. E. Stiriba, H. Frey, and R. Haag, *Angew. Chem. Int. Ed. Engl.* **41**, 1329 (2002).
- [79] S. Rosenfeldt et al., *Macromol. Chem. Phys.* **203**, 1995 (2002).

-
- [80] W. Chen, D. A. Tomalia, and J. L. Thomas, *Macromolecules* **33**, 9169 (2000).
- [81] C. N. Likos and M. Ballauff, Equilibrium structure of dendrimers - results and open questions, in *Functional Molecular Nanostructures*, volume 245 of *Top. Curr. Chem.*, pages 239–252, Springer Berlin / Heidelberg, 2005.
- [82] S. Huißmann, C. N. Likos, and R. Blaak, *J. Mater. Chem.* **20**, 10486 (2010).
- [83] J. Dzubiella and J.-P. Hansen, *J. Chem. Phys.* **119**, 12049 (2003).
- [84] D. Cakara, J. Kleinmann, and M. Borkovec, *Macromolecules* **36**, 4201 (2003).
- [85] W. L. Jorgensen, J. D. Madura, and C. J. Swenson, *J. Am. Chem. Soc.* **106**, 6638 (1984).
- [86] H. J. C. Berendsen, J. P. M. Postma, W. F. van Gunsteren, A. DiNola, and J. R. Haak, *J. Chem. Phys.* **81**, 3684 (1984).
- [87] D. M. Ferguson, *J. Comp. Chem.* **16**, 501 (1995).
- [88] P. G. Kusalik and I. M. Svishchev, *Science* **265**, 1219 (1994).
- [89] K. Bagchi, S. Balasubramanian, and M. L. Klein, *J. Chem. Phys.* **107**, 8561 (1997).
- [90] A. Wallqvist, *Chem. Phys. Lett.* **165**, 437 (1990).
- [91] A. Kohlmeyer, W. Witschel, and E. Spohr, *Chem. Phys.* **213**, 211 (1996).
- [92] F. Bresme and A. Wynveen, *J. Chem. Phys.* **126**, 044501 (2007).
- [93] M. Lingenheil, R. Denschlag, R. Reichold, and P. Tavan, *J. Chem. Theory Comput.* **4**, 1293 (2008).
- [94] H. C. Andersen, *J. Chem. Phys.* **72**, 2384 (1980).
- [95] F. H. Stillinger, *J. Solution Chem.* **2**, 141 (1973).
- [96] A. Kohlmeyer, C. Hartnig, and E. Spohr, *J. Mol. Liq.* **78**, 233 (1998).

-
- [97] M. T. Morgan et al., *J. Am. Chem. Soc.* **125**, 15485 (2003).
- [98] A. Jusufi, R. H. D. Vane, W. Shinoda, and M. L. Klein, *Soft Matter* **7**, 1139 (2011).
- [99] D. Kannaiyan and . Imae, *Langmuir* **25**, 5282 (2009).
- [100] F. A. Detcheverry, D. Q. Pike, P. Nealey, M. Müller, and J. J. de Pablo, *Faraday Discuss.* **144**, 111 (2010).
- [101] C. Mayer et al., *Nat. Mater.* **7**, 780 (2008).
- [102] E. Stiakakis, D. Vlassopoulos, C. N. Likos, J. Roovers, and G. Meier, *Phys. Rev. Lett.* **89**, 208302 (2002).
- [103] M. Camargo and C. N. Likos, *J. Chem. Phys.* **130**, 204904 (2009).
- [104] M. Camargo and C. N. Likos, *Phys. Rev. Lett.* **104**, 078301 (2010).
- [105] M. P. Lettinga, J. K. G. Dhont, Z. Zhang, S. Messlinger, and G. Gompper, *Soft Matter* **6**, 4556 (2010).
- [106] Q. Yan and J. J. de Pablo, *Phys. Rev. Lett.* **91**, 018301 (2003).
- [107] D.-W. Yin, F. Horkay, J. F. Douglas, and J. J. de Pablo, *J. Chem. Phys.* **129**, 154902 (2008).
- [108] A. Z. Panagiotopoulos, *J. Phys.: Condens. Matter* **21**, 424113 (2009).
- [109] X. Li et al., *Soft Matter* **7**, 618 (2011).
- [110] D. Vlassopoulos and G. Fytas, *Adv. Polym. Sci.* **236**, 1 (2010).
- [111] D. Vlassopoulos, *J. Polym. Sci. Part B: Polym. Phys.* **42**, 2931 (2004).
- [112] E. Stiakakis et al., *Europhys. Lett.* **72**, 664 (2005).
- [113] M. E. Helgeson, N. J. Wagner, and D. Vlassopoulos, *J. Rheol.* **51**, 297 (2007).
- [114] E. Stiakakis, D. Vlassopoulos, and J. Roovers, *Langmuir* **19**, 6645 (2003).

-
- [115] S. Asakura and F. Oosawa, *J. Polym. Sci.* **33**, 183 (1958).
- [116] F. Sciortino and P. Tartaglia, *Adv. Phys.* **54**, 471 (2005).
- [117] K. N. Pham et al., *Science* **296**, 104 (2002).
- [118] A. Vrij, *Pure Appl. Chem.* **48**, 471 (1976).
- [119] C. N. Likos, C. Mayer, E. Stiakakis, and G. Petekidis, *J. Phys.: Condens. Matter* **17**, S3363 (2005).
- [120] J. K. G. Dhont et al., *Faraday Discuss.* **123**, 157 (2003).
- [121] B. Loppinet et al., *Macromol. Chem. Phys.* **206**, 163 (2005).
- [122] A. Fernández-Nieves, A. Fernández-Barbero, B. Vincent, and F. J. D. las Nieves, *J. Chem. Phys.* **119**, 10383 (2003).
- [123] B. R. Saunders and B. Vincent, *Colloid. Polym. Sci.* **275**, 9 (1997).
- [124] J. Roovers et al., *Macromolecules* **26**, 4324 (1993).
- [125] P. Strunz, J. Saroun, U. Keiderling, A. Wiedenmann, and R. Przenioslo, *J. Appl. Cryst.* **33**, 829 (2000).
- [126] D. Richter et al., *J. Phys. IV* **C8**, 3 (1993).
- [127] L. Willner et al., *Macromolecules* **27**, 3821 (1994).
- [128] W. D. Dozier, J. S. Huang, and L. J. Fetters, *Macromolecules* **24**, 2810 (1991).
- [129] C. M. Marques, D. Izzo, T. Chariat, and E. Mende, *Eur. Phys. J. B* **3**, 353 (1998).
- [130] M. C. G. J. S. Pedersen, *Macromolecules* **29**, 531 (1996).
- [131] H. Benoit and J. Higgins, *Polymers and Neutron Scattering*, Oxford Science Publications, New York, 1994.
- [132] J. Roovers, *Macromolecules* **27**, 5359 (1994).

-
- [133] M. Rubinstein and R. H. Colby, *Polymer Physics*, Oxford University Press, New York, 2003.
- [134] F. S. Bates, G. D. Wignall, and W. C. Koehler, *Phys. Rev. Lett.* **55**, 2425 (1985).
- [135] A. N. Semenov et al., *Langmuir* **15**, 358 (1999).
- [136] A. A. Louis, P. G. Bolhuis, E. J. Meijer, and J. P. Hansen, *J. Chem. Phys.* **116**, 10547 (2002).
- [137] Y. O. T. Ohta, *Phys. Lett. A* **89**, 460 (1982).
- [138] C. Mayer and C. N. Likos, *Macromolecules* **40**, 1196 (2007).
- [139] P. L. Taylor, B.-C. Xu, F. A. Oliveira, and T. P. Doerr, *Macromolecules* **25**, 1694 (1992).
- [140] I. Lee, B. D. Athey, A. W. Wetzel, W. Meixner, and J. R. B. Jr., *Macromolecules* **35**, 4510 (2002).
- [141] Z. A. Rycerz and P. W. M. Jacobs, *Molecular Simulation* **8**, 197 (1992).

Danksagung

Hiermit möchte ich allen Personen meinen großen Dank aussprechen, die mich im Verlauf der Promotion unterstützt und begleitet haben.

Ich bedanke mich herzlich bei Dr. Ronald Blaak für die wunderbare Unterstützung und die unzähligen Diskussionen und wertvollen Denkanstöße. Seine humorvolle Art und Zuversichtlichkeit haben in hohem Maß zum Gelingen der Arbeit beigetragen. Mein besonderer und ebenso großer Dank gilt Prof. Dr. Christos N. Likos für die außerordentlich gute Betreuung, die denkbar beste Unterstützung, seine große Geduld und seine vielen sehr wertvollen Tips und Ratschläge, die weit über das Gebiet der Wissenschaft hinausgingen. Durch seine großartige Fürsorge habe ich mich zu jedem Zeitpunkt sehr gut in seiner Gruppe aufgehoben gefühlt. Ich danke ihm besonders dafür, dass ich dadurch sehr viel lernen und insbesondere großen Spaß an der Arbeit haben konnte. Es war mir stets eine besondere Ehre und es bereitete mir große Freude mit ihm zusammenzuarbeiten.

Außerdem bedanke ich mich bei Prof. Dr. Jürgen Horbach dafür, dass er sich freundlicherweise als Gutachter für meine Dissertation zur Verfügung gestellt hat. Ein Dankeschön geht auch an alle Kollegen und Freunde, speziell an Manuel Caramago, Dominic Lenz, Dr. Arturo Narros, Charbel Abou Jaoudeh und Katja Hauswald, die mich mit konstruktiven und lebensfrohen Diskussionen begleitet, tatkräftig unterstützt und mir eine vitalisierende Abwechslung verschafft haben.

Meiner ganzen Familie und besonders meinen Eltern gilt ein besonders großer Dank. Denn sie waren immer für mich da, konnten mich ermutigen und haben für viel Spaß und Erholung außerhalb der Arbeit gesorgt.

Zu guter Letzt bedanke ich mich bei meiner Frau Tamuna für die unbezahlbar wertvolle Unterstützung an jedem einzelnen Tag. Vor allem mit ihrer ansteckenden Neugier hat sie mir immer wieder deutlich gemacht, was das Herz der Wissenschaft ist und mein Leben damit auf unbeschreibliche Art bereichert.

Die hier vorgelegte Dissertation habe ich eigenständig und ohne unerlaubte Hilfe angefertigt. Die Dissertation wurde in der vorgelegten oder in ähnlicher Form noch bei keiner anderen Institution eingereicht. Ich habe bisher keine erfolglosen Promotionsversuche unternommen.

Düsseldorf, den 02.05.2011

(Sebastian Huißmann)